Title
Metal Organic Frameworks: From Structure to Property

Permalink
https://escholarship.org/uc/item/1rs8g3rn

Author
Bu, Fei

Publication Date
2016

UNIVERSITY OF CALIFORNIA
RIVERSIDE

Metal Organic Frameworks: From Structure to Property

A Dissertation submitted in partial satisfaction
of the requirements for the degree of

Doctor of Philosophy

in

Chemistry

by

Fei Bu

March 2016

Dissertation Committee:

       Dr. Pingyun Feng, Chairperson
       Dr. Vincent Lavallo
       Dr. Yadong Yin

This Dissertation of Fei Bu is approved:

_____

_____

_____

Committee Chairperson

University of California, Riverside

Acknowledgements

Foremost, I would like to express my deepest gratitude to my grandmother for her continuous support in the past five years. Her understanding and optimism always encourage me to move forward. I feel lucky that I have such an American relative, who is always standing with me. This dissertation would not have been completed without her tremendous encouragement. My deep thanks also go out to my hard working parents for their selfless support and patient teaching. Their love is my valuable treasure, which help me to keep strong.

I would like to express my great thanks to my advisor Dr. Pingyun Feng, who helped me a lot in the past many years. Without her, I wouldn't achieve so much. She often encouraged me when I felt depressed. And she frequently provided me with pivotal helps when I had troubles.

I owe a debt of gratitude to my brilliant and helpful group members, who shared great experiences with me. Especially, I would like to thank Dr. Rui Liu. He selflessly provided me with pivotal help in my first quarter, making me have a great start at UCR. I would also thank Dr. Qipu Lin, Dr. Tao Wu, Dr. Xiang Zhao, Dr. Fan Zuo and Dr. Le Wang for providing valuable suggestions to me in my research and taking care of me in daily life. Other significant contributors include Dr. Quanguo Zhai, Dr. Shoutian Zheng, Dr. Guiyuan Jiang, Dr. Puhong Liao, Dr. Zhenyu Zhang, Dr. Yang Hou, Dr. Xaio Wei, Dr. Lei Ge, Zhao Zhao, Shilei Xie, Chengyu Mao, Koroush Sasan, Xitong Chen and Yuan Wang.

I want to give my special thanks to my committee members Professor Vincent Lavallo, Professor Yadong Yin for taking time to join my defense and providing me with valuable suggestions. Dr. Lavallo was also my committee member in my oral exam. He was quite patient when I made mistakes, and gave me lots of suggestions. Dr. Yin was quite nice to me when we met at campus. And he encouraged me a lot before my defense. I feel so lucky that I have these knowledgeable and friendly professors as my committee members.

I also want to thank my first teacher in the United States, Dr. Christopher Reed. I had a hard time in his classes and in my oral exam. But I am sure Dr. Reed is the teacher who really wants the students to be good. I learned a lot in his classes and really felt confident after that.

Besides, I would like to express my heart-felt gratitude to my Teaching Assistant Advisor Dr. Kevin Simpson. He does a great job and makes me work happily. In my first year, I had a difficult time getting adapt to the environment. Dr Simpson's super strong organizing ability made me work easily. And his patience encouraged me to keep improving. I hope I can be a great teacher like him.

I will never forget that our Graduate Student Affairs Officer, Ms. Christina Youhas, encouraged me during my candidate exam. Her encouragement was warm and much more valuable than any academic suggestions. She was one of limited people in the United States who encouraged me and made me feel that I was needed during my hard time.

I also want to take this opportunity to thank all my students. They are talented and respectful. Interacting with these interesting people is no doubt my most wonderful memory at UCR.

Last but not least, I thank Yiding Liu, Yongsheng Xiao, Lei Guo (in Dr.Yinsheng Wang's group), Lei Guo (in Dr. Francisco Zaera's group), Jill Luo, Mingsheng Wang, Yuanhang Huang, Chen Yang, Yang Li, Fan Zhang, Elizabeth Dickinson, Consuelo Beecher, David Ruiz, Ryan Kudla and all other friends who have helped me and experienced great time with me. It is amazing that I meet these great people at UCR.

Dedication

To my grandmother, my parents and my friends

Copyright Acknowledgements

The text and figures in Chapter 2, in part or full, are reprinted with permission from: F. Bu, Q. Lin, Q. Zhai, L. Wang, T. Wu, S. Zheng, X. Bu, P. Feng, *Angew. Chem. Int. Ed*. **2012**, *51*, 8538.

The text and figures in Chapter 3, in part or full, are a reprint of the material as it appears in: F. Bu, Q. Lin, Q. Zhai, X. Bu, P. Feng, *Dalton Transactions*. **2015**, *44*, 16671.

The text and figures in Chapter 4, in part or full, are reprinted with permission from: Q. Lin, X. Bu, A. Kong, C. Mao, X. Zhao, F. Bu, P. Feng, *J. Am. Chem. Soc*. **2015**, *137*, 2235.

Figure 1.1, Figure 2.9 are reprinted or adapted with permission from: H. Li, M. Eddaoudi, M. O'Keeffe and O. M. Yaghi, *Nature*. **1999**, *402*, 276.

Figure 1.2 is reprinted or adapted with permission from: H. Furukawa, K. Cordova, M. O'Keeffe, O. M. Yaghi, *Science*. **2013**, *341*, 123044.

Figure 1.3 is reprinted or adapted with permission from: H. Deng, S. Grunder, K. Cordova, C. Valente, H. Furukawa, M. Hmadeh, F. Gándara, A. Whalley, Z. Liu, S. Asahina, H. Kazumori, M. O'Keeffe, O. Terasaki, J. Stoddart, O. M. Yaghi, *Science*. **2012**, *336*, 1018.

Figure 1.4 is reprinted or adapted from: K. Yee, N. Reimer, J. Liu, S. Cheng, S. Yiu, J. Weber, N. Stock, Z. Xu, *J. Am. Chem. Soc*. **2013**, *135*, 7795.

Figure 1.5, Scheme 1.2 are reprinted or adapted with permission from: R. Banerjee, A. Phan, B. Wang, C. Knobler, H. Furukawa, M. O'Keeffe, O. M. Yaghi, *Science*. **2008**, *319*, 939.

Scheme 1.3 is reprinted or adapted with permission from: D. Zhao, D. Timmons, D. Yuan, H. C. Zhou, *Accounts of Chemical Research*. **2011**, *44*, 123.

Scheme 1.4 and Figure 2.1 are reprinted or adapted from: H. Furukawa, J. Kim, N. M. Ockwig, M. O'Keeffe, O. M. Yaghi, *J. Am. Chem. Soc*. **2008**, *130*, 11650.

Figure 1.6 is reprinted or adapted with permission from: G. Ferey, *Chem. Soc. Rev*. **2008**, *37*, 191.

Scheme 1.5 is reprinted or adapted with permission from: J. Zhang, J. Bu, S. Chen, T. Wu, S. Zheng, Y. Chen, R. Nieto, P. Feng, X. Bu, *Angew. Chem. Int. Ed*. **2010**, *49*, 8876.

Figure 2.2 is reprinted or adapted with permission from: H. Furukawa, K. Cordova, M. O'Keeffe, O. M. Yaghi, *Science*. **2013**, *341*, 974.

Scheme 2.1 and Figure 2.3 are reprinted or adapted from: S. Chen, J. Zhang, T. Wu, P. Feng, X. Bu, *J. Am. Chem. Soc*. **2009**, *131*, 16027.

Figure 2.4 is reprinted or adapted from: S. T. Zheng, J. Bu, Y. Li, T. Wu, F. Zuo, P. Feng, X. Bu, *J. Am. Chem. Soc*. **2010**, *132*, 17062.

Figure 2.5 is reprinted or adapted with permission from: S. T. Zheng, T. Wu, B. Irfanoglu, F. Zuo, P. Feng, X. Bu, *Angew. Chem*. **2011**, *123*, 8184; *Angew. Chem. Int. Ed*. **2011**, *50*, 8034.

Figure 2.6 is reprinted or adapted with permission from: Q. F. Sun, T. Murase, S. Sato, M. Fujita, *Angew. Chem*. **2011**, *123*, 10502; *Angew. Chem. Int. Ed*. **2011**, *50*, 10318.

Figure 3.1 is reprinted or adapted with permission from: P. Ramaswamy, R. Matsuda, K. Kosaga, G, Akiyama, H. Jeon, S. Kitagawa, *Chem. Commun*. **2014**, *50*, 1144.

Figure 4.1 is reprinted or adapted from: J. Cavka, S. Jakobsen, U. Olsbye, N. Guillou, C. Lamberti, S. Bordiga, K. Lillerud, *J. Am. Chem. Soc*. **2008**, *130*, 13850.

Figure 4.2 is reprinted or adapted with permission from: S. Wang, W. Yao, J. Lin, Z. Ding, X. Wang, *Angew. Chem. Int. Ed*. **2014**, *53*, 1034.

ABSTRACT OF THE DISSERTATION

Metal Organic Frameworks: From Structure to Property

by

Fei Bu

Doctor of Philosophy, Graduate Program in Chemistry
University of California, Riverside, March 2016
Dr. Pingyun Feng, Chairperson

Porous Materials are an important class of materials due to their large-scale industrial

applications in gas adsorption, gas separation, heterogeneous catalysis and so on. Among

many kinds of porous materials, metal organic frameworks (MOFs) have emerged as one

of the favorites in the past fifteen years. MOFs are crystalline porous materials that are

mainly made of inorganic metal containing units and organic ligands.

Compared to commercial inorganic porous materials, zeolites, which are based on

Al^{3+} and Si^{4+}, MOFs can accommodate most types of metal ions and a large number of

organic ligands. This makes it possible for MOFs to adopt some fantastic features: (1) in

principle the pore size and the surface area of MOFs can be tuned by changing the organic

linkers, which allows MOFs to have a wider range of pore size and surface area than

zeolites; (2) functionality can be built into linkers; (3) in MOFs, the solvents have weak

interaction with frameworks and therefore can easily leave the structure at relatively low

temperature, which will provide useful and readily accessible porosity. Furthermore, the

removal of coordinated solvent molecules can provide unsaturated metal centers, which are quite meaningful for gas adsorption and catalysis.

We focus on developing MOFs with zeolite topologies and analyzing how different factors affect the construction of the final products. We also evaluated the potential applications of synthesized MOFs in gas adsorption/separation, proton conductivity and oxygen reduction reaction.

In chapter 2, we reported a rare MOF in which two zeolitic frameworks (SOD and ACO) are within one MOF. The construction of this exceptional structure is simply realized by using di-functional organic ligands. Different inorganic building units ZnO_4 tetramer, trimer and Zn^{2+} monomer appear in one MOF. The inner cages in this structure are bridged by the outer cages through Zn^{2+} monomers. The work also proved how important the bent angle of ligands is in the synthesis of MOFs.

In chapter 3, by using the same ligand, and varying synthetic conditions, we obtained three unique building blocks of indium, demonstrating charge-switching from positive trimer to negative monomer and leading to synthesis of In-MOFs with tunable framework charge. We further demonstrated the variations of gas sorption properties and proton conduction behaviors in such materials.

In chapter 4, we developed a series of zirconium-porphyrin frameworks. Different metal ions are trapped within phorphyrin rings. The frameworks have exceptional stability and uniform pores. These make them become excellent candidates for being the precursors of catalysis for oxygen reduction reaction. This work demonstrated a novel method to develop noble metal free catalysts for electrochemical reactions.

Table of Contents

List of Tables

List of Figures

List of Schemes

Chapter 1

General Overview

1.1 Introduction

Over the past decades, Metal-organic frameworks (MOFs) are widely investigated because of their tunable pore size, extra-high surface area, diverse structures and fantastic properties in gas adsorption, heterogeneous catalysis, ion exchange, drug release, proton conductivity and so on.[1-8]

MOFs are crystalline porous materials that are mainly made of inorganic metal-containing units (secondary building units, also called SBUs), organic ligands and templates. The templates can balance the charge of frameworks or act as pore-filling agents. Sometimes, the templates are from solvent molecules.[9-15] As it is shown in Figure 1.1, MOF-5 is a typical framework that is constructed by metal cluster $Zn_4(O)O_{12}C_6$ and linker 1,4-dicarboxybenzene.[11]

The interest of MOFs originates from another kind of crystalline porous materials, zeolites. The application of zeolites plays an important role in the global economy as zeolites are widely used in petroleum industry, water softening and purification. As inorganic porous materials, zeolites are constructed by tetrahedral $Si(Al)O_4$ units and two connected O atoms. So far, more than 150 types of frameworks have been developed.[16, 33] MOFs are different from zeolites in that organic linkers replace O atoms to bridge different metal ions or metal clusters.

Compared to zeolites, MOFs have some promising features that will make them be widely used in the future: (1) while zeolites are mainly synthesized by using Si^{4+}, Al^{3+}, P^{3+}, Ga^{3+}, Ge^{4+}, MOFs can accommodate most types of metal ions and a large number of organic ligands. Introducing different metal cations will result in different SBUs (Figure 1.2a). Since SBUs usually serve as the vertexes in the frameworks, diverse metal cations will enrich the connection modes of frameworks. Organic ligands with different shapes will greatly affect the topologies of the final structures. By designing and using different organic ligands, the structures of MOFs will be more diverse than zeolites (Figure 1.2b);[17] (2) in principle the pore size and the surface area of MOFs can be tuned by changing the organic linkers, which allows MOFs to have a wider range of pore size and surface area than zeolites.[18-25] For example, by using ligands with the same shape but different lengths, O. M. Yaghi et al successfully synthesized a series of MOFs which have the same structure but different pore apertures (Figure 1.3).[26] While the Brunauer–Emmett–Teller (BET) surface area of zeolites are between 300 to 800 $m^2\ g^{-1}$, the BET surface area of MOFs can be higher than 7000 $m^2\ g^{-1}$;[27-30] (3) functionality can be built into linkers. For example, by reasonably using "hard and soft (lewis) acids and bases" (HSAB) theory, Xu et al had developed two frameworks which can effectively absorb mercury (Figure 1.4).[31] They used $ZrCl_4$ or $AlCl_3$ to react with 2,5-dimercapto-1,4-benzenedicarboxylic acid (H_2DMBD). Hard Zr (IV) or Al (III) will bind strongly to hard oxygen of carboxylates of the ligand, forming a robust 3D frameworks with free-standing thiol (-SH). The soft sulfur of thiol can bind to mercury from aqueous solution of $HgCl_2$ and Hg(0) vapor; (4) in MOFs, the solvents have weak

2

interaction with frameworks and therefore can easily leave the structure at relatively low

temperature, which will provide useful and readily accessible porosity. Furthermore, the

removal of coordinated solvent molecules can provide unsaturated metal centers, which

are quite meaningful for gas adsorption and catalysis. Although the relatively low thermal

stability of MOFs (rarely more than 500 °C) rules out their utilities at high temperature,

MOFs have great potential in various applications, especially when scientists have a

better understanding of synthetic mechanism of MOFs and can develop MOFs with the

tailored functionality.[32-39]
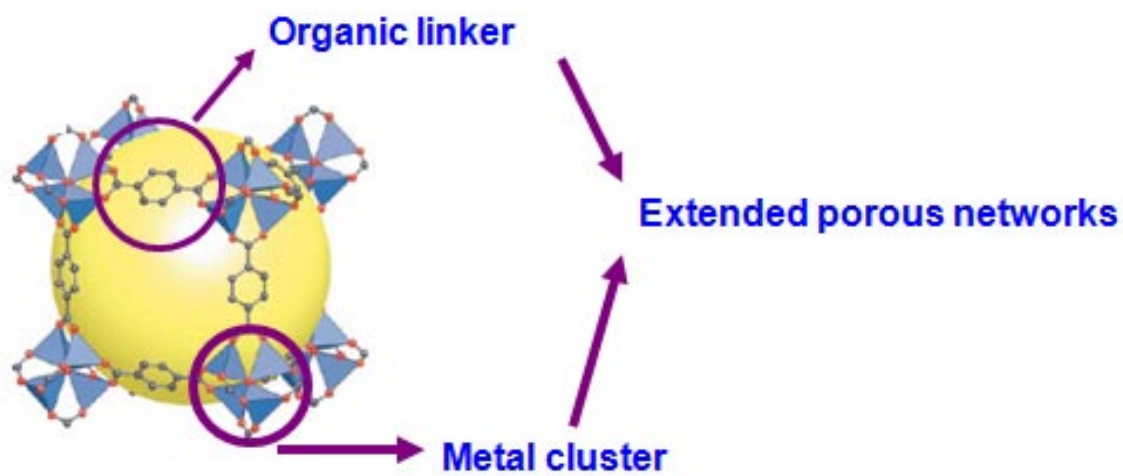
Figure 1.1 The construction of MOF-5.[11]

A

Zn$_4$O(CO$_2$)$_6$

M$_3$O(CO$_2$)$_6$ (M = Zn, Cr, In, and Ga)

M$_2$(CO$_2$)$_4$ (M = Cu, Zn, Fe, Mo, Cr, Co, and Ru)

Zr$_6$O$_4$(OH)$_4$ (CO$_2$)$_{12}$

Zr$_8$O$_8$(CO$_2$)$_8$

M$_3$O$_3$(CO$_2$)$_3$ (M = Zn, Mg, Co, Ni, Mn, Fe, and Cu)

Al(OH)(CO$_2$)$_2$ VO(CO$_2$)$_2$

In(C$_5$HO$_4$N$_2$)$_4$

Na(OH)$_2$(SO$_3$)$_3$

Cu$_2$(CNS)$_4$

Zn(C$_3$H$_3$N$_2$)$_4$

Ni$_4$(C$_3$H$_3$N$_2$)$_8$

B

Oxalic acid

Fumaric acid

H$_2$BDC

H$_2$BDC-X (X = Br, OH, NO$_2$, and NH$_2$)

H$_4$DOT

H$_2$BDC-(X)$_2$ (X = Me, Cl, COOH, OC$_3$H$_5$, and OC$_7$H$_7$)

H$_3$BTC

H$_3$BTE (X = C≡C) H$_3$BBC (X = C$_6$H$_4$)

H$_4$ATC

H$_3$THBTS

H$_3$ImDC

H$_3$BTP

DTOA

H$_3$BTB (X = CH) H$_3$TATB (X = N)

H$_4$ADB

TIPA

Gly-Ala

ADP

H$_8$BTETCA

H$_6$TPBTM (X = CONH) H$_6$BTEI (X = C≡C) H$_6$BTPI (X = C$_6$H$_4$) H$_6$BHEI (X = C≡C–C≡C) H$_6$BTTI (X = (C$_6$H$_4$)$_2$) H$_6$PTEI (X = C$_6$H$_4$–C≡C) H$_6$TTEI (X = C≡C–C$_6$H$_4$–C≡C) H$_6$BNETPI (X = C≡C–C$_6$H$_4$–C≡C–C≡C) H$_6$BHEHPI (X = (C$_6$H$_4$–C≡C)$_2$)

DCDPBN

BPP34C10DA

Ir(H$_2$DPBPyDC)(PPy)$_2$+

H$_4$DH9PhDC

H$_4$DH11PhDC

Figure 1.2 (a) Various secondary building units that are constructed by different metal cations. C black, O red, N green, S yellow, P purple, Cl light green, metal ions blue polyhedral; (b) Different ligands that can be used in the synthesis of MOFs. H atoms are omitted for clarity. AIPA, tris(4-(1H-imidazol-1-yl)phenyl)amine; ADP, adipic acid; TTFTB4$^-$,4,4′,4″,4‴-([2,2′-bis(1,3-dithiolylidene)]-4,4′,5,5′-tetrayl)tetrabenzoate.[17]

(a)

(b)

(c)
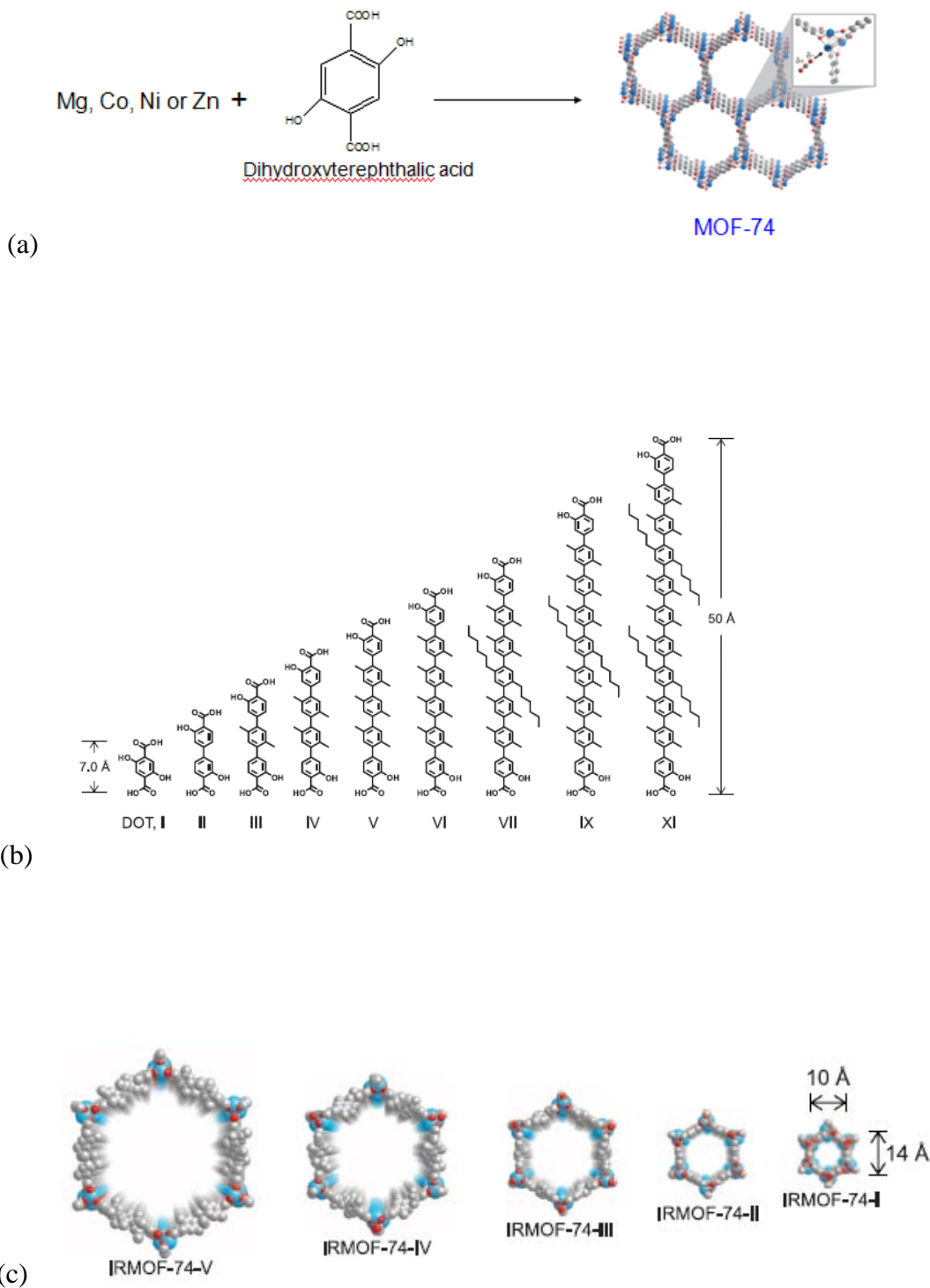
Figure 1.3 (a) Synthesis of MOF-74; (b) Ligands with same shape but different sizes were used to synthesize expanded version of MOF-74; (c) Perspective views of one-dimensional channels in the synthesized MOFs. C gray, O red, Mg blue.[26]

5
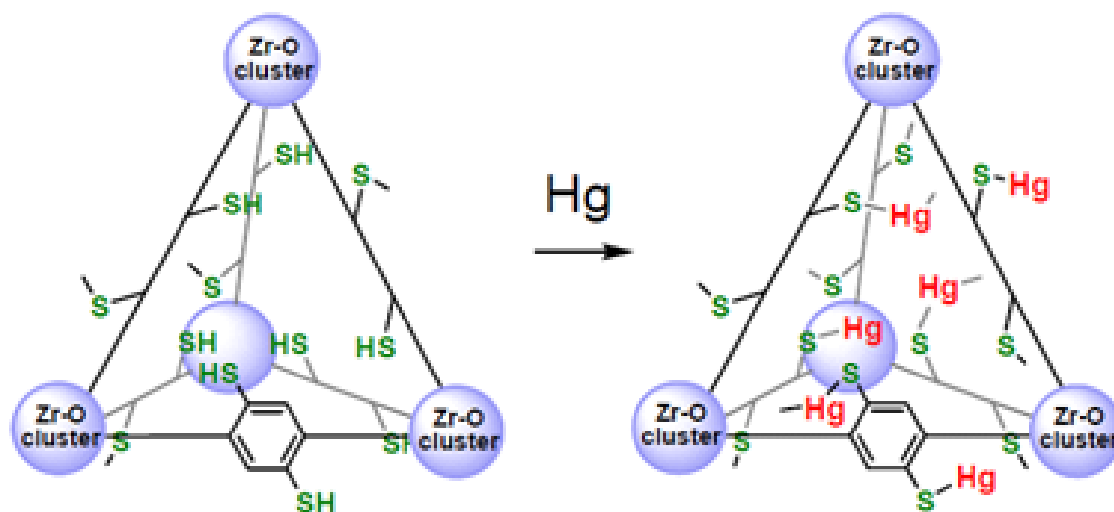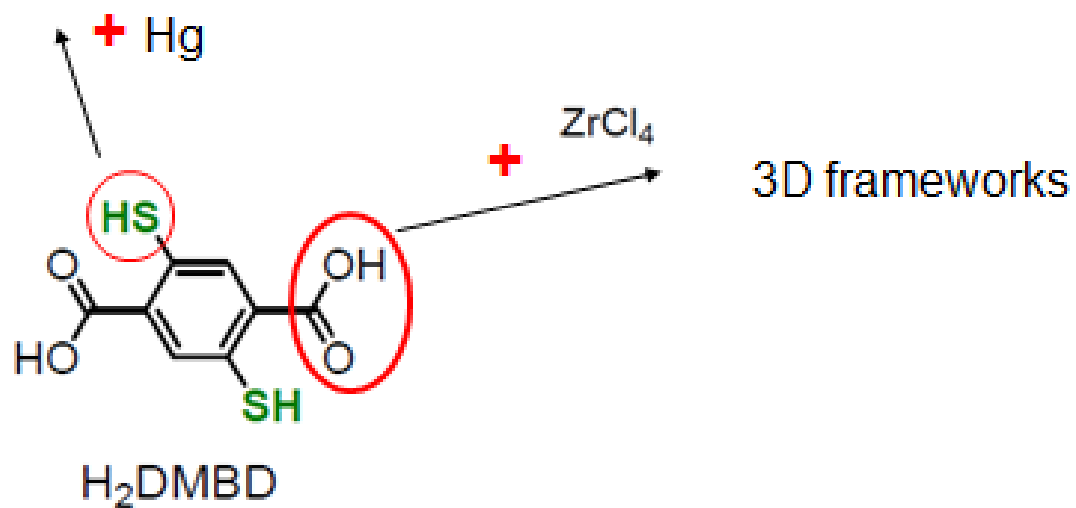
Figure 1.4 HSAB theory was used to develop MOFs that can effectively absorb mercury. Zr cations bind to carboxylates of H$_2$DMBD to form frameworks, while free standing thiols can bind to mercury later.[31]

1.2 Zeolitic Imidazolate Frameworks (ZIFs) and Carboxylate-based Metal Organic frameworks

Currently, lots of organic ligands have been used in the synthesis of MOFs, such as pipyridine, azoles, imidazolate, di- or muti-carboxylate containing molecules. Among them, imidazolate and its derivatives, and carboxylate-containing molecules gain more attention and contribute to the formation of two kinds of important MOFs in MOFs family.

Because of the widespread application and excellent stability of zeolites, developing MOFs with zeolite topologies has attracted tremendous interest. Imidazolate and its derivatives are found to be effective in the synthesis of zeolitic metal organic frameworks (ZMOFs), because these molecules have a bent angle of approximately 145°, which is close to the Si-O-Si bond angle typically found in zeolites (Scheme 1.1, Scheme 1.2, Figure 1.5).[33] Through reacting with divalent metal ions, such as Zn^{2+}, Co^{2+}, Cu^{2+}, Cd^{2+}, more than 100 metal organic frameworks with different zeolite topologies have been developed. They are named as zeolitic imidazolate frameworks (ZIFs). In the formation of ZIFs, each metal ion is tetrahedrally coordinated by four imidazolate ligands and serves as a four-connected vertex in the 3D network, and each imidazolate ligand bridges two metal ions. These can be compared to tetrahderal $Si(Al)O_4$ units and two connected O atoms in zeolites. Some ZIFs have shown promising properties in gas adsorption, molecule separation, catalysis and so on.[33, 44]

Currently, most zeolitic frameworks are synthesized based on imidazolate ligands. However, it is well known that zeolite topologies can have a large range of bent angles.

For example, in the zincoarsenates ($As_2O_8Zn_3$, AsO_4 is the tetrahedral unit), longer T-O bond results a smaller T-O-T bent angle of 123.8°.[45] This leads people to use carboxylate-containing ligands to synthesize MOFs with zeolite topologies. Carboxylate-containing ligands can not only form tetrahedral units, but also introduce different angles into the final structures and help forming topologies. Some zeolitic frameworks have been synthesized by carboxylate-containing ligands.[38-51] Compared to imidazolate ligands, carboxylate-containing ligands have some advantages that make them predominate in the synthesis of MOFs: (1) carboxylate-containing ligands have a greater diversity than imidazolate ligands. This makes them can contribute to the diversity and complexity of frameworks; (2) carboxylate-containing ligands can coordinate to different metals in different modes (Figure 1.2a). Since metal-containing units play an important role in the formation of MOFs, different metal-ligand coordination modes have an insightful effect on the structural features and stabilities of MOFs; (3) by reasonable design, different functional groups can be incorporated into carboxylate-containing ligands. And ligands with different sizes but same shapes can also be synthesized. These can greatly affect the pore sizes, surface area and functions of synthesized MOFs (Scheme 1.3, Scheme 1.4).[52, 53] Lots of famous MOFs, such as MOF-5, MOF-117, HKUST-1, have been synthesized by carboxylate-containing ligands (Figure 1.6).[2]

M-IM-M   Si-O-Si
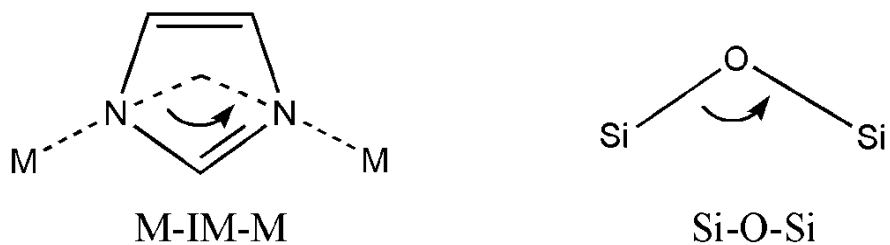
Scheme 1.1 The bridging angles in ZIFs (left) and zeolites (right).

IM   mIM   eIM   nIM   dcIM

bIM   Pur   cbIM   mbIM
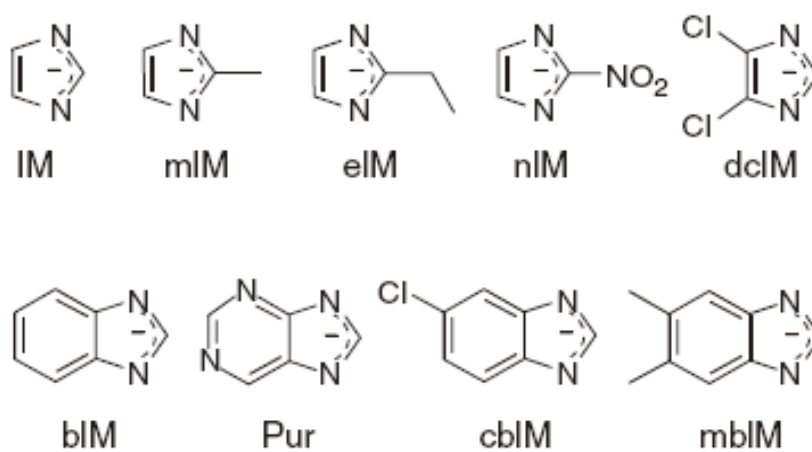
Scheme 1.2 Imidazole and some of its derivatives that are used in the synthesis of ZIFs.[33]
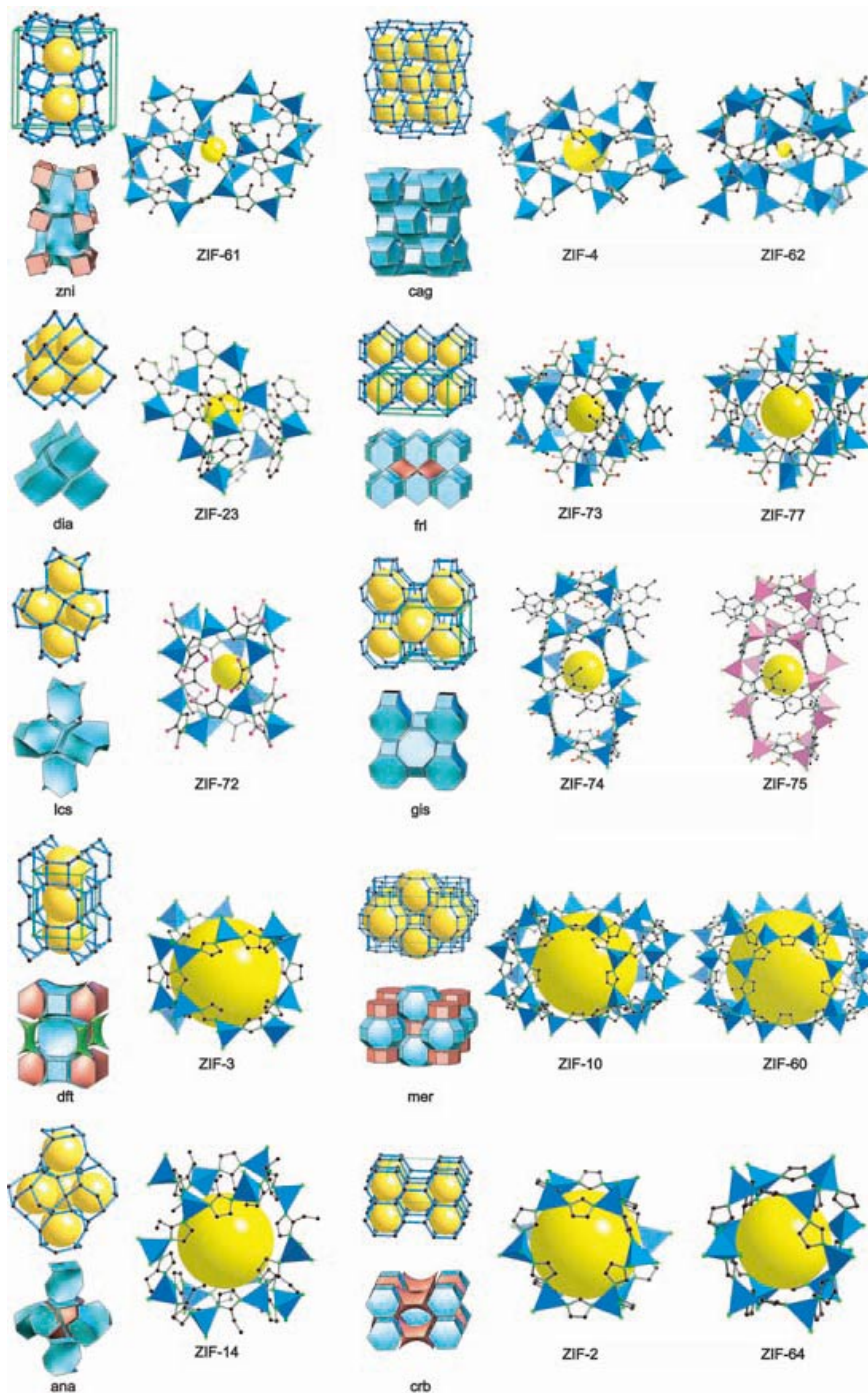
Figure 1.5 The single crystal structures of some ZIFs. In each row, the net is shown by using blue lines and black dots, and the subdivision of space (various polyhedrons with different colors) of net is represented by the tiles that are in the middle. At the bottom of the row, there is a three-letter net symbol that is used to label the net. The sizes of yellow spheres represent the free pore space. H atoms are omitted for clarity. C black, N green, O red, Cl pink.[33]

10
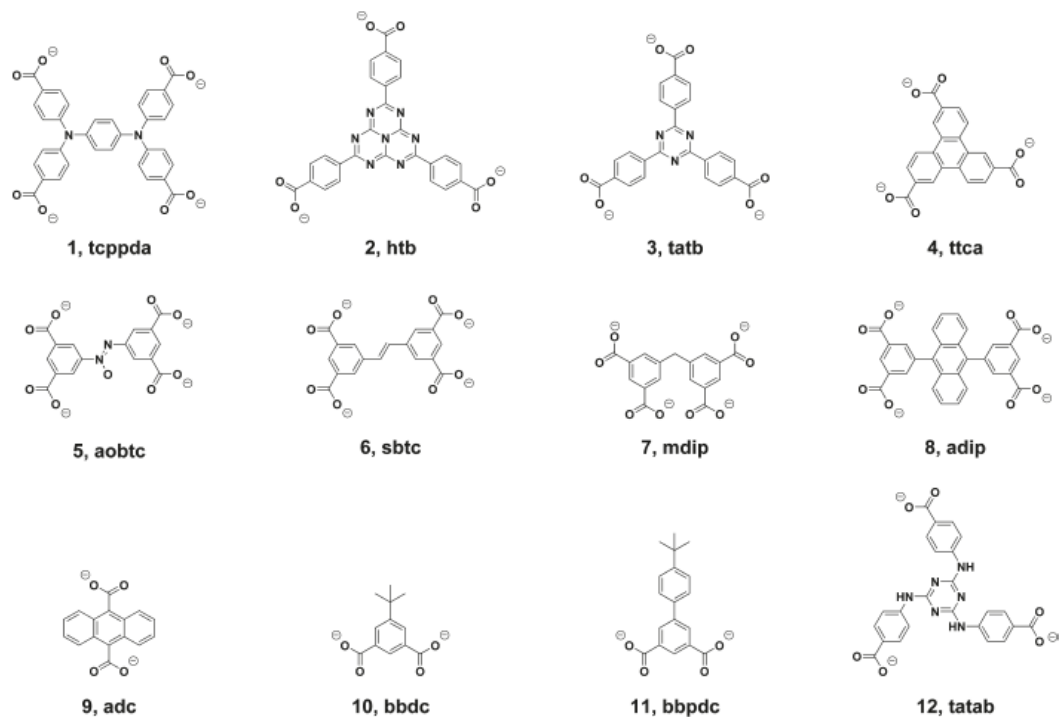
Scheme 1.3 Carboxylate ligands with similar shape but different sizes. They are used in Hongcai Zhou's group.[52]
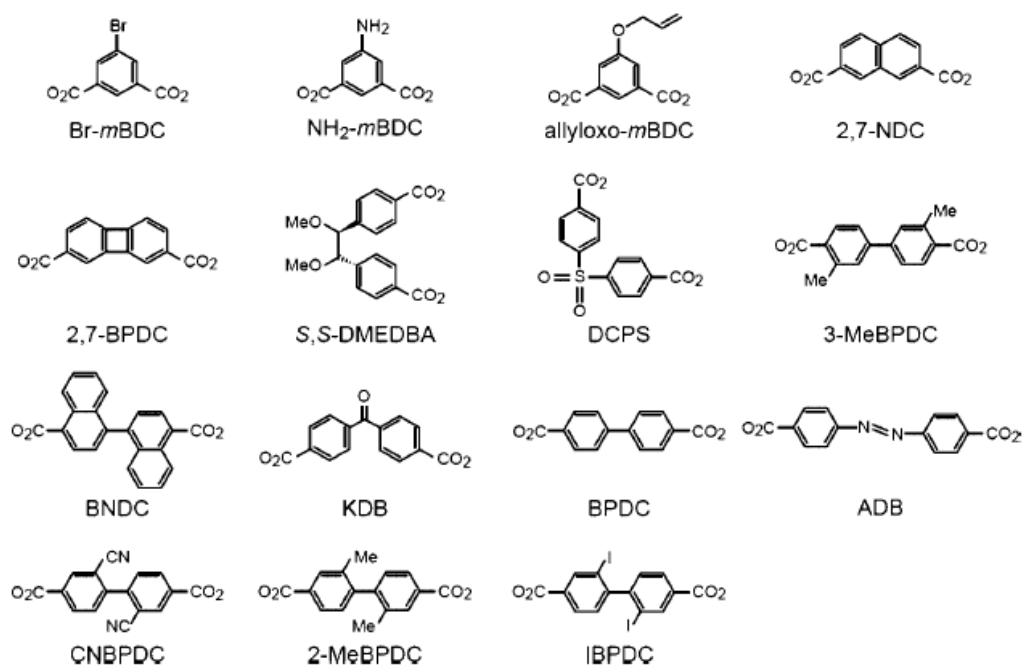
Scheme 1.4 Carboxylate ligands with similar shape but different side groups.[53]
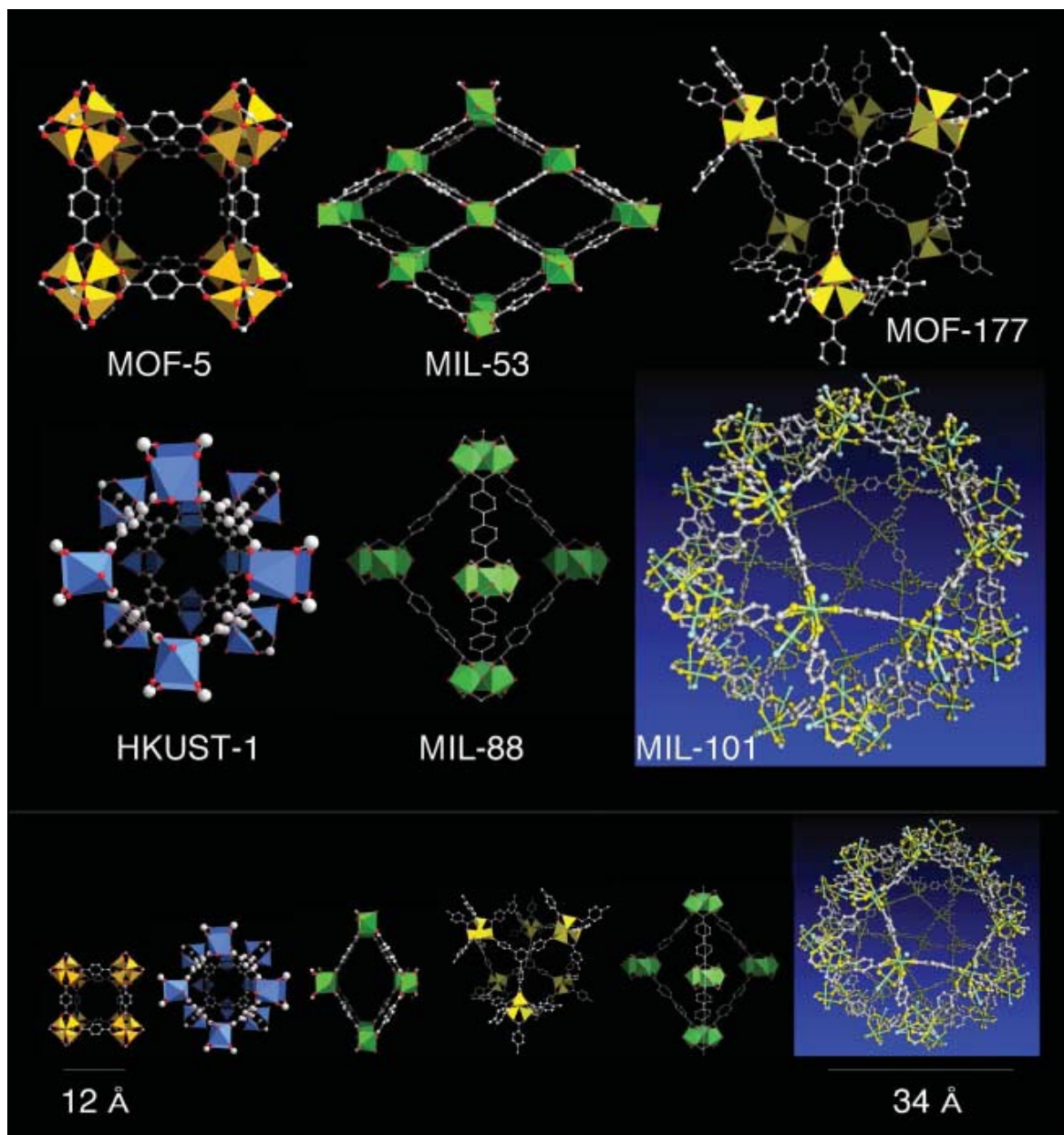
Figure 1.6 Some most cited MOFs. They are all constructed by various carboxylate ligands. Their cages are at the bottom of this figure.[2]

1.3 Synthetic Methods and Strategies

The formation of MOFs is the spontaneous assembly of multiple subunits into 3D, functional structures. The resulting structure is highly sensitive to even a slight change of one component, such as ratio of metal to ligands, temperature, pH, solvents, the charge of metal ion, the shape of ligands. The typical synthetic procedure is: the desired transition metal salts, organic ligands, structure directing agents (templates) and solvents are put in a glass vial that is heated at a temperature ranging from 80 to 150 °C. Finally, the reaction vial will be cooled to room temperature. And the single crystals will be rinsed by some solvents so that they can be analyzed later.

Different metal salts and organic ligands may be used in one reaction with the hope that they are all incorporated into the final structure and bring new properties to the framework.

Being similar to the synthesis of zeolites, structure directing agents may be needed to fill the pores and balance the charge of the frameworks. Different ammonium salts are frequently used in the synthesis of MOFs. The sizes and chirality of these templates may greatly affect gas adsorption properties and chirality of the framworks.[54-61]

Solvent plays an important role in the synthesis of MOFs. It's not rare that a specific structure can only be gained by using a specific solvent and different structures can be produced from the same reactants by different solvents and co-solvents. In the synthesis of zeolites, hydrothermal method in which water is the main or only solvent is widely used, although non-aqueous synthesis is also tried to some extent. Because the diversity of reactants in the synthesis of MOFs, many more organic solvents have been

used in MOFs synthesis. This process is called solvothermal synthesis. Some organic

solvents can not only improve the dissolution of metal salts and ligands, but also serve as

templates to fill the pores of the frameworks. For example, the decomposed product of

dimethylformamide (DMF), $(CH_3)_2NH_2^+$, frequently serves as templates to fill the pores

and balance the negative charge of frameworks. Thus DMF and its derivatives are widely

used to develop new MOFs.[62-65] Urea and its derivatives are also quite effective in the

synthesis of MOFs. The process of using urea and its derivatives to synthesize MOFs is

called urothermal synthesis. In the urothermal synthesis, urea and its derivatives are used

as additives or solvents directly based on their melting points. It is found that urothermal

synthesis can easily help people develop a large amount of MOFs based on different

metals. Furthermore, urea molecules will bind to metal ions during the self-assembly of

MOFs and can be easily removed later, producing lots of open metal sites and accessible

porosity.[66]

The pH also has an important effect in the synthesis of MOFs. Different base or

acid may be added to the reaction system to deprotonate the ligands or enhance the

dissolution of reactants. We expect that organic superbase will be promising in MOFs,

although they are not explored a lot currently. The reasons are: (1) compared to amines,

superbases have high proton affinity and low nucleophilicity. This makes them easily

remove the protons of ligands without binding to metal cations; (2) Some superbases'

melting points are so low that they can serve as solvent directly, for example, the melting

point of 1,8-Diazabicyclo[5.4.0]undec-7-ene (DBU) is -70°C; (3) In addition to help

generate anionic (e.g., by deprotonation of imidazole), the protonated form of organic

superbases is cationic and can serve as template to balance the charge of negative

frameworks that are often encountered in the synthesis of porous frameworks. Some

interesting results have been got by using superbases in the synthesis of another crystalline

frameworks, chalcogenide clusters.[67]
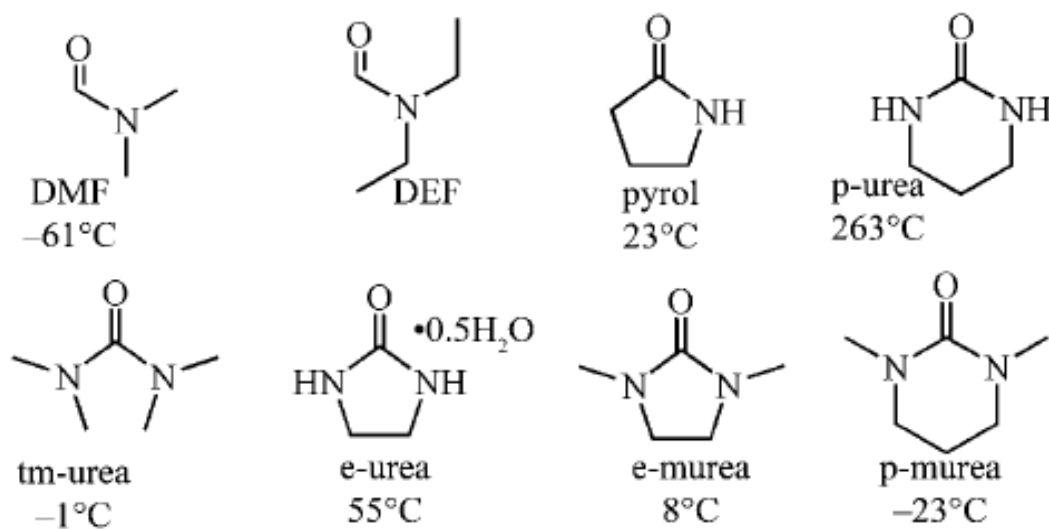
Scheme 1.5 DMF, DEF, pyrol and some urea derivatives that can be used in urothermal synthesis. Their melting points are also provided. DMF = dimethylformamide, DEF = diethylformamide, pyrol = 2-pyrrolidinone, p-urea = propyleneurea, tm-urea = tetramethylurea, e-urea = ethyleneurea, e-murea = 1,3-dimethyl-2-imidazolidinone, p-murea = 1,3-dimethylpropyleneurea.[66]

1.4 Scope of the Dissertation

Currently, great efforts are being put to develop new strategies to synthesize

MOFs with specific topologies and properties. Our group focuses on developing zeolitic

frameworks and analyzing their potential applications in gas adsorption/separation,

proton conductivity and oxygen reduction reaction.

The ligands we used were 2,5-furandicarboxylic acid (FDA),

thiophene-2,5-dicarboxylic acid (THB) and

5,10,15,20-Tetrakis(4-carboxybiphenyl)porphyrin (TCBPP) (Scheme 1.6). FDA and

THB have the bent angles of 129° and 147°, respectively. This can help us understand

how the bent angle affects the final structure. Metalloporphyrin-based MOFs can easily

trap different metal ions within the porphyrin rings. The structural features of MOFs,

such as uniform pores, and trapped metal ions within the porphyrin rings make this kind

of MOFs have a great potential to be used as heterogeneous catalysts.

Other factors were systematically changed so that we could analyze the

mechanism of self-assembly of MOFs.
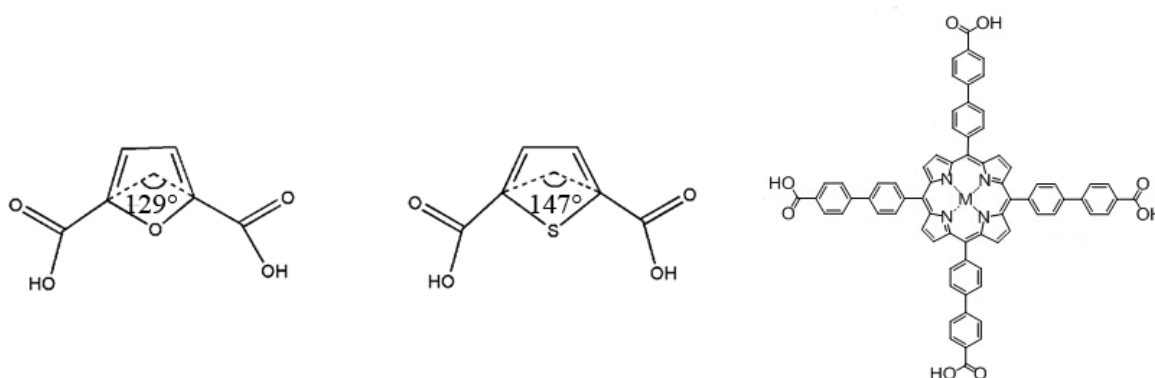
Scheme 1.6 The structures of FDA, THB, TCBPP-M (from left to right). M is H_2 or metal ions that are trapped within the porphyrin ring.

In chapter 2, we reported a rare MOF in which two zeolitic frameworks (SOD and ACO) are within one MOF. The construction of this exceptional structure is simply realized by using di-functional organic ligands, 2,5-furandicarboxylic acid. Different inorganic building units ZnO_4 tetramer, trimer and Zn^{2+} monomer appear in one MOF. Being different from other cage-within-cage structures in which the connection of inner cages and outer cages is realized by using polyfunctional ligands, the inner cages in this structure are bridged by the outer cages through Zn^{2+} monomers. The work also proved how important the bent angle of ligands is in the synthesis of MOFs.[68]

In chapter 3, we reported three indium MOFs made from the same ligand, 2,5-furandicarboxylic acid. One fascinating thing about In-MOFs is their various structural building blocks such as negative $[In(COO)_4]^-$ monomer and positive $[In_3(O)(COO)_6]^+$ trimer. An added interest in such building blocks is their different charges which can be utilized to design either cationic or anionic MOFs, in addition to common neutral MOFs. During the past several years, a large number of high-impact manuscripts have been published based on In-MOFs built from each unit or their combinations. What has always intrigued us is that prior to each synthetic exploration, it is almost always a matter of luck (or art) as to predict when a particular building block can be formed.

In this work, recognizing the difference in In/carboxylate ratios in the building units, we explored various synthetic conditions including varying In/carboxylate ratios to investigate key synthetic factors affecting the formation of different building blocks. By using the same ligand, 2,5-furandicarboxylic acid (FDA), and varying synthetic

conditions (especially In^{3+}/FDA ratio), it is possible to access three unique building

blocks of indium, demonstrating charge-switching from positive trimer to negative

monomer and leading to synthesis of In-MOFs with tunable framework charge. We

further demonstrated the variations of gas sorption properties and proton conduction

behaviors in such materials.[69]

In chapter 4, we developed a series of zirconium-porphyrin frameworks. The

frameworks are constructed by Zr^{4+} and TCBPP. Different metal ions (Zn, Co, Fe) are

trapped within phorphyrin rings. The frameworks have exceptional stability and uniform

pores. These make them become excellent candidates for being the precursors of catalysis

for oxygen reduction reaction (ORR). The electrochemical properties of the carbonized

products of these MOFs had been tested. One of them showed excellent ORR activity

that could be compared to commercial catalyst 20% Pt/C in alkaline and acidic

environments. This work demonstrated a novel method to develop noble metal free

catalysts for electrochemical reactions.[70]

1.5 References

(1)   O. M. Yaghi, M. O'Keeffe, N. Ockwig, H. Chae, M. Eddaoudi, J. Kim, *Nature*. **2003**, *423*, 705.

(2)   G. Ferey, *Chem. Soc. Rev*. **2008**, *37*, 191.

(3)   Caubère, *Chemical Reviews*. **1993**, *93*, 2317.

(4)   J. Lee, O. Farha, J. Roberts, K. A. Scheidt, S. T. Nguyen and J. T. Hupp, *Chem. Soc. Rev*. **2009**, *38*, 1450.

(5)   J. Li, R. J. Kuppler and H. Zhou, *Chem. Soc. Rev*. **2009**, *38*, 1477.

(6)   T. Uemura, N. Yanaia and S. Kitagawa, *Chem. Soc. Rev*. **2009**, *38*, 1228.

(7)   L. J. Murray, M. Dinca and J. R. Long, *Chem. Soc. Rev*. **2009**, *38*, 1294.

(8)   A. U. Czaja, N. Trukhanb and U. Muller, *Chem. Soc. Rev*. **2009**, *38*, 1284.

(9)   H. Zhou, J. Long, O. M. Yaghi, *Chem. Reviews*. **2012**, *112*, 673.

(10)   M. O'Keeffe, O. M. Yaghi, *Chem. Rev*. **2012**, *112*, 675.

(11)   H. Li, M. Eddaoudi, M. O'Keeffe and O. M. Yaghi, *Nature*. **1999**, *402*, 276.

(12)   J. Sun, L. Weng, Y. Zhou, J. Chen, Z. Chen, Z. Liu, D. Zhao, *Angew. Chem. Int. Ed*. **2002**, *41*, 4471.

(13)   X. Gu, Z. H. Luab, Q. Xu, *Chem. Commun*. **2010**, *46*, 7400.

(14)   Z. Lin, F. Jiang, L. Chen, C. Yue, D. Yuan, A. Lan, M. Hong, *Cryst. Growth Des*. **2007**, *7*, 1712.

(15)   L. Liu, J. Eubank, A. Cairns, J. Eckert, V. Kravtsov, R. Luebke, M. Eddaoudi, *Angew. Chem. Int. Ed*. **2007**, 46, 3278.

(16)   K. S. Park, Z. Ni, A. P. Cote, J. Y. Choi, R. Huang, F. J. Uribe-Romo, H. K. Chae, M. O'Keeffe, O. M. Yaghi, O. M. Proc. *Natl. Acad. Sci. U. S. A*. **2006**, *103*, 10186.

(17)   H. Furukawa, K. Cordova, M. O'Keeffe, O. M. Yaghi, *Science*. **2013**, *341*, 123044.

(18) R. Davies, P. Raithby, R. Snaith, *Organometallics*. **1996**, *15*, 4355.

(19) T. Boyle, T. Alam, K. Peters, M. Rodriguez, *Inorg. Chem.* **2001**, *40*, 6281.

(20) A. Cheetham, G. Férey, T. Loiseau, *Angew. Chem. Int. Ed*. **1999**, *38*, 3268.

(21) S. Batten, R. Robson, *Angew. Chem. Int. Ed*. **1998**, *37*, 1460.

(22) M. Davis, *Nature*. **2002**, *417*, 813.

(23) S. Kitagawa, R. Kitaura, S. Noro, *Angew. Chem. Int. Ed*. **2004**, *43*, 2334.

(24) R. Morris, P. Wheatley, *Angew. Chem. Int. Ed*. **2008**, *47*, 4966.

(25) M. Latroche, S. Surble, C. Serre, C. Mellot-Draznieks, P. Llewellyn, J. Lee, J. Chang, S. Jhung, G. Ferey, *Angew. Chem. Int. Ed*. **2006**, *45*, 8227.

(26) H. Deng, S. Grunder, K. Cordova, C. Valente, H. Furukawa, M. Hmadeh, F. Gándara, A. Whalley, Z. Liu, S. Asahina, H. Kazumori, M. O'Keeffe, O. Terasaki, J. Stoddart, O. M. Yaghi, *Science*. **2012**, *336*, 1018.

(27) G. Férey, C. Mellot-Draznieks, C. Serre, F. Millange, J. Dutour, S. Surble, I. Margiolaki, *Science*. **2005**, *309*, 2040.

(28) S. Chui, S. Lo, J. Charmant, A. Orpen, I. Williams, *Science*. **1999**, *283*, 1148.

(29) J. Rowsell, O. M. Yaghi, Angew. *Chem. Int. Ed*. **2005**, *44*, 4670.

(30) N. Rosi, J. Eckert, M. Eddaoudi, D. Vodak, J. Kim, M. O'Keeffe, O. M. Yaghi, *Science*. **2003**, *300*, 1127.

(31) K. Yee, N. Reimer, J. Liu, S. Cheng, S. Yiu, J. Weber, N. Stock, Z. Xu, *J. Am. Chem. Soc*. **2013**, *135*, 7795.

(32) M. Eddaoudi, J. Kim, N. Rosi, D. Vodak, J. Wachter, M. O'Keeffe, O. M. Yaghi, *Science*. **2002**, *295*, 469.

(33) R. Banerjee, A. Phan, B. Wang, C. Knobler, H. Furukawa, M. O'Keeffe, O. M. Yaghi, O. M. *Science*. **2008**, *319*, 939.

(34) J. Roswell, O. M. Yaghi, *J. Am. Chem. Soc*. **2006**, *128*, 1304.

(35) S. Han, J. Mendoza-Cortés, W. Goddard III, *Chem. Soc. Rev*. **2009**, 38, 1460.

(36) T. Ong, K. Kavuru, T. Nguyen, R. Cantwell, L. Wojtas, M. Zaworotko, *J. Am. Chem. Soc*. **2011**, *133*, 9224.

(37) B. Abrahams, M. Grannas, T. Hudson, R. Robson, *Angew. Chem. Int. Ed*. **2010**, *49*, 1087.

(38) K. Sumida, M. Hill, S. Horike, A. Dailly, J. Long, *J. Am. Chem. Soc*. **2009**, *131*, 15120.

(39) S. Han, W. Deng, W. Goddard III, *Angew. Chem. Int. Ed*. **2007**, *46*, 6289.

(40) S. Hausdorf, F. Baitalow, T. Bohle, D. Rafaja, F. Mertens, *J. Am. Chem. Soc*. **2010**, *132*, 10978.

(41) A. Phan, C. Doonan, F. Uribe-Romo, C. Knobler, M. O'keeffe, O. M. Yaghi, *Acc. Chem. Res*. **2009**, *43*, 58.

(42) E. Bloch, D. Britt, C. Doonan, F. Uribe-Romo, H. Furukawa, J. Long, O. M. Yaghi, J. Am. Chem. Soc. 2010, 132, 14382.

(43) M. Dincă, J. Long, *J. Am. Chem. Soc*. **2005**, *127*, 9376.

(44) W. Zhan, Q. Kuang, J. Zhou, X. Kong, Z. Xie, L. Zheng, *J. Am. Chem. Soc*. **2013**, *135*, 1926.

(45) S. Zheng, F. Zuo, T. Wu, B. Irfanoglu, C. Chou, R. Nieto, P. Feng, X. Bu, *Angew. Chem. Int. Ed*. **2011**, *50*, 1849.

(46) C. Volkringer, D. Popov, T. Loiseau, N. Guillou, G. Férey, M. Haouas, F. Taulelle, C. Mellot-Draznieks, M. Burghammer, C. Riekel, *Nat. Mater*. **2007**, *6*, 760.

(47) T. Loiseau, L. Lecroq, C. Volkringer, J. Marrot, G. Férey, M. Haouas, F. Taulelle, S. Bourrely, P. Llewellyn, M. Latroche, *J. Am. Chem. Soc*. **2006**, *128*, 10223.

(48) T. Loiseau, C. Serre, C. Huguenard, G. Fink, F. Taulelle, M. Henry, T. Bataille, G. Férey, *Chem. Eur. J*. **2004**, *10*, 1373.

(49) S. Caskey, A. Wong-Foy, A. Matzger, *J. Am. Chem. Soc*. **2008**, *130*, 10870.

(50) P. Dietzel, R. Blom, H. Fjellvåg, *Eur. J. Inorg. Chem*. **2008**, 3624.

(51)   D. Britt, H. Furukawa, B. Wang, T. Glover, O. M. Yaghi, *PNAS*. **2009**, *106*, 20637.

(52)   D. Zhao, D. Timmons, D. Yuan, H. C. Zhou, *Accounts of Chemical Research*. **2011**, *44*, 123.

(53)   H. Furukawa, J. Kim, N. Ockwig, M. O'Keeffe, O. M. Yaghi, *J. Am. Chem. Soc*. **2008**, *130*, 11650.

(54)   W. Zhou, H. Wu, T. Yildirim, *J. Am. Chem. Soc*. **2008**, *130*, 15268.

(55)   E. Anokhina, M. Vougo-Zanda, X. Wang, A. Jacobson, *J. Am. Chem. Soc*. **2005**, *127*, 15000.

(56)   C. Volkringer, M. Meddouri, T. Loiseau, N. Guillou, J. Marrot, G. Férey, M. Maouas, F. Taulelle, N. Audebrand, M. Latroche, *Inorg. Chem*. **2008**, *47*, 11892.

(57)   S. Wang, T. Zhao, G. Li, L. Wojtas, Q. Huo, M. Eddaoudi, Y. Liu, *J. Am. Chem. Soc*. **2010**, *132*, 18038.

(58)   D. Sava, V. Kravtsov, F. Nouar, L. Wojtas, J. Eubank, M. Eddaoudi, *J. Am. Chem. Soc*. **2008**, *130*, 3768.

(59)   Y. Liu, V. Kravtsov, M. Eddaoudi, *Angew. Chem. In. Ed*. **2008**, *47*, 8446.

(60)   S. Han, Y. Wei, C. Valente, I. Lagzi, J. Gassensmith, A. Coskun, J. Stoddart, B. Grzybowski, *J. Am. Chem. Soc*. **2010**, *132*, 16358.

(61)   H. Jiang, Y. Tatsu, Z. Lu, Q. Xu, Q. *J. Am. Chem. Soc*. **2010**, *132*, 5586.

(62)   M. Maes, L. Alaerts, F. Vermoortele, R. Ameloot, S. Couck, V. Finsy, J. Denayer, D. De Vos, *J. Am. Chem. Soc*. **2010**, *132*, 2284.

(63)   L. Alaerts, M. Maes, L. Giebeler, P. Jacobs, J. Martens, J. Denayer, C. Kirschhock, D. De Vos, *J. Am. Chem. Soc*. **2008**, *130*, 14170.

(64)   B. Chen, C. Liang, J. Yang, D. Contreras, Y. Clancy, E. Lobkovsky, O. M. Yaghi, S. Dai, *Angew. Chem. Int. Ed*. **2006**, *45*, 1390.

(65)   Z. Jin, H. Zhao, X. Zhao, Q. Fang, J. Long, G. Zhu, *Chem. Commun*. **2010**, *46*, 8612.

(66) J. Zhang, J. Bu, S. Chen, T. Wu, S. Zheng, Y. Chen, R. Nieto, P. Feng, X. Bu, *Angew. Chem. Int. Ed*. **2010**, *49*, 8876.

(67) T. Wu, X. Bu, P. Liao, L. Wang, S. Zheng, R. Ma, P. Feng, *J. Am. Chem. Soc*. **2012**, *134*, 3619.

(68) F. Bu, Q. Lin, Q. Zhai, L. Wang, T. Wu, S. Zheng, X. Bu, P. Feng, *Angew. Chem. Int. Ed*. **2012**, *51*, 8538.

(69) F. Bu, Q. Lin, Q. Zhai, X. Bu, P. Feng, *Dalton Transactions*. **2015**, *44*, 16671.

(70) Q. Lin, X. Bu, A. Kong, C. Mao, X. Zhao, F. Bu, P. Feng, *J. Am. Chem. Soc*. **2015**, *137*, 2235.

Chapter 2

Two Zeolite-Type Frameworks in One Metal-Organic Framework with $Zn_{24}@Zn_{104}$ Cube-in-Sodalite Architecture

2.1 Introduction

Over the past several decades, the self-assembly process driven by coordination chemistry has allowed the creation of many fascinating materials that range from discrete molecular cages to 3D porous frameworks.[1-15] A high level of synthetic control over such assembly processes has been achieved, as demonstrated by the increasing size of discrete assemblies (called coordination cages or metal-organic polyhedra (MOPs)) (Figure 2.1) and the ever-increasing variety of topologies in metal-organic frameworks (MOFs) (Figure 2.2).[4, 16, 17-47]

For several years, we have been interested in the development of synthetic methodologies for the engineering of geometric pore spaces. For example, we were able to use a number of extra-framework organic cations of different sizes to control the utilization of pore space in a series of porous anionic indium-BTC (H_3BTC = trimesic acid) frameworks (denoted CPM-1, CPM = crystalline porous materials), leading to a significant tunability in gas sorption properties (Scheme 2.1 and Figure 2.3).[5]

More recently, we created two types of cage-in-cage coreshell-like porous frameworks, called CPM-6 (or isostructural CPM-5) and CPM-24.[42,55] In both CPM-6 and CPM-24, the trifunctional ligand (BTC) interconnects outer and inner cages.
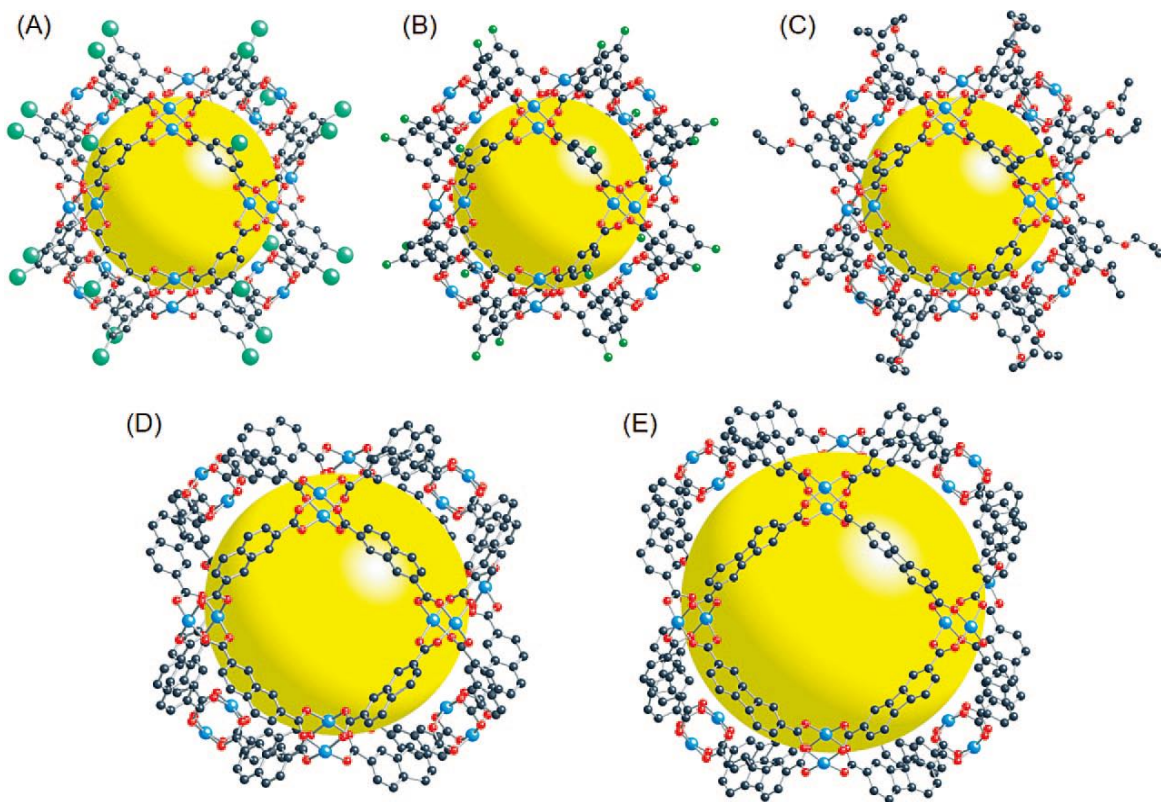
Figure 2.1 The structures of a series of MOP compounds. They are synthesized by ligands with different lengths and have different sizes. The sizes of yellow spheres represent the free pore space. Cu blue, O red, C black, Br green.[4]

CPM-6 is synthesized by indium cations and BTCs. As it is illustrated in Figure 2.4, in this $In_{12}@In_{24}$ structure, the outer In_{24} cage is constructed from In monomers.[42] In each monomer, In^{3+} is eight coordinated by the chelate bonds from the carboxylates of BTC and serves as the four-connected node. Any two monomers are bridged by two carboxylates of BTC to form the outer sodalite cage. The third carboxylate of BTC points into the cavity of the outer cage and contributes to the formation of In trimers, which are the SBUs of the inner In_{12} cage. The overall structure can be treated as a 0D MOP@3D MOF architecture, as the outer sodalite cages are packed to form a framework and the inner cages are discretely connected to corresponding sodalite cages.

CPM-24 is a nested $Co_{24}@Co_{48}$ structure that is developed by mixed ligands strategy.[55] Each outer cage is constructed by 24 V-shaped Co-OH-Co dimers and 48 deprotonated isonicotinic acid (IN) molecules. The inner cages are formed by Co-Co paddlewheels and the BTC ligands. Here the BTC ligands not only contribute to the construction of inner cages, but also serve as the bridges to connect the inner cages and outer cages. Each BTC uses two of its carboxylates to form Co-Co paddlewheel and connects the paddlewheels to build the inner Co_{24} cage. Then, the third carboxylate of BTC binds to two Co cations in the outer cage, bridging the inner cage and the outer cage (Figure 2.5). Being different from CPM-6, CPM-24 is a 3D MOF@3D MOF structure. The inner cages are connected by Co-Co paddlewheels to form an inner framework (Figure 2.5).

Interestingly, the similar mechanism based on the intercage crosslinking by polyfunctional organic ligands was also found in the formation of discrete sphere-in-sphere coordination polyhedra with the same inside and outside cages as in CPM-24 (Figure 2.6).[47]

One of the most fundamental aspects in the assembly of the nested cages is the mechanism for the interconnection between inside and outside cages. Since the original discovery of the nesting mechanism based on trifunctional organic ligand in CPM-6, we have been faced with the question whether the use of a polyfunctional ligand is the only way to create the nested cage-in-cage architecture.[47-57] The work reported in this chapter provides an unequivocal answer to this question by showing a new way in which the intercage connection is accomplished by monomeric Zn^{2+} sites anchored at the face

center of eight hexagonal rings of the sodalite cage. In contrast, the original mechanism for the intercage connection as found in CPM-6 is based on the carboxy group anchored off the edge center of sodalite cages. The new material (denoted CPM-7) is a rare example in which two zeolite-type frameworks are in one metal-organic framework.
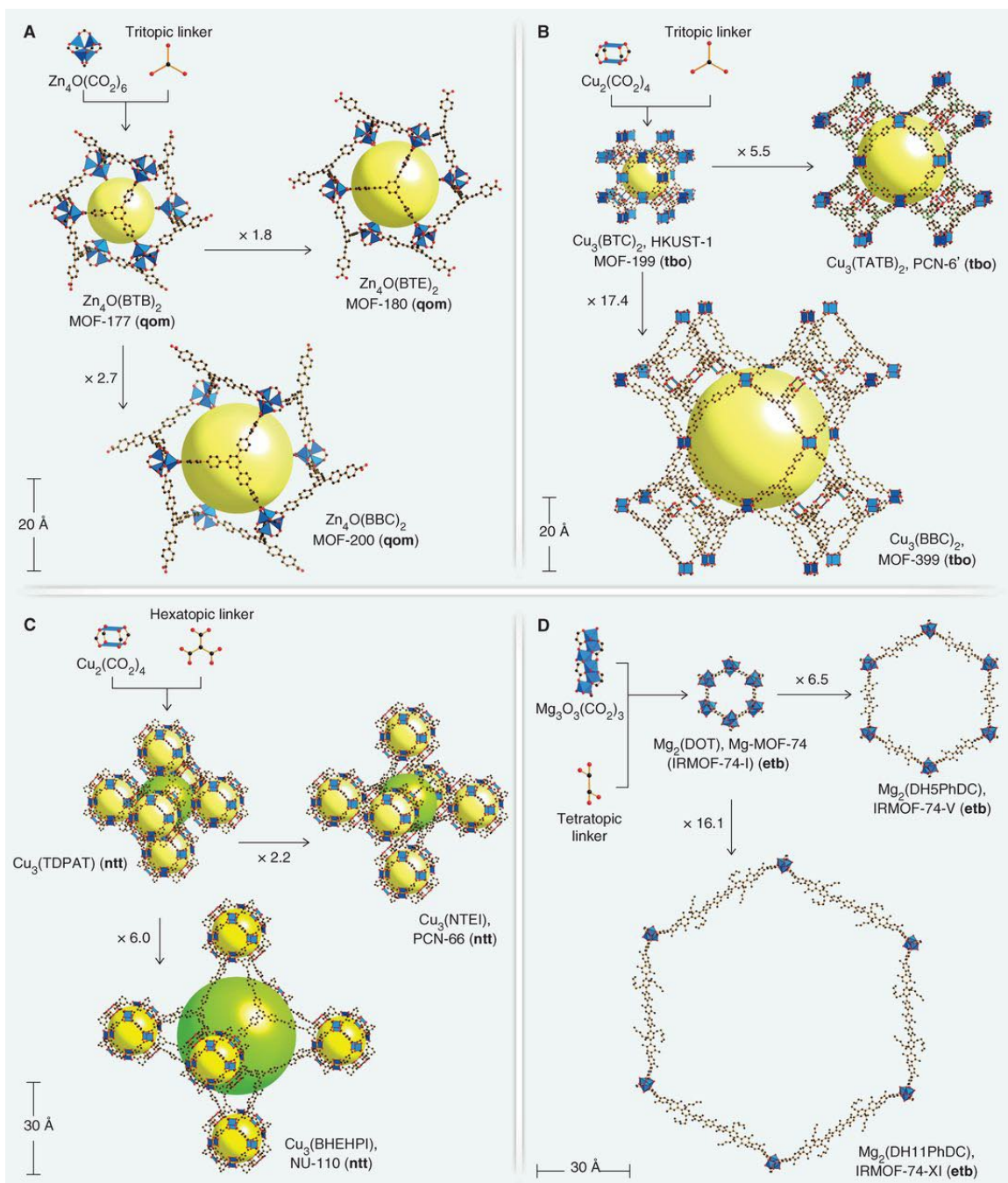
Figure 2.2 Development of expanded versions of MOFs with qom (A), tbo (B), ntt (C) and etb (D) topologies.[16]
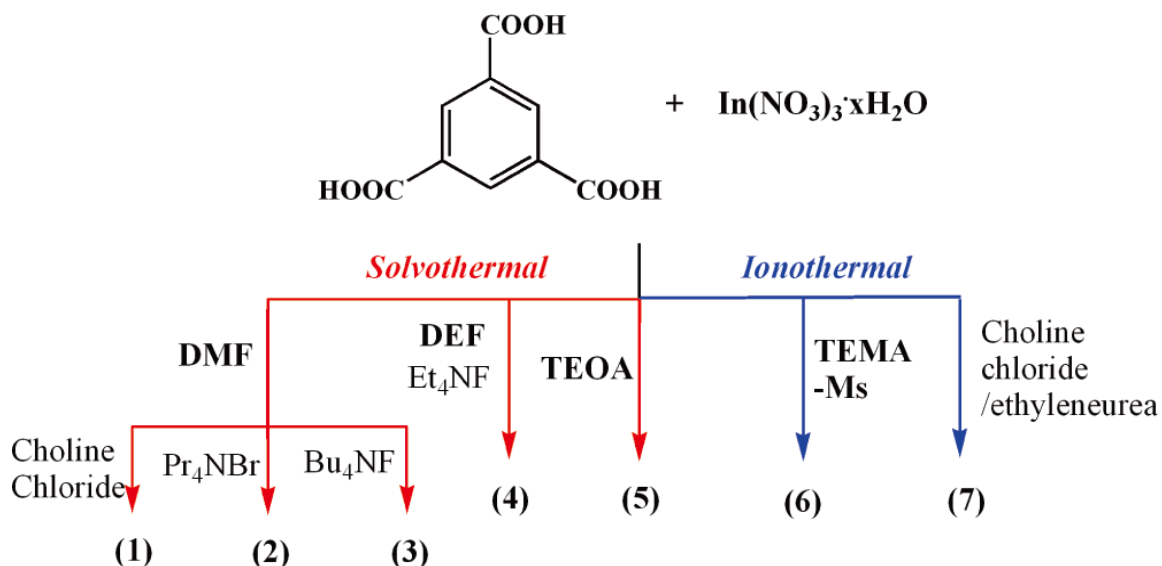
Scheme 2.1 Six different cationic templates are encapsulated in the same MOF. choline = $[(CH_3)_3NCH_2CH_2OH]^+$; Pr_4N = tetrapropylammonium; Bu_4N = tetrabutylammonium; TEOA = triethanolamine; TEMA = tris(2-hydroxyethyl)methylammonium; eurea = ethyleneurea; DMF = Dimethylformamide; DEF = Diethylformamide.[5]
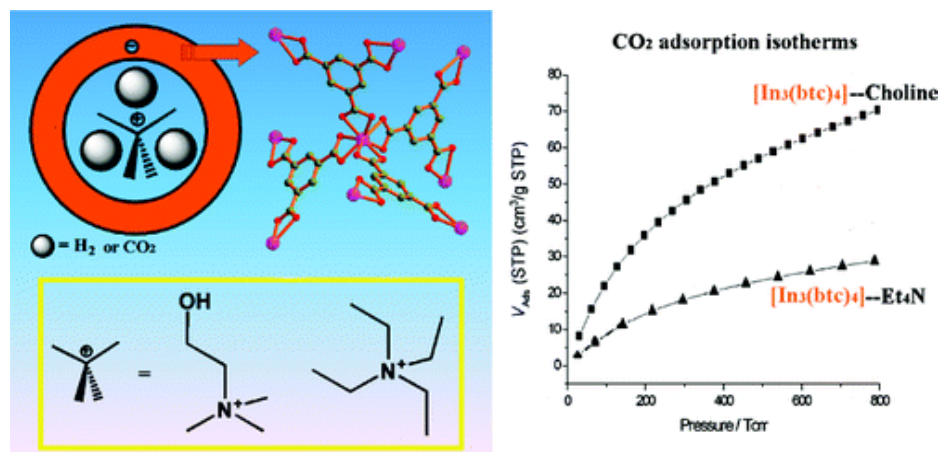
Figure 2.3 Changing the templates of MOFs can improve the gas sorption properties.[5]
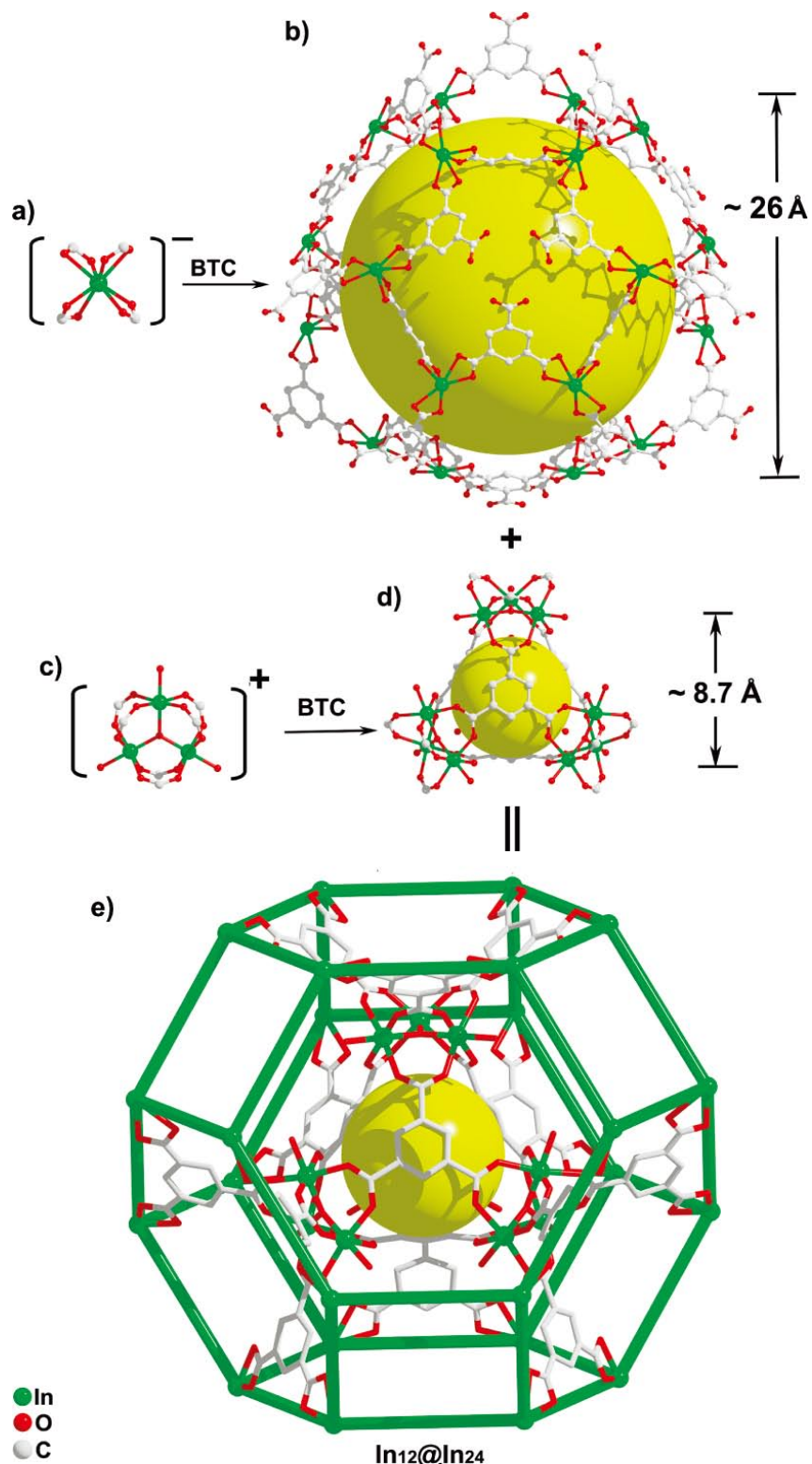
Figure 2.4 In-trimers based In$_{12}$ cage is bridged to the In-monomers based In$_{24}$ cage through the third carboxylic groups of BTCs.[42]
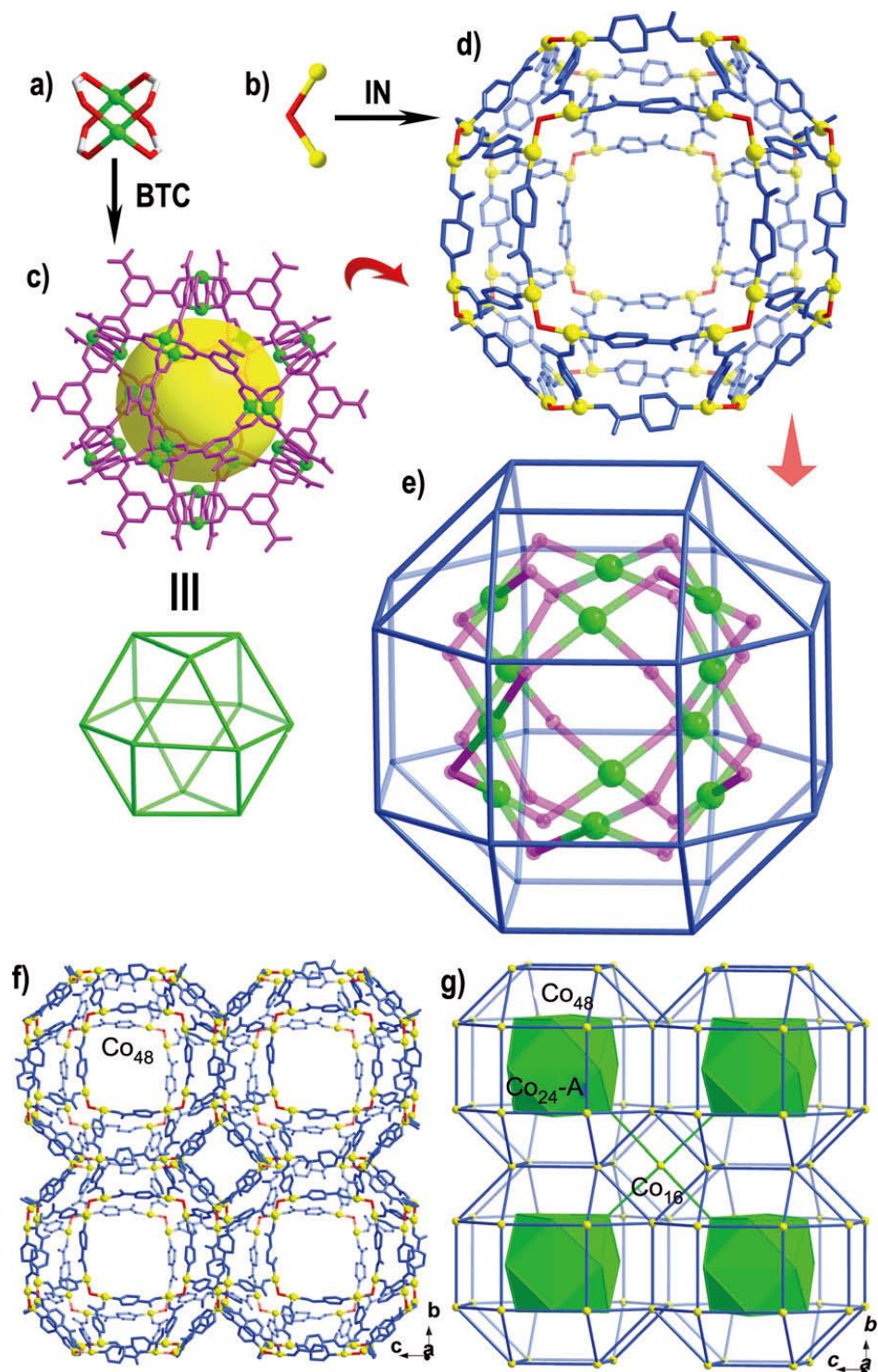
Figure 2.5 (a) Co-Co paddlewheel, Co green, O red, C gray; (b) V-Shaped dimer, Co yellow, OH^- red; (c) Inner Co_{24} cage, Co green, BTC^{3-} purple; (d) Outer Co_{48} cage, IN^- blue, Co yellow, OH^- red; (e) Cage within cage; (f) Formation of outer frameworks; (g) Connection of inner cages within outer frameworks.[55]
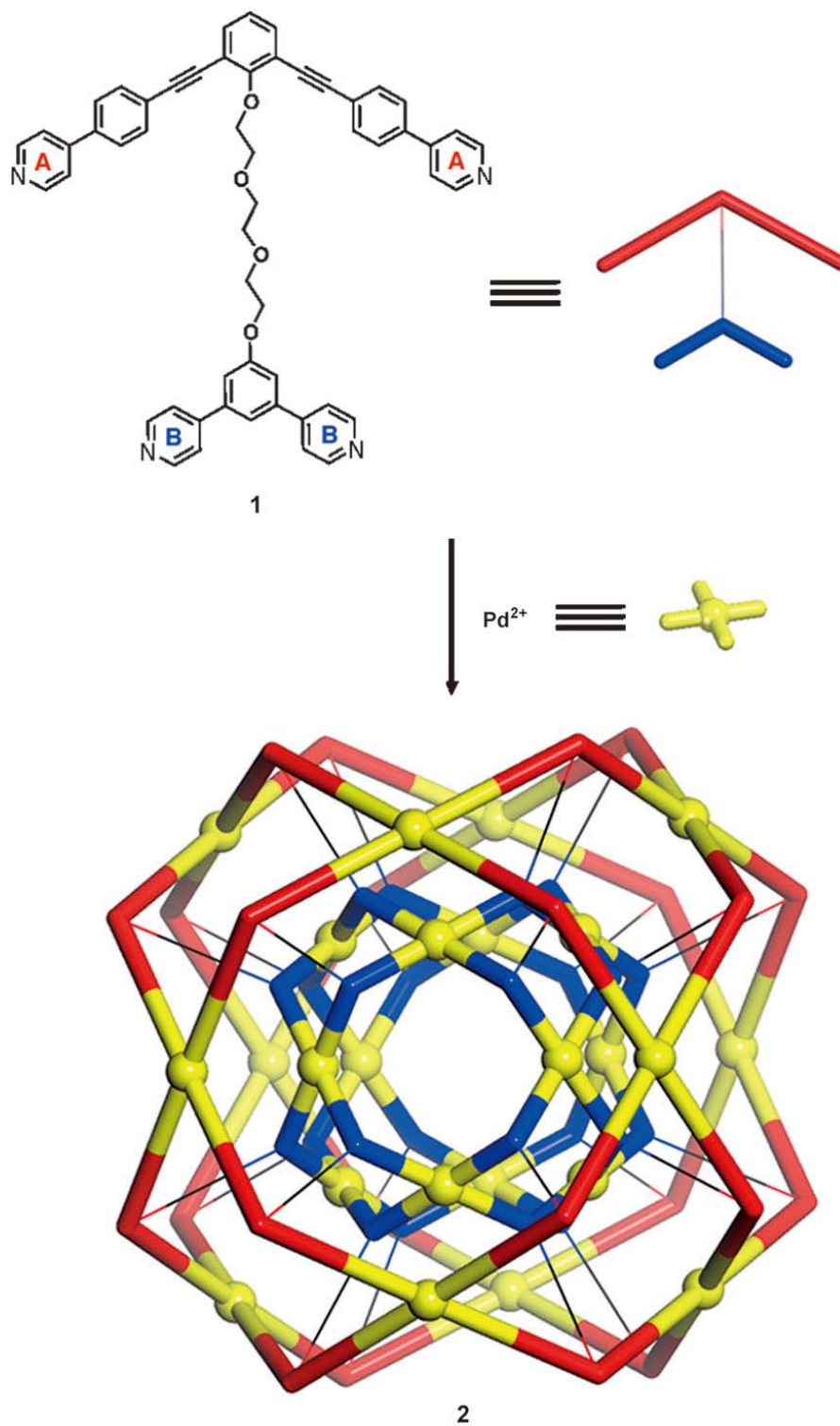
Figure 2.6 Sphere-in-sphere structure **2** is constructed by polyfunctional ligand **1**.[47]

2.2 Experimental Section

2.2.1 Synthesis of Zn$_{24}$@Zn$_{104}$ cube-sodalite frameworks

All reactants and solvents were commercially available. 2,5-furandicarboxylic acid (FDA) was bought directly from TCI. Zinc nitrate hexahydrate, N,N-diethylformamide and methanol were bought directly from Sigma-Aldrich. They were all used without further treatment.

A mixture of 2,5-furandicarboxylic acid (0.0193 g), Zn(NO$_3$)$_2$·6H$_2$O (0.037 g), N,N-diethylformamide (1.0 8g) and methanol (4.10 g) were stirred in a 23 ml vial for 20 minutes and then heated at 120 °Cfor 3 days. After cooled to room temperature and washed by ethanol, yellow cubic crystals were obtained (yield: about 91.1% based on Zn(NO$_3$)$_2$·6H$_2$O). Elemental analysis (%), calcd for Zn$_{52}$H$_{538}$C$_{446}$O$_{300}$N$_{34}$: C, 36.75; H, 3.72; N, 3.27. Found: C, 36.3; H, 3.66; N, 3.28.

2.2.2 Thermal Analysis

The thermogravimetric analysis (TGA) was performed on a TA Instruments TGA Q500 apparatus in the temperature range of 20 °C to 800 °C under N$_2$ flow at a heating rate of 5 °C/min.

2.2.3 Gas Adsorption Measurement

The measurements (N$_2$, H$_2$ and CO$_2$) were performed on a Micromeritics ASAP 2020 surface-area and pore-size analyzer.

The as-synthesized sample was activated by immersing crystals in methanol for three days. The sample was then degassed at 160 °C for 24 hours prior to gas adsorption/desorption measurements.

2.2.4 Single Crystal X-ray Diffraction

Crystal was collected on a Bruker APEX II diffractometer equipped with a fine focus, 2.0 kW sealed tube X-ray source (MoK radiation, $\lambda = 0.71073$ Å) operating at 50 kV and 30 mA. The empirical absorption correction was based on equivalent reflections. Structure was solved by direct methods followed by successive difference Fourier methods. Computations were performed using SHELXTL and final full-matrix refinements were against F^2.

Crystal data of CPM-7: cubic, *I23*, $a = 30.9836(3)$ Å, $V = 29743.75(50)$ Å^3. A total of 8726 reflections were collected in the range of $0.93° \leq \theta \leq 24.98°$, 6210 of which are unique ($R_{int} = 0.0885$). $R_1(wR_2) = 0.0526$ (0.1114) for 465 parameters and 8735 reflections ($I > 2\sigma(I)$). GOF = 0.939. CCDC 867864 contains the supplementary crystallographic data for this crystal. These data can be obtained free of charge from The Cambridge Crystallographic Data Centre via www.ccdc.cam.ac.uk/data_request/cif.
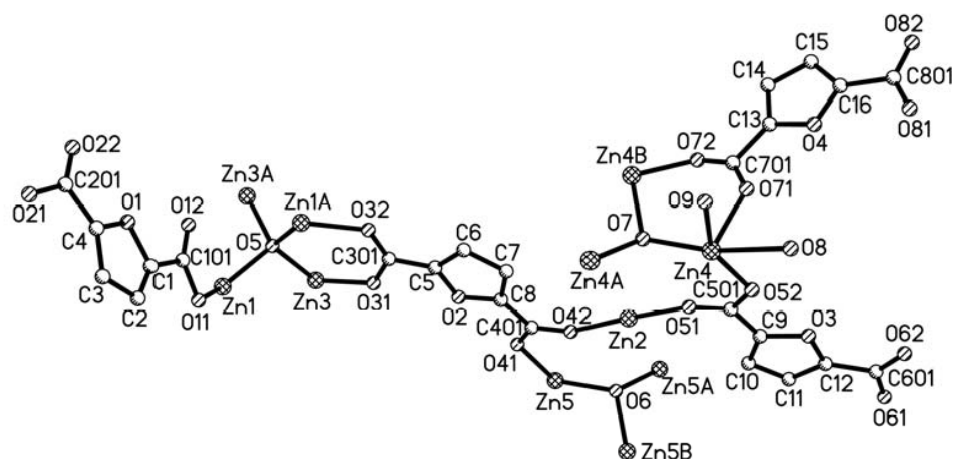
Figure 2.7 Local coordination environment of CPM-7. The figure was drawn by using SHELXTL.

2.2.5 Powder X-ray Diffraction

The experiments were performed on a Bruker D8 Advance X-ray powder diffractometer operating at 40 kV and 40 mA (CuKα radiation, λ =1.5418 Å). The test was performed with a step size of 0.03° and counting time of 1s per step. The range of 2-theta is from 3° to 40°.

The simulated powder XRD pattern was obtained based on the single-crystal data.

2.3 Results and Discussion

2.3.1 Structure Description

The chemical composition of CPM-7, determined by single-crystal X-ray analysis and formulated per sodalite cage in the sequence of [amine-template][monomer][trimer1-trimer2][tetramer][solvent], is $[(CH_3CH_2)_2NH_2]_{12}\cdot[Zn(FDA)_3]_4\cdot[Zn_3(OH)(FDA)_{3/2}\cdot Zn_3(OH)(FDA)_{3/2}\cdot(H_2O)_6]_4[Zn_4O(FDA)_4]_6\cdot[(DEF)_{22}]$. Despite this apparently complicated formula, the topological structure of CPM-7 is in fact quite simple. In the above formula, $[Zn_4O(FDA)_4]_6$ represents a sodalite cage formed from the Zn_4O tetramer and FDA, while $[Zn_3(OH)(FDA)_{3/2}\cdot Zn_3(OH)(FDA)_{3/2}\cdot(H_2O)_6]_4$ is just a collection of eight $Zn_3(OH)$ trimers joined by FDA into a cube inside the sodalite cage. The $[Zn(FDA)_3]_4$ unit represents the monomeric Zn^{2+} site at the face center (6-ring face only) of the sodalite cage and has the role of cube-to-sodalite intercage connection. Note that because this is a 3D framework, the number of metal nodes and ligands in the above notation does not match with those based on zero dimensional discrete cages.

CPM-7 crystallizes in a highly symmetric cubic space group *I23* with a relatively large unit cell (a= 30.98 Å). Its structure is built from four crystallographically different building units, Zn_4O tetramer, two kinds of $Zn_3(OH)$ trimers, and Zn monomer (Figure 2.8). While the coexistence of all these different building blocks (from the same metal ion) is in itself very unusual, their very exotic bonding pattern is even more unusual. For example, the Zn_4O tetramer, in which Zn^{2+} sites occupy four tetrahedral corners and one oxygen is at the center of the tetrahedron, should "by default" be a six connected tetramer,

just like in MOF-5 (Figure 2.9).[34] Yet, it is eight connected in CPM-7 (Figure 2.10, Figure 2.13). Such a bonding mode is very unusual and, to the best of our knowledge, has never been observed before.

There are eight FDA ligands attached to the Zn_4O tetramer and they can be divided into two sets. The first set consists of four bidentate chelating COO-Zn links in which one COO group of FDA chelates to one Zn site in the Zn_4O tetrahedron (Figure 2.8a). This bonding pattern is common in indium MOFs,[5, 42] but it is quite unusual for Zn^{2+}. In the second set, there are four bidentate bridging $COO-Zn_2$ links in which one COO group of FDA bridges two Zn sites on the edge of the Zn_4O tetrahedron (as in MOF-5). These two sets of ligands play very different roles in the framework construction. Through four chelating COO-Zn links, each Zn_4O tetramer is joined to four other Zn_4O tetramers to forma sodalite framework (Figure 2.8b, Figure 10, Figure 2.14). On the other hand, each bridging $COO-Zn_2$ link uses the other end of FDA to also bridge two Zn sites that come from one Zn monomer and one Zn trimer, respectively (Figure 2.10, Figure 2.11, Figure 2.13).

There are in fact two crystallographically different trimers: water-free $[Zn_3(OH)(O_2CR)_3]^{2+}$ (trimer **1**) and water-containing $[Zn_3(OH)(O_2CR)_3(H_2O)_6]^{2+}$ (trimer **2**). In trimer **1**, each Zn is four-coordinated, while in trimer **2**, each Zn is six-coordinated because of the presence of two terminal water molecules (Figure 2.8c and Figure 11). Topologically, however, trimer **1** and trimer **2** are equivalent, because the presence of water molecules does not affect the intercluster connectivity in any way.

Each trimer **1** is connected to six bridging FDA ligands. Three of these FDA ligands connect to three separate trimers **2**, thus leading to a cube (in a cube, each corner is always connected to three other corners) with four trimers **1** and four trimers **2** as corners of the cube (Figure 2.8c, Figure 2.15). The other three FDA ligands bridge between trimer **1** and the Zn monomer. Similarly, each trimer **2** is also connected to the Zn^{2+} monomer by three bridging FDA ligands, thus leading to the six-coordinated monomeric Zn^{2+} site.

While each monomeric Zn^{2+} site is six-coordinated, it is topologically eight-connected. This is because six FDA ligands around the monomeric Zn^{2+} site contribute a total of twelve oxygen sites (at the other end of FDA ligands) around the Zn monomer. Six of these connect to the Zn_4O tetramers, while the other six oxygen sites work in two groups and connect directly to the Zn sites in trimer **1** and trimer **2**, respectively. As a result, the eight-connected Zn monomer has two roles. It uses two connections to join the cubes into the zeolitic ACO topology (in the ACO topology, primitive cubes are packed into a body-centered cubic pattern; Figure2.8d). And it uses the remaining six connections to join to the six nodes of the hexagonal rings of the sodalite cage (Figure 2.8e, Figure 2.11, Figure 2.12, Figure 2.13).

The aforementioned unusual coexistence of various inorganic building blocks and unusual bonding patterns between them lead to the unprecedented nested $Zn_{24}@Zn_{104}$ cage-in-cage architecture in which a larger sodalite cage encapsulates a smaller cubic cage (Figure 2.16). In this case, the larger Archimedean cage (sodalite) with an overall negative charge is formed by Zn_4O tetramers, while the smaller neutral Platonic cage

(cube) is formed by $Zn_3(OH)$ trimers. Each cube in the ACO network is connected to adjacent cubes through hexagonal windows of sodalite. The monomer is at the center of the window and is bonded to six vertices of the hexagon (Figure 2.8f, Figure 2.16).
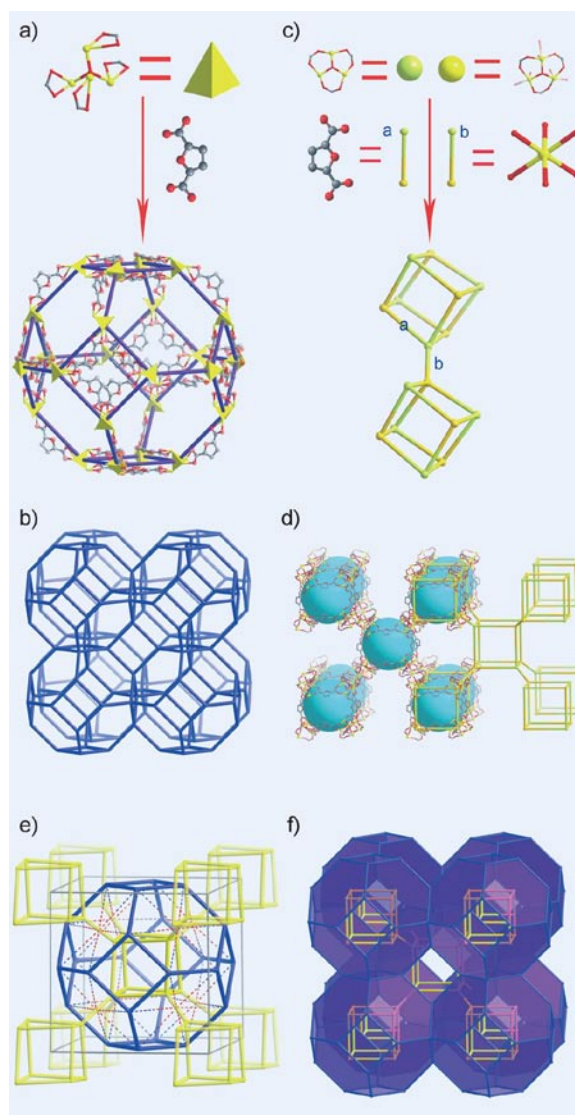
Figure 2.8 (a) 24 Zn_4O tetramers are connected by FDAs to form a sodalite cage; (b) 3D sodalite-type framework; (c) Four trimers **1** (green) and four trimers **2** (yellow) are joined into a cube by FDA ligands (shown as type **a** linkage). Two adjacent cubes are linked through one Zn^{2+} monomer (shown as type **b** linkage); (d) 3D ACO type framework (Zn yellow, O red, C grey); (e) Nested $Zn_{24}@Zn_{104}$ cages joined together by monomeric Zn^{2+} sites (shown as dashed lines) at the center of the hexagonal windows of the sodalite cage; (f) 3D nested cage-in-cage and framework-in-framework structure of CPM-7.
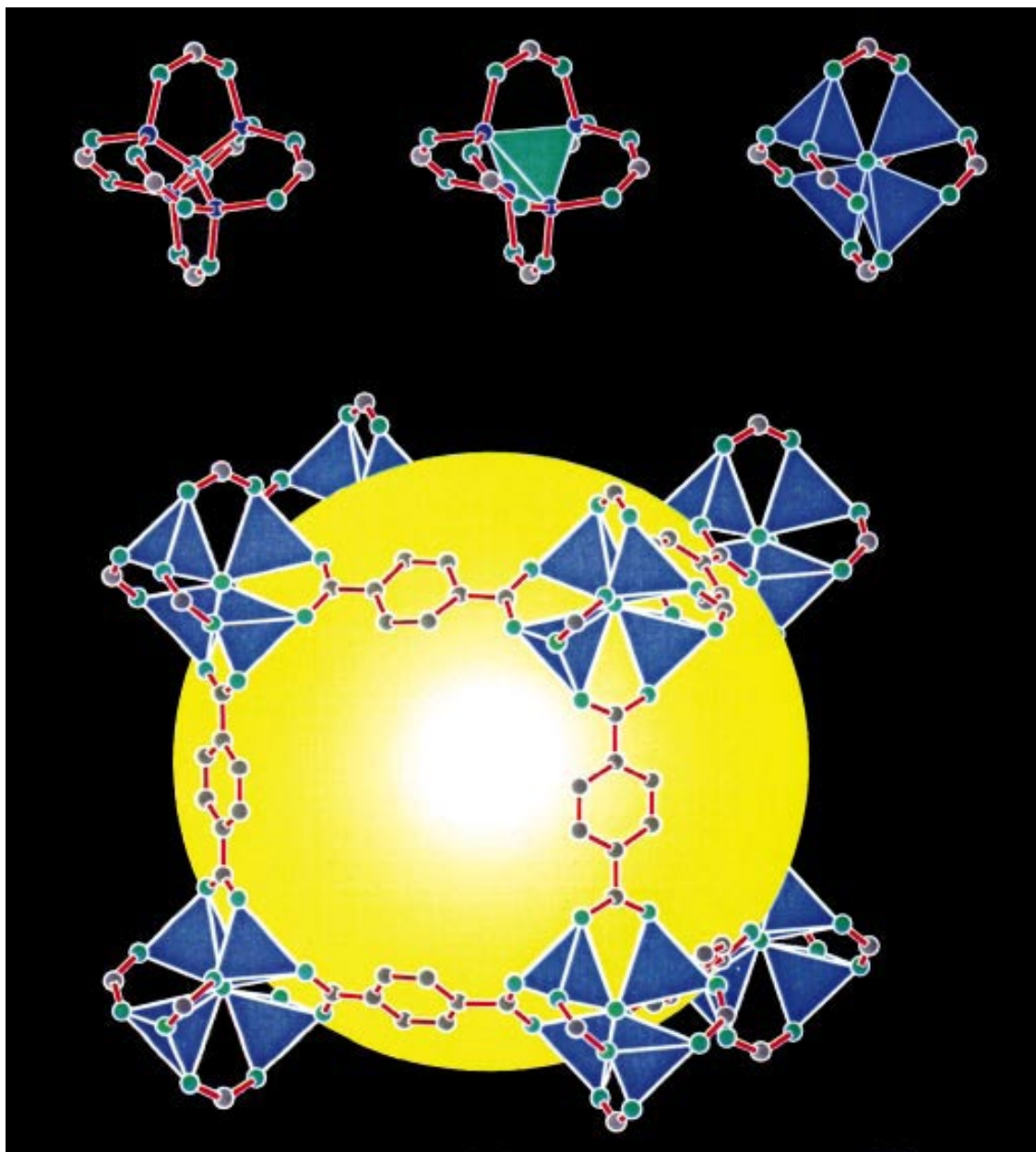
Figure 2.9 MOF-5 is constructed by $Zn_4(O)O_{12}C_6$ tetramers. Top, same $Zn_4(O)O_{12}C_6$ tetramer is represented by different ways. Left, ball and stick mode. Middle, same tetramer, green tetrahedron represents Zn_4O. Right, same tetramer, blue tetrahedrons represent ZnO_4. Each tetramer is six connected. Bottom, single cage in MOF-5 is constructed by tetramers. Zn purple, O green, C gray.[34]
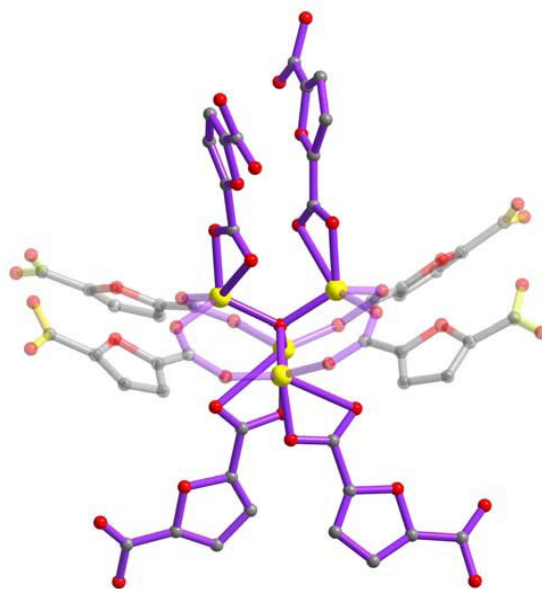
Figure 2.10 Local coordination environment of tetramer in CPM-7. Zn yellow, O red, C gray.
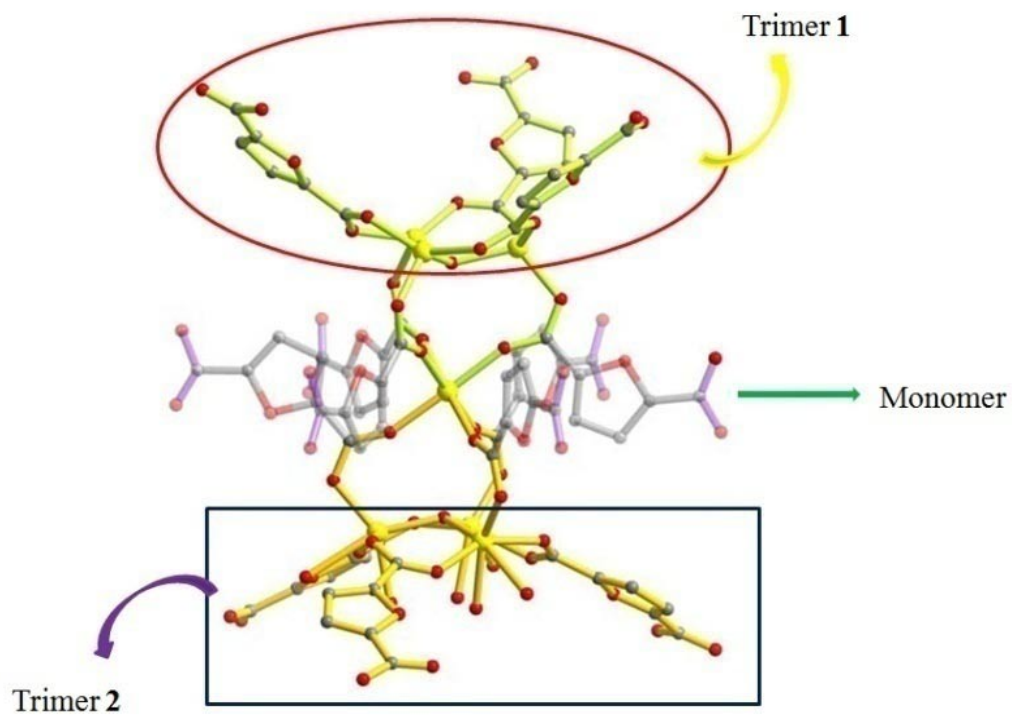
Figure 2.11 Local coordination environment of trimer **1**, trimer **2** and monomer in CPM-7. Zn yellow, O red, C gray.
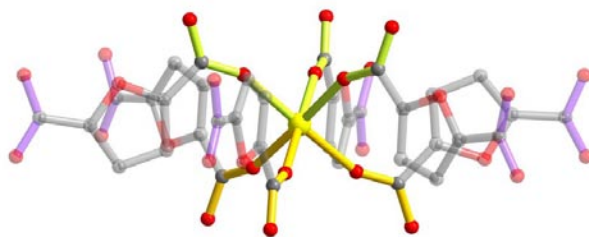
Figure 2.12 Local coordination environment of monomer in CPM-7. Zn yellow, O red, C gray.
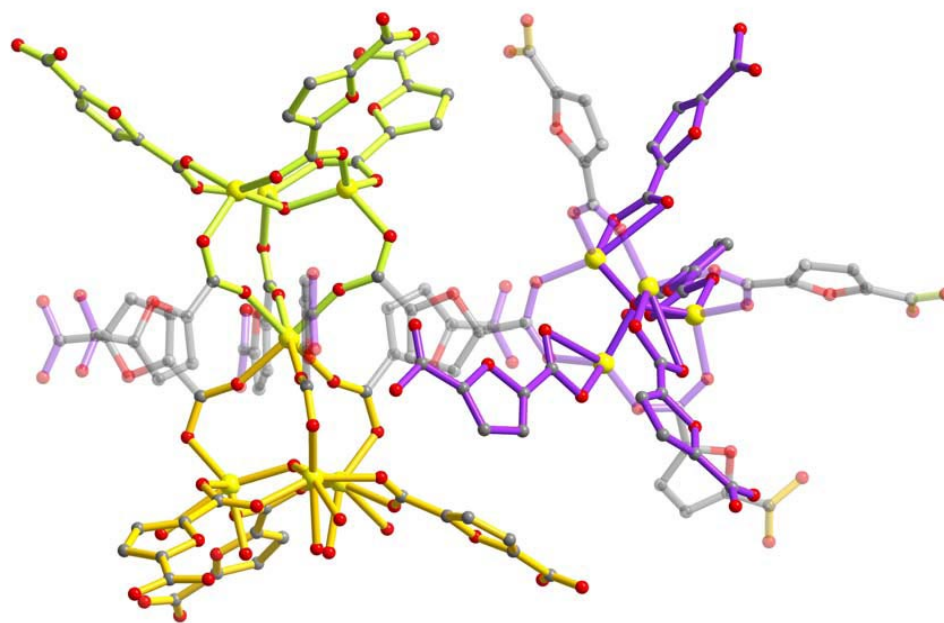
Figure 2.13 The connectivity of tetramer, trimer **1**, trimer **2** and monomer in CPM-7. Zn yellow, O red, C gray.
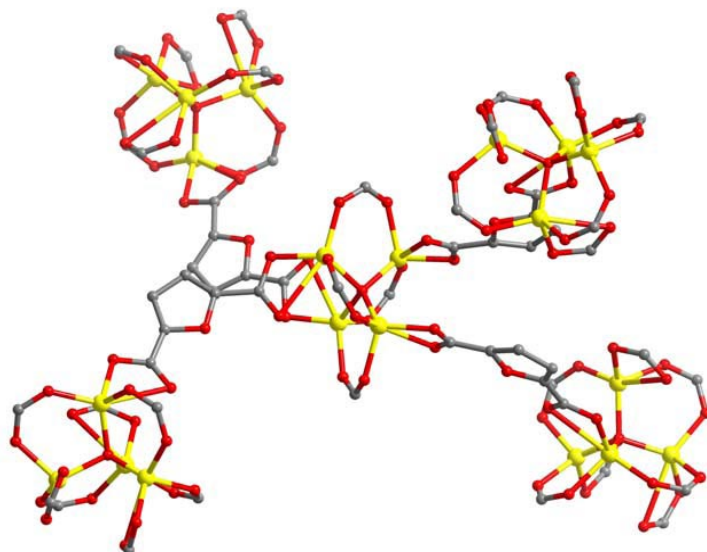
Figure 2.14 Tetramers serve as 4 connected vertexes in sodalite framework. Zn yellow, O red, C gray.
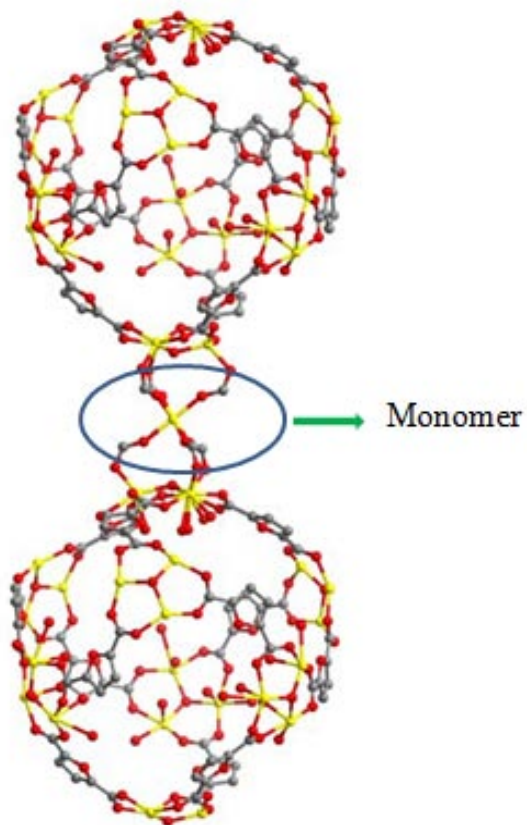
Figure 2.15 Trimers serve as 3 connected vertexes in cubes. Monomer bridges every two cubes. Zn yellow, O red, C gray.
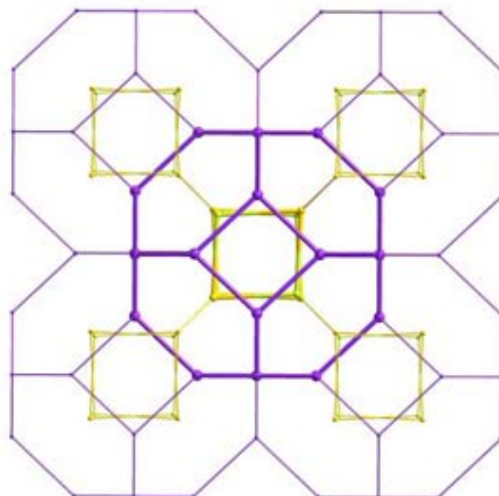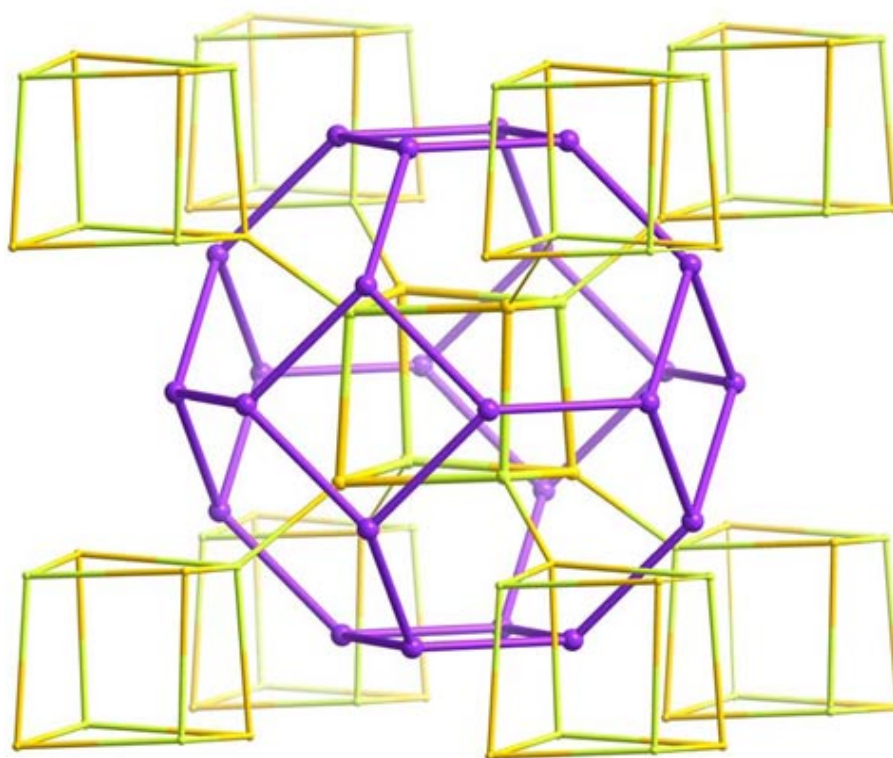
Figure 2.16 (a) The packing of SOD cages (purple) with cubes (yellow or yellow green) inside them, view from a axis; (b) The packing of cubes. Outer SOD cages except the central one, H atoms are omitted for clarity.

2.3.2 Analysis of Properties

Thermogravimetric analysis of CPM-7 showed that the removal of solvents occured in the temperature range of 100-140 °C (Figure 2.17). Powder X-ray diffraction further confirmed that CPM-7 retained its crystallinity up to approximately 240 °C (Figure 2.18).

The gas adsorption/desorption measurements were performed and the results are show in Figure 2.19. The CO_2 uptake reached 28.6 $cm^3 g^{-1}$ at 760 Torr and 273 K. In comparison, H_2 adsorption only gave an uptake of 5.4 $cm^3 g^{-1}$ at 760 Torr and 77 K. We observed that for many MOFs, the H_2 uptake in $cm^3 g^{-1}$ at 760 Torr and 77 K is often significantly higher than (sometimes approximately twice) the CO_2 uptake (also in $cm^3 g^{-1}$) at 760 Torr and 273 K. For example, CPM-5 exhibits a CO_2 uptake capacity of 81.3 $cm^3 g^{-1}$ at 273 K and 760 Torr while for H_2 gas, CPM-5 can absorb 139.2 $cm^3 g^{-1}$ of H_2 at 77 K and 760 Torr. Apparently, there is a significant difference between CPM-5 and CPM-7, in terms of the interactions between gas molecules and frameworks.

So far there are very few cage-within-cage structures. Our main interest in such a configuration is to accomplish efficient partition of pore space to optimize usage of pore space for gas sorption, based on the assumption that excessively large pore cavity has its own limitations, particularly for low-pressure gas sorption applications. There are, however, a number of parameters in the cage-in-cage configuration that strongly affect the gas sorption properties. In addition to variations in intercage connectivity, strategies for achieving different types of outside and inside cages are critically important for enhanced gas sorption.
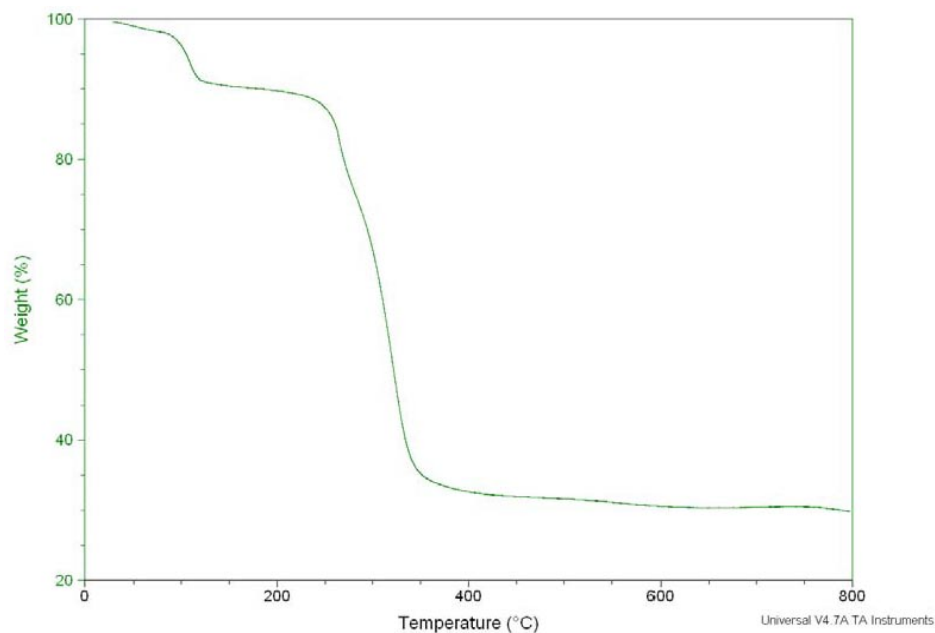
Figure 2.17 Thermogravimetric analysis (TGA) curve of CPM-7.
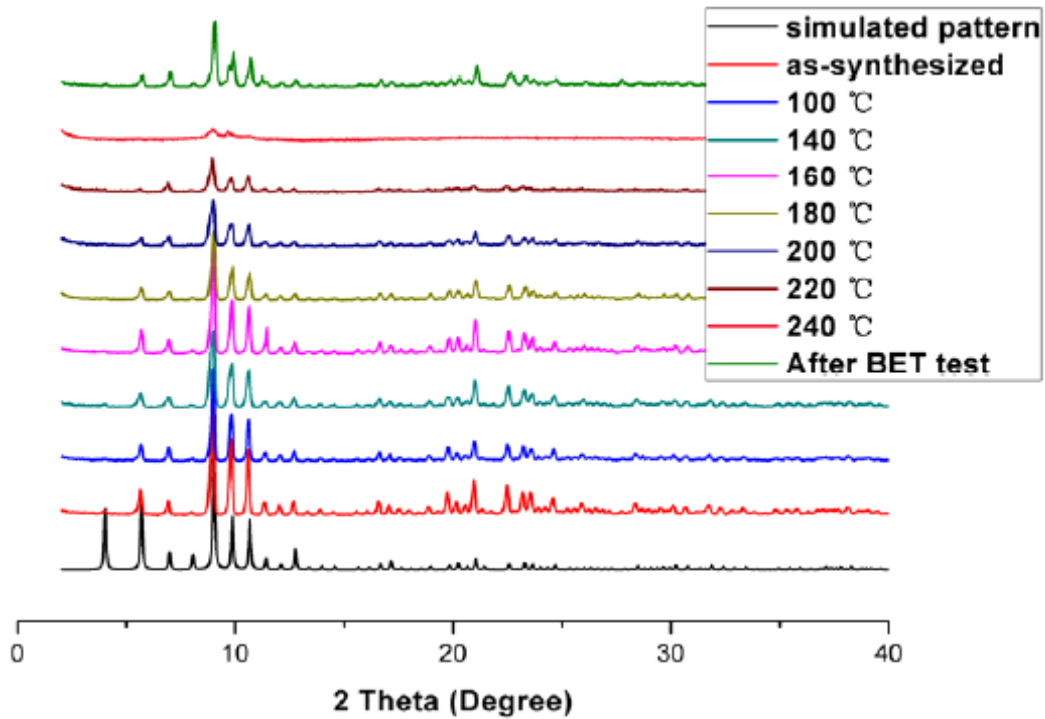
Figure 2.18 PXRD patterns of the as-synthesized sample CPM-7, CPM-7 after being heated at different temperature and CPM-7 after BET test. The simulated powder XRD pattern was obtained based on the single-crystal data.
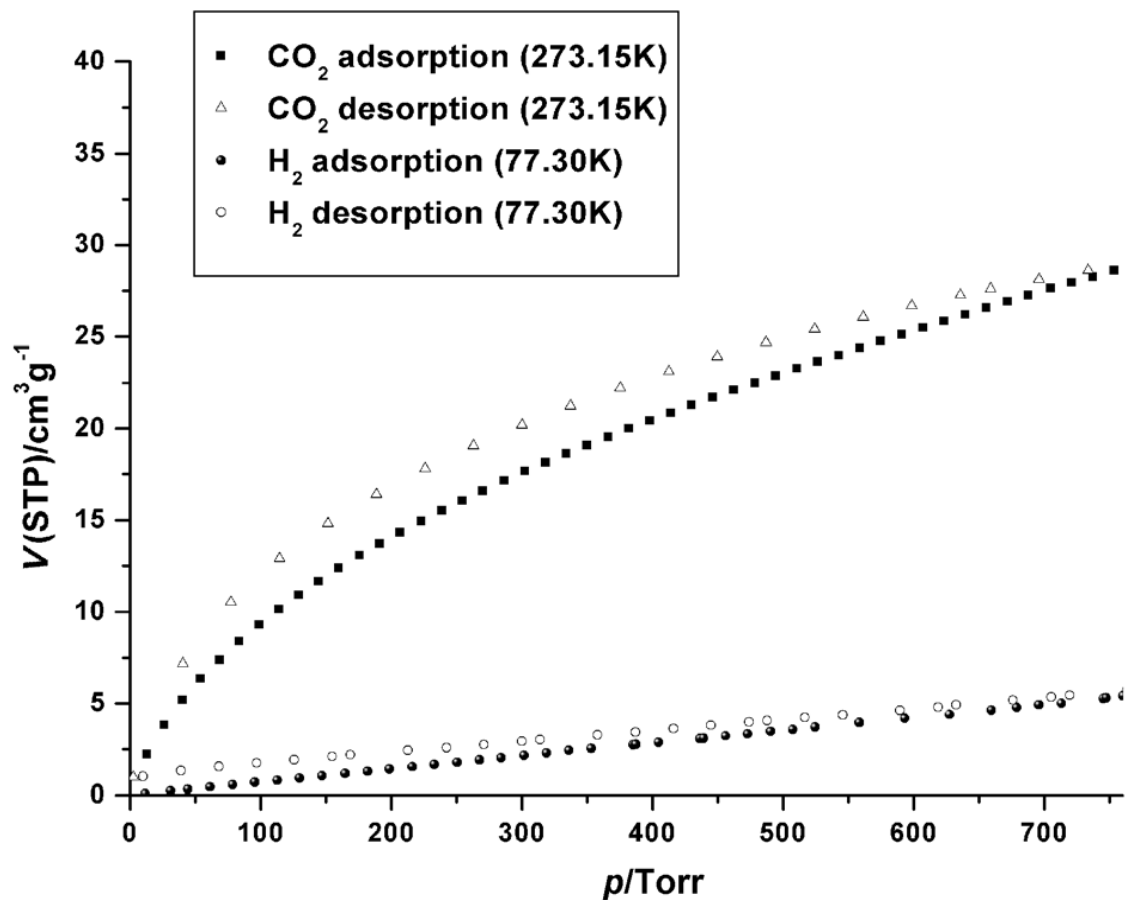
Figure 2.19 CO_2 and H_2 adsorption and desorption isotherms of CPM-7. STP = standard temperature and pressure.

2.4 Conclusion

We reported a cage-within-cage porous material that has highly unusual building blocks, such as eight connected Zn_4O tetramer, and combines multiple different building blocks (tetramer, trimer, as well as monomer). Two types of polyhedral cages are formed (sodalite cage from tetramers and cubic cage from trimers), each of which forms a different zeolite-type topology (SOD and ACO). This is the first example of two types of zeolite frameworks nested in the same material, and it also demonstrates a new mechanism for the formation of nested cage structure that is distinctly different from the previously reported mechanism based on polyfunctional ligands.[58-65] This new type of intercage linking mechanism through metal sites might be adapted for the synthesis of discrete coordination polyhedra as well, which may lead to the creation of sophisticated coordination assemblies, and perhaps a better understanding of self assembly processes in both synthetic and natural systems.

2.5 Outlook

Although CPM-7 has demonstrated the feasibility to create a highly sophisticated architecture, its adsorption ability is only moderate. The main reason may be that the bulky inner framework partially blocks the pores and occupies too much pore space of the outer cages. We propose to extend our strategy by synthesizing new frameworks, some of which will have similar structure with CPM-7, but contain larger pore size and space. This will allow us to tune and optimize properties of MOFs in adsorption and catalysis.

First of all, smaller templates will be investigated in this reaction system. In CPM-7, it's the decomposition product of DEF that serves as the template to balance the negative charge of frameworks. We can use similar molecules such as DMF, NMF (*N*-Methylformamide) and formamide as solvent or co-solvent to replace DEF in the synthesis so that the templates can occupy less pore space.

Secondly, rigid linkers will be exploited in synthesizing lengthened versions of FDA, and the synthesized ligands will be used to synthesize new versions of CPM-7 with larger pore size and space. It's worth noting that the bent angle of FDA plays an important role in the construction of CPM-7 and the new ligands formed by rigid linkers will have the same bent angle as FDA. As a result, these ligands will likely allow the construction of frameworks similar to that formed by FDA. One example of a new ligand design is illustrated in Scheme 2.2.

In addition to geometrical control through lengthening FDA, the starting FDA can be modified by 4-aminobenzonic acid to construct a new ligand. This new ligand will

introduce amide group into the final structures (Scheme 2.3) and may enhance their

ability of absorbing carbon dioxide.[66] More interestingly, amide functionalized MOFs

may have the potential to be used in the catalysis of Knoevenagel condensation reaction,

which can be catalyzed by weak base.[67] Solid frameworks with amide groups on the

surface may exhibit high catalytic activity because amide groups are located on the

surface and the formation of hydrogen bonds among amide can be avoided. This type of

new ligands based on the flexible amide linkage may have potential for constructing

many interesting frameworks, including expanded versions of CPM-7. With the amide

groups and desirable architecture, the new material may serve as highly efficient and

selective heterogeneous catalyst in the Knoevenagel condensation reaction.
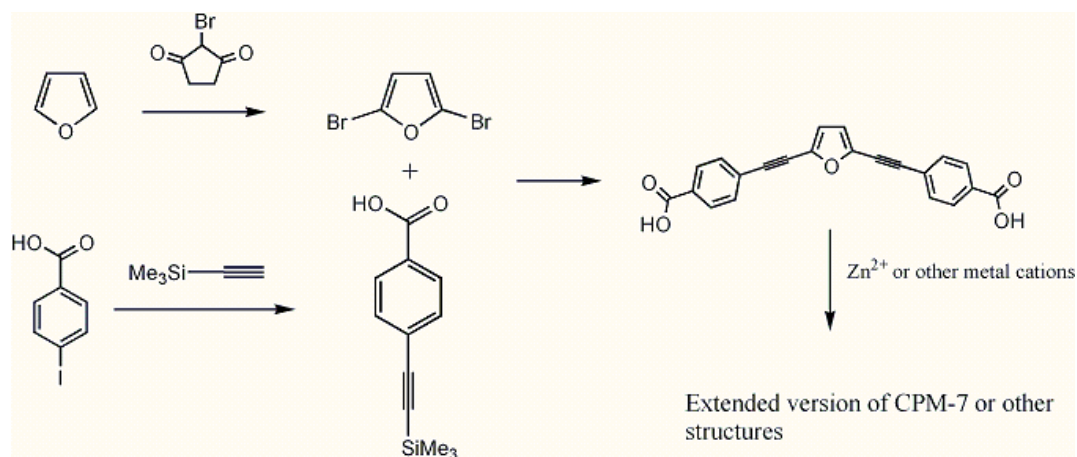
Scheme 2.2 Synthesis of expanded version of CPM-7 or other porous materials.
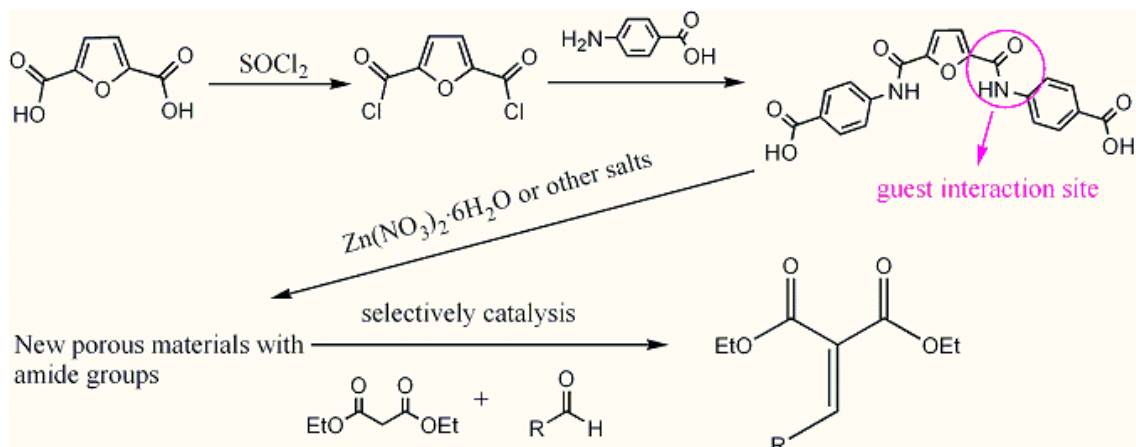
Scheme 2.3 Construction of amide functionalized porous materials for catalysis.

2.6 References

(1)   M. Eddaoudi, J. Kim, J. Wachter, H. Chae, M. O'Keeffe, O. M. Yaghi, *J. Am. Chem. Soc*. **2001**, *123*, 4368.

(2)   S. R. Seidel, P. J. Stang, *Acc. Chem. Res*. **2002**, *35*, 972.

(3)   Q. H. Yuan, L. J. Wan, H. Jude, P. J. Stang, *J. Am. Chem. Soc*. **2005**, *127*,16279.

(4)   H. Furukawa, J. Kim, N. M. Ockwig, M. O'Keeffe, O. M. Yaghi, *J. Am. Chem. Soc*. **2008**, *130*, 11650.

(5)   S. Chen, J. Zhang, T. Wu, P. Feng, X. Bu, *J. Am. Chem. Soc*. **2009**, *131*, 16027.

(6)   Z. Q. Jiang, G. Y. Jiang, F. Wang, Z. Zhao, J. Zhang, *Chem. Commun*. **2012**, *48*, 3653.

(7)   R. E. Morris, P. S. Wheatley, *Angew. Chem*. **2008**, *120*, 5044; *Angew. Chem. Int. Ed*. **2008**, *47*, 4966.

(8)   D. J. Tranchemontagne, Z. Ni, M. O'Keeffe, O. M. Yaghi, *Angew. Chem*. **2008**, *120*, 5214; *Angew. Chem. Int. Ed*. **2008**, *47*, 5136.

(9)   S. Sato,Y. Ishido, M. Fujita, *J. Am. Chem. Soc*. **2009**, *131*, 6064.

(10)   J. R. Li, R. Kuppler, H. C. Zhou, *Chem. Soc. Rev*. **2009**, *38*, 1477.

(11)   X. Zhao, T. Wu, S. T. Zheng, L. Wang, X. Bu, P. Feng, *Chem. Commun*. **2011**, *47*, 5536.

(12)   M. J. Zaworotko, *Chem. Soc. Rev*. **2009**, *38*, 1400.

(13)   M. Yoshizawa, J. K. Klosterman, M. Fujita, *Angew. Chem*. **2009**, *121*, 3470; *Angew. Chem. Int. Ed*. **2009**, *48*, 3418.

(14)   Q. C. Zhang, I. Chung, J. I. Jang, J. B. Ketterson, M. G. Kanatzidis, *J. Am. Chem. Soc*. **2009**, *131*, 9896.

(15)   L. R. MacGillivray, *Angew. Chem*. **2012**, *124*, 1136; *Angew. Chem. Int. Ed*. **2012**, *51*, 1110.

(16) H. Furukawa, K. Cordova, M. O'Keeffe, O. M. Yaghi, *Science*. **2013**, *341*, 974.

(17) T. O. Salami, X. Fan, P. Y. Zavalij, S. R. J. Oliver, *Dalton. Trans*. **2006**, 1574.

(18) W. M. Chang, M. Y. Cheng, Y. C. Liao, M. C. Chang, S. L. Wang, *Chem. Mater*. **2007**, *19*, 6114.

(19) S. R. J. Oliver, *Chem. Soc. Rev*. **2009**, *38*, 1868.

(20) G. Férey, S. Christian, *Chem. Soc. Rev*. **2009**, *38*, 1380.

(21) Y. Liu, P. D. Kanhere, C. L. Wong, Y. F. Tian, Y. H. Feng, F. Boey, T. Wu, H. Y. Chen, T. J. White, Z. Chen, Q. C. Zhang, *J. Solid State Chem*. **2010**, *183*, 2644.

(22) N. L. Rosi, J. Eckert, M. Eddaoudi, D. T. Vodak, J. Kim, M. O'Keeffe, O. M. Yaghi, *Science*. **2003**, *300*, 1127.

(23) J. W. Cheng, J. Zhang, S. T. Zheng, M. B. Zhang, G. Y. Yang, *Angew. Chem*. **2006**, *118*, 79; *Angew. Chem. Int. Ed*. **2006**, *45*, 73.

(24) R. E. Morris, X. Bu, *Nat. Chem*. **2010**, *2*, 353.

(25) Q. C. Zhang, Y. Liu, X. Bu, T. Wu, P. Feng, *Angew. Chem*. **2008**, *120*, 119; *Angew. Chem. Int. Ed*. **2008**, *47*, 113.

(26) G.Férey, *Dalton. Trans*. **2009**, *23*, 4400.

(27) S. T. Zheng, J. Zhang, X. X. Li, W. H. Fang, G. Y. Yang, *J. Am. Chem. Soc*. **2010**, *132*, 15102.

(28) H. X. Zhang, F. Wang, H. Yang, Y. X. Tan, J. Zhang, X. Bu, *J. Am. Chem. Soc*. **2011**, *133*, 11884.

(29) A. P. Cote, A. I. Benin, N. W. Ockwig, M. O'Keeffe, A. J. Matzger, O. M. Yaghi, *Science*. **2005**, *310*, 1166.

(30) F. Wang, Z. S. Liu, H. Yang, Y. X. Tan, J. Zhang, *Angew. Chem*. **2011**, *123*, 470; *Angew. Chem. Int. Ed*. **2011**, *50*, 450.

(31) G. Z.Liu, S. T. Zheng, G. Y. Yang, *Angew. Chem*. **2007**, *119*, 2885; *Angew. Chem. Int. Ed*. **2007**, *46*, 2827.

(32) G. Férey, *Chem. Soc. Rev.* **2008**, *37*, 191.

(33) G. Férey, S. Christian, D. Thomas, M. Guillaume, J. Herve, L. Philip, D. W. Guy, V. Alexandre, D. Marco, J. S. Chang, *Chem. Soc. Rev.* **2011**, *40*, 550.

(34) H. Li, M. Eddaoudi, M. O'Keeffe, O. M. Yaghi, *Nature.* **1999**, *402*, 276.

(35) M. B. Zhang, J. Zhang, S. T. Zheng, G. Y. Yang, *Angew. Chem.* **2005**, *117*, 1409; *Angew. Chem. Int. Ed.* **2005**, *44*, 1385.

(36) H. He, G. J. Cao, S. T. Zheng, G. Y. Yang, *J. Am. Chem. Soc.* **2009**, *131*, 15588.

(37) J. C. Xiao, S. W. Liu, Y. Liu, L. Ji, X. W. Liu, H. Zhang, X. W. Sun, Q. C. Zhang, *Chem. Asian J.* **2012**, *7*, 561.

(38) Y. X. Tan, Y. P. He, J. Zhang, *Chem. Commun.* **2011**, *47*, 10647.

(39) F. j. Liu, T. Willhammar, L. Wang, L. F. Zhu, Q. Sun, X. J. Meng, W. Carrillo-Cabrera, X. D. Zou, F. S. Xiao, *J. Am. Chem. Soc.* **2012**, *134*, 4557.

(40) S. H. Huang, C. H. Lin, W. C. Wu, S. L. Wang, *Angew. Chem.* **2009**, *121*, 6240; *Angew. Chem. Int. Ed.* **2009**, *48*, 6124.

(41) G. Férey, *Struct. Bonding (Berlin)*, **2009**, *132*, 87.

(42) S. T. Zheng, J. Bu, Y. Li, T. Wu, F. Zuo, P. Feng, X. Bu, *J. Am. Chem. Soc.* **2010**, *132*, 17062.

(43) M. Moliner, T. Willhammar, W. Wan, J. Gonalez, F. Rey, J. Jorda, X. D. Zou, A. Corma, *J. Am. Chem. Soc.* **2012**, *134*, 6473.

(44) Y. C. Yang, S. L. Wang, *J. Am. Chem. Soc.* **2008**, *130*, 1146.

(45) S. T. Zheng, J. Zhang, G. Y. Yang, *Angew. Chem.* **2009**, *121*, 7312; *Angew. Chem. Int. Ed.* **2009**, *48*, 7176.

(46) H. H. Fei, L. U. Paw, D. L. Rogow, M. Bresler, Y. Abdollahian, S. R. J. Oliver, *Chem. Mater.* **2010**, *22*, 2027.

(47) Q. F. Sun, T. Murase, S. Sato, M. Fujita, *Angew. Chem.* **2011**, *123*, 10502; *Angew. Chem. Int. Ed.* **2011**, *50*, 10318.

(48) P. Horcajada, C. Serre, M. Vallet-Regi, M. Sebban, F. Taulellle, G. Férey, *Angew. Chem.* **2006**, *118*, 6120; *Angew. Chem. Int. Ed*. **2006**, *45*, 5974.

(49) Y. L. Lai, K. H. Lii, S. L. Wang, *J. Am. Chem. Soc*. **2007**, *129*, 5350.

(50) S. T. Zheng, J. Zhang, G. Y. Yang, *Angew. Chem.* **2008**, *120*, 3973; *Angew. Chem. Int. Ed*. **2008**, *47*, 3909.

(51) Z. Y. Guo, H. Wu, G. Srinivas, Y. M. Zhou, S. C. Xiang, Z. X. Chen, Y. T. Yang, W. Zhou, M. O'Keeffe, B. L. Chen, *Angew. Chem.* **2011**, *123*, 3236; *Angew. Chem. Int. Ed*. **2011**, *50*, 3178.

(52) R. Banerjee, A. Phan, B. Wang, C. Knobler, H. Furukawa, M. O'Keeffe, O. M. Yaghi, *Scinece*. **2008**, *319*, 939.

(53) L. H. Huang, Y. C. Lai, H. C. Lai, Y. W. Chiang, J. H. Huang, S. L. Wang, *Inorg. Chem*. **2009**, *48*, 11882.

(54) H. H. Fei, D. L. Rogow, S. R. J. Oliver, *J. Am. Chem. Soc. **2010**,* 132, 7202.

(55) S. T. Zheng, T. Wu, B. Irfanoglu, F. Zuo, P. Feng, X. Bu, *Angew. Chem.* **2011**, *123*, 8184; *Angew. Chem. Int. Ed*. **2011**, *50*, 8034.

(56) Z. E. Lin, J. Zhang, J. T. Zhao, S. T. Zheng, C. Y. Pan, G. M. Wang, G. Y. Yang, *Angew. Chem.* **2005**, *117*, 7041; *Angew. Chem. Int. Ed*. **2005**, *44*, 6881.

(57) C. Livage, P. M. Forster, N. Guillou, M. M. Tafoya, A. K. Cheetham, G. Férey, *Angew. Chem.* **2007**, *119*, 5981; *Angew. Chem. Int. Ed*. **2007**, *46*, 5877.

(58) Y. Q. Sun, J. Zhang, Y. M. Chen, G. Y. Yang, *Angew. Chem.* **2005**, *117*, 5964; *Angew. Chem. Int. Ed*. **2005**, *44*, 5814.

(59) J. W. Cheng, J. Zhang, S. T. Zheng, M. B. Zhang, G. Y. Yang, *Angew. Chem.* **2007**, *119*, 2885; *Angew. Chem. Int. Ed*. **2007**, *46*, 2827.

(60) A. C. McKinlay, R. E. Morris, P. Horcajada, G. Férey, R. Gref, P. Couvreur, C. Serre, *Angew. Chem.* **2010**, *122*, 6400; *Angew. Chem. Int. Ed*. **2010**, *49*, 6260.

(61) H. H. Fei, S. R. J. Oliver, *Angew. Chem.* **2011**, *123*, 9232; *Angew. Chem. Int. Ed*. **2011**, *50*, 9066.

(62)   Y. Liu, M. J. W. Tan, F. X. Wei, Y. F. Tian, T. Wu, C. Kloc, F. W. Huo, Q.
         Y. Yan, H. H. Hng, J. Ma, Q. C. Zhang, *CrystEngComm*. **2012**, *14*, 75.

(63)   B. Wang, A. P. Cote, H. Furukawa, M. O'Keeffe, O. M. Yaghi, *Nature*.
         2008, *453*, 207.

(64)   P. C. Jhang, N. T. Chuang, S. L. Wang, *Angew. Chem.* **2010**, *122*, 4296;
         Angew. Chem. Int. Ed. **2010**, *49*, 4200.

(65)   Y. Han, D. L. Zhang, L. L. Chng, J. L. Sun, L. Zhao, X. D. Zou, J. Y. Ying,
         Nat. Chem. **2009**, *1*, 123.

(66)   B. Arstad, H. Fjellvag, K. O. Kongshaug, O. Swang, R. Blom, *Adsorption*.
         2008, *14*, 755.

(67)   S. Hasegawa, S. Horike, R. Matsuda, S. Furukawa, K. Mochizuki, Y.
         Kinoshita, S. Kitagawa, *J. Am. Chem. Soc*. **2007**, *129*, 2607.

Chapter 3

Charge-Tunable Indium-Organic Frameworks Built from Cationic, Anionic, and Neutral Building Blocks

3.1 Introduction

Metal-organic frameworks (MOFs) have attracted widespread interest over the past three decades because of their potential applications in gas storage and separation, catalysis, drug delivery, ion exchange etc.[1-29] Such broad range of potential applications stem from the structural diversity of these crystalline materials which can be tuned by varying metal nodes, organic linkers, and reaction conditions. For example, by using Zn^{2+} and 5-sulfoisophthalic acid (5-sipH$_3$) and 4,4'-bipyridine (bpy) or 1,2-di(4-pyridyl)ethyrene (bpe), S. Kitagawa et al synthesized three MOFs in which -SO$_3$ (protonated or non-protonated) groups are non-coordinated (these frameworks were called PCP, porous coordination polymers, which is another name of MOFs). These -SO$_3$ groups are positioned on the channel surface of MOFs and uniformly aligned inside the channel. Thus they can form hydrogen bonds with guest molecules such as water or ammonium ion. This will facilitate the transfer of the protons as the protons can hop via hydrogen bonds. And the open channels of MOFs also provide excellent environment for the transfer of the protons. Thus the synthesized MOFs showed high proton conductivity (Figure 3.1).[30]

Recently, MOFs have also been shown as promising candidates for proton conduction, which has inspired efforts in developing MOFs that can be used to produce proton conductive films. Some MOFs have achieved proton conductivity comparable to the proton conductivity of Nafion.[31-38]

We are particularly interested in In-MOFs, because in addition to being capable of typical octahedral coordination of 3d transition metal ions which allows indium to adopt various structural patterns such as $[In_3O(COO)_6]^+$ trimers, indium can also exhibit pseudotetrahedral 8-coordinate and 4-connected monomeric $[In(COO)_4]^-$ form which allow access to even greater variety of materials types.[39, 40] For example, the integration of monomeric and trimeric indium building blocks led to an unusual cage-within-cage architecture (Figure 2.4).[39, 40]

It is worth noting that different types of inorganic building blocks from the same metal ion such as In^{3+} often have different metal/COO- ratio. For example, $[In_3O(COO)_6]^+$ trimer and $[In(COO)_4]^-$ monomer have an In^{3+}/COO^- ratio of 3/6 and 1/4, respectively. As such, different inorganic building blocks can not only lead to different structures and framework topologies, but also affect the charge of the building blocks and the overall framework charge. Thus the synthetic control of the metal/COO$^-$ ratio can provide a way in the design of MOF building units and associated frameworks with different charge.

In this work, by using the same ditopic ligand (2, 5-furandicarboxylic acid) and varying synthetic conditions, we are able to access three very different building blocks of indium, trimer, monomer, and chain, respectively. More interestingly, these different

structural building blocks carry different charges, leading to positive, negative, and neutral frameworks (Figure. 3.2), respectively (denoted Compound-**1**, Compound-**2**, and Compound-**3**). Compound-**1** and Compound-**2** with positive and negative frameworks respectively showed very good proton conductivity at room temperature and 99.5% relative humidity (RH). Compound-**3** with the neutral framework has much lower conductivity under comparable measurement conditions.
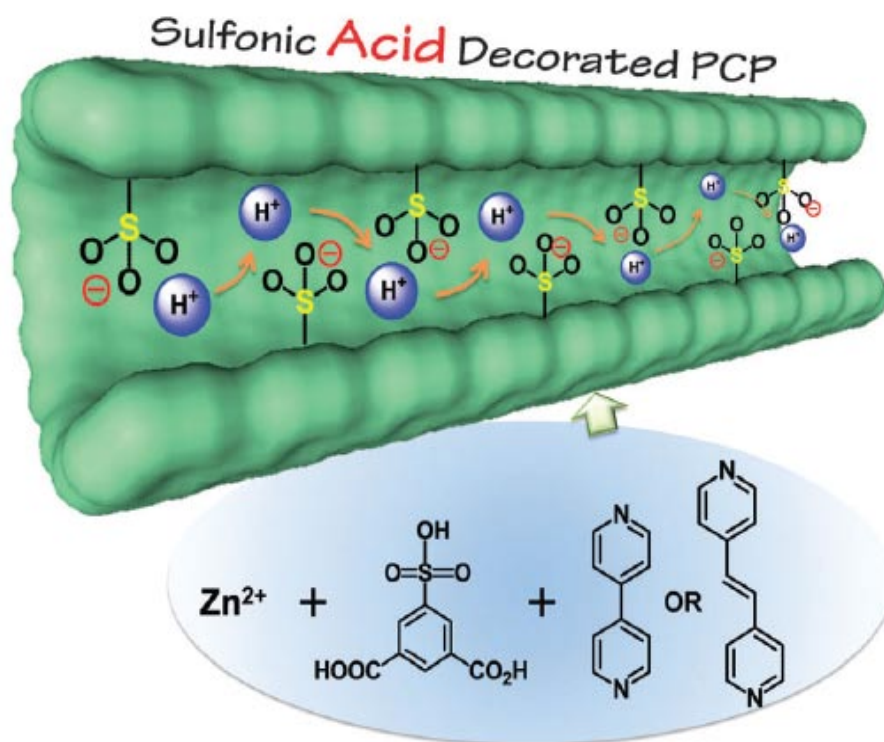
Figure 3.1 MOFs that formed by Zn^{2+} and 5-sulfoisophthalic acid (5-sipH$_3$) and 4,4'-bipyridine (bpy) or 1,2-di(4-pyridyl)ethyrene (bpe). -SO$_3$ (protonated or non-protonated) groups are not coordinated to metal ions. They are positioned on the channel surface of MOFs and uniformly aligned inside the channel. This structural feature facilitates the transfer of the protons.[30]
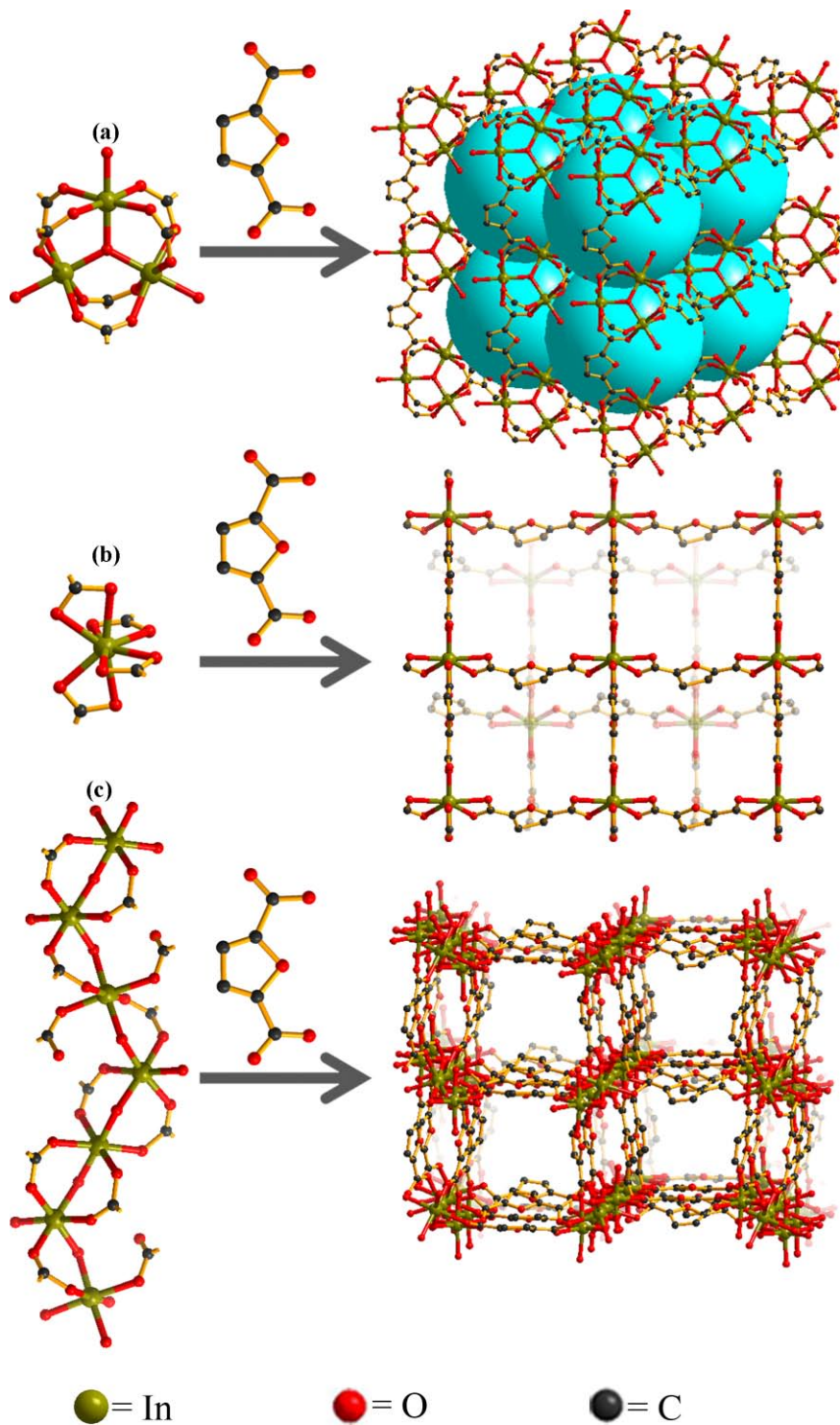
Figure 3.2 (a) Compound-**1** with 3D positive framework built of the trimers, $[In_3O(H_2O)_3(OOC^-)_6]^+$; (b) Compound-**2** with 2D negative framework built of the monomers, $[In(OOC^-)_4]^-$; (c) Compound-**3** with 3D neutral framework built of the 1D chains, $[In_2(OH)_2(H_2O)(OOC^-)_4]$.

3.2 Experimental Section

3.2.1 Synthesis of the In-Compounds

All reactants and solvents were commercially available. They were all used without further treatment.

Synthesis of Compound-1: A mixture of 2,5-furandicarboxylic acid (0.03 g), $In(NO_3)_3 \cdot xH_2O$ (0.0 3g), 2-(2-aminoethylamino)ethanol (0.01 g), concentrated nitric acid (0.02 g), dimethylacetamide (1.02 g) and methanol (4.10 g) were stirred in a 23 ml vial for 25 minutes and then heated at 120 °C for 3 days. After cooled to room temperature and washed by methanol, brown crystals were obtained.

Synthesis of Compound-2: A mixture of 2,5-furandicarboxylic acid (0.03 g), $In(NO_3)_3 \cdot xH_2O$ (0.015 g), 2-(2-aminoethylamino)ethanol (0.01 g), concentrated nitric acid (0.02 g), dimethylacetamide (4.01 g) and methanol (1.02 g) were stirred in a 23 ml vial for 25 minutes and then heated at 120 °C for 3 days. After cooled to room temperature and washed by methanol, brown crystals were obtained.

Synthesis of Compound-3: A mixture of 2,5-furandicarboxylic acid (0.015 g), $In(NO_3)_3 \cdot xH_2O$ (0.03 g), 3-amino-5-mercapto-1,2,4-triazole (0.012 g), tetramethylurea (1.08 g) and water (4.01 g) were stirred in a 23 ml vial for 25 minutes and then heated at 80 °C for 3 days. After cooled to room temperature and washed by water, clear crystals were obtained.

3.2.2 Thermal Analysis

The thermogravimetric analysis (TGA) was performed on a TA Instruments TGA Q500 apparatus. All the experiments were performed in the temperature range of 20 $^{\circ}$C to 800 °C under N_2 flow at a heating rate of 5 $^{\circ}$C/min.

3.2.3 Gas Adsorption Measurement

The measurements were performed on a Micromeritics ASAP 2020 surface-area and pore-size analyzer.

The as-synthesized samples were activated by immersing crystals in CH_2Cl_2 solution for 3 days. Then the samples were degassed at 80 °C for 24 hours prior to measurements. The adsorption data of CO_2 and C_2H_2 at 273.15 K in Compound-**1** and Compound-**3** were collected.

3.2.4 Single Crystal X-ray Diffraction

Single-crystal X-ray analysis was performed on a Bruker Smart APEX II CCD area diffractometer with N_2-flow temperature controller using graphite-monochromated MoKα radiation. The SADABS program was used for absorption correction. The structure was solved by direct methods and the structure refinements were based on $|F^2|$. All non-hydrogen atoms were refined with anisotropic displacement parameters. All crystallographic calculations were conducted with the SHELXTL software and final full-matrix refinements were against F^2.

Crystal data and Structure Refinements for these compounds can be found in table 3.1.

CCDC 1045859-104586 contain the supplementary crystallographic data for this crystal. These data can be obtained free of charge from The Cambridge Crystallographic Data Centre via www.ccdc.cam.ac.uk/data_request/cif.

3.2.5 Powder X-ray Diffraction

The experiments were performed on a Bruker D8 Advance X-ray powder diffractometer operating at 40 kV and 40 mA (CuKα radiation, $\lambda = 1.5418$ Å). All the tests were performed with a step size of 0.03° and counting time of 1s per step. The range of 2-theta is from 5° to 40°.

The simulated powder XRD patterns were obtained based on the single-crystal data.

3.2.6 Conductivity Measurements

The proton conductivity measurements were carried out for not only the single crystal samples but also the compacted powder samples.

Single crystal sample of Compound-**2** (S = 4.57×10^{-5} cm^2, L = 0.0099 cm) was selected to measure the proton conductivity at 22.5 °C and 99.5% RH (Relative Humidity), 84.5% RH and 75.5% RH.

Pellet sample Compound-**1** (S = 1.327 cm^2, L = 0.097 cm) was selected to measure the proton conductivity at various temperatures and 99.5% RH condition.

Another pellet sample Compound-**1** (S = 1.327 cm^2, L = 0.050 cm) was selected to measure the proton conductivity at 22.5 °C and various RH conditions.

Pellet sample Compound-**2** (S = 1.327 cm^2, L = 0.114 cm) was selected to measure the proton conductivity at 22.5 °C, and 99.5% RH and 84.5% RH.

63

Another pellet sample Compound-**3** (S = 1.327 cm^2, L = 0.120 cm) was selected to measure the proton conductivity at 22.5 °C and 99.5% RH.

The compacted powder samples for conductivity measurements were prepared by pressing the single crystal samples into pellets at 50 Mpa (S = 1.327 cm^2). The pellets were sandwiched between two blocking stainless-steel electrodes and fixed with a clamp for measurements.

AC impedance spectroscopy measurements were performed by using a Solartron 1260 impedance/gain-phase analyzer connected to a Solartron1287 electrochemistry interface. Zplot 2.6b was used as the control software and ZView 2.6b was used as the analysis software. A typical measurement was made over a frequency range between 3 MHz to 0.1 Hz and a 100 mV (peak voltage) was applied as AC signals. Variable impedance spectra were collected over different humidity and temperatures obtained by saturated salt solutions and the water bath.

Ionic conductivity (S/cm) was calculated using the formula $\sigma = L/SR$, where L is the pellet thickness and S is the pellet area in contact with the stainless-steel electrodes. R is the complex impedance obtained from Nyquist plot.

Table 3.1 Crystal data and structure refinements for the In-MOFs in this study.

Compound reference	Compound-**1**	Compound-**2**	Compound-**3**
Chemical formula	$C_{18}H_{12}In_3O_{19} \cdot (NO_3)$	$C_{12}H_4InO_{10} \cdot (C_2H_8N)$	$C_{12}H_8In_2O_{13}$
Formula Mass	938.70	469.70	589.79
Crystal system	Rhombohedral	Tetragonal	Monoclinic
$a/$ Å	13.9508(19)	9.7460(4)	10.7435(6)
$b/$ Å	13.9508(19)	9.7460(4)	21.4819(12)
$c/$ Å	22.402(7)	31.081(2)	10.7721(7)
$\alpha/°$	90.00	90.00	90.00
$\beta/°$	90.00	90.00	105.1130(10)
$\gamma/°$	120.00	90.00	90.00
Unit cell volume/ Å^3	3775.9(14)	2952.2(3)	2400.1(2)
Temperature/K	195(2)	195(2)	195(2)
Space group	*R*32	*I*4(1)*/amd*	*P*2(1)*/m*
No. of formula units per unit cell, *Z*	3	4	4
No. of reflections measured	7331	6628	8139
No. of independent reflections	1277	725	4274
R_{int}	0.0502	0.0276	0.0252
Final R_1 values ($I > 2\sigma(I)$)	0.0571	0.0445	0.0279
Final $wR(F^2)$ values ($I > 2\sigma(I)$)	0.1850	0.1263	0.0774
Final R_1 values (all data)	0.0579	0.0461	0.0376
Final $wR(F^2)$ values (all data)	0.1863	0.1285	0.0804
Goodness of fit on F^2	1.035	1.040	1.036

$R_1 = \sum ||F_o| - |F_c||/\sum|F_o|$, $wR = \{\sum w[(F_o)^2 - (F_c)^2]^2/\sum w[(F_o)^2]^2\}^{1/2}$.

3.3 Results and Discussion

3.3.1 Structure Description

Compounds **1**-**3** were synthesized by the reactions of indium nitrate hydrate and FDA. The use of different additives or solvents helps promote crystallization of the final frameworks.

Compound-**1**, $[In_3O(FDA)_3(H_2O)_3]\cdot[NO_3]$, crystallizes in rhombohedral space group $R32$. The framework is constructed from indium trimers, in which three indium cations are bonded to a central O^{2-}, and each pair of indium sites are bridged by four oxygens from two carboxylate groups. There is a water molecule bonded to each indium site (Figure 3.2a). As a result, the charges of trimer and framework are both positive and balanced by NO_3^-. Each trimer serves as a 6-connected node, leading to the formation of a 3D pcu network (Figures 3.2a, Figure 3.3).

Under similar synthetic condition to Compound-**1**, but with the amount of indium salt reduced by half, Compound-**2**, $[NH_2(CH_3)_2]\cdot[In(FDA)_2]$, was obtained. It is worth noting that compared to Compound-**1** with the In^{3+}/FDA ratio of 1, the In^{3+}/FDA ratio in Compound-**2** is 1/2 which seems to be correlated with the change in the synthetic conditions (i.e., In^{3+}/FDA ratio in the starting mixture, synthetic details in **3.2.1**). Compound-**2** crystallizes in tetragonal space group $I4_1/amd$. It is of particular interest to note the transition of inorganic building blocks from 6-connected In^{3+} trimer in compound-**1** to 4-connected In^{3+} monomer in compound-**2** as the synthetic conditions were varied. Compound-**2** has a 4-connected 2D square net (Figure 3.2b, Figure 3.4). Since the monomer is constructed by one indium cation and four carboxylates, the charge

of the framework is negative and is balanced by the decomposition product of dimethylacetamide (DMA), $NH_2(CH_3)_2^+$. The decomposition of amide solvents in In-MOF synthesis is commonly observed.[14]

Compound-**3**, $In_2(\mu_2\text{-}OH)_2(FDA)_2(H_2O)$, was synthesized with the addition of tetramethylurea following a procedure previously described as urothermal synthesis.[41]It crystallizes in monoclinic space group $P2_1/m$. The 3D framework is built by infinite chains cross linked by FDA. The chains are formed from octahedrally coordinated indiums (Figures 3.2c, Figure 3.5).
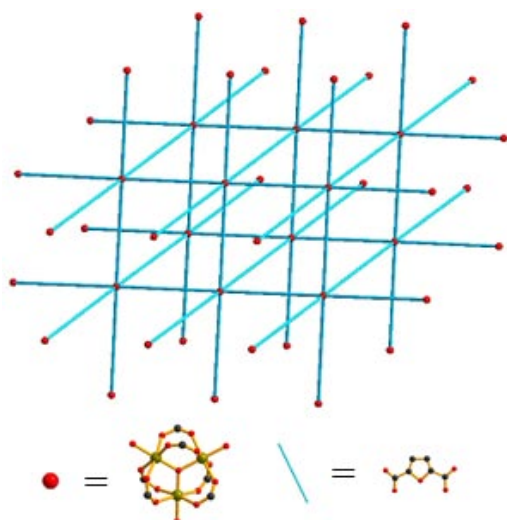
Figure 3.3 The pcu network formed by indium trimer and FDA.
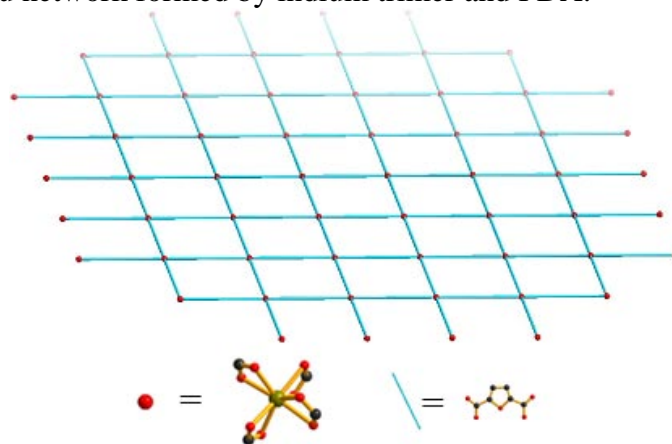
Figure 3.4 The 2D network formed by indium monomer and FDA.
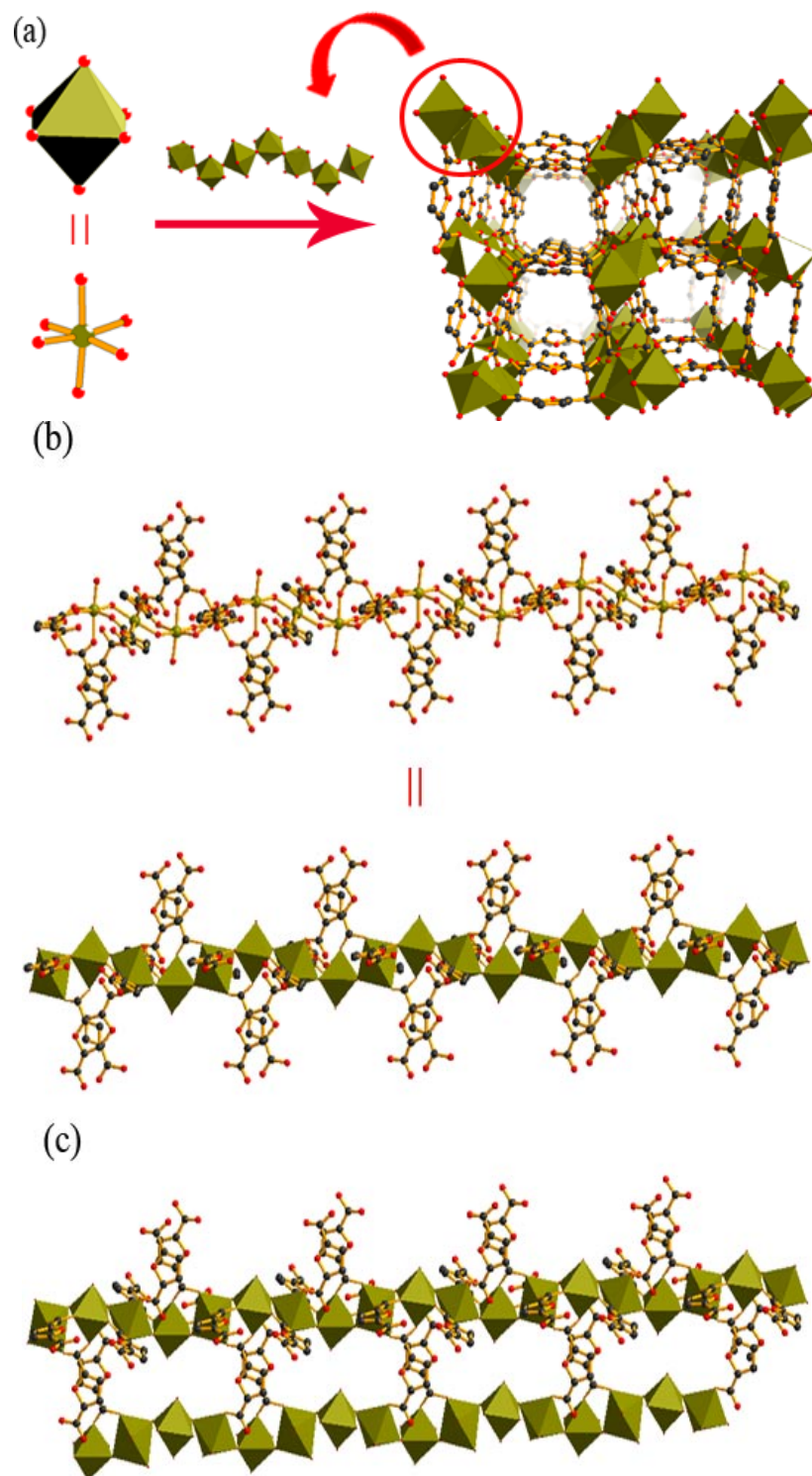
Figure 3.5 (a) 3D framework, Compound-3, formed by octahedrally coordinated indiums; (b) The chains in Compound-**3** are constructed by octahedrally coordinated indiums; (c) The connection between two chains.

3.3.2 Analysis of Properties

AC impedance analyses were performed on the pellet samples of Compound-**1**, Compound-**2**, and Compound-**3**, and single crystal sample of Compound-**2**. Both Compound-**1** and Compound-**2** displayed relatively high proton conductivities at room temperature and 99.5% relative humidity (Figure. 3.6). The proton conductivity of Compound-**1** reached 1.0×10^{-4} S cm^{-1}. We also tested the proton conductivity of Compound-**1** at various temperatures, which showed that the conductivity increased with temperature (Figure 3.7). The humidity dependence of Compound-**1** at 25 °C was also determined based on four sets of data shown in Figure 3.8.

Compound-**2** displayed a conductivity of 6.7×10^{-6} S cm^{-1} at 22.5 °C and 99.5% RH. The conductivity increased significantly to 1.0×10^{-4} S cm^{-1} at 30.5 °C and 99.5% RH (Figure 3.6b and Figure 3.6d). Single crystal conductivity measurements showed that the conductivity of Compound-**2** reached 9.5×10^{-3} S cm^{-1} at 22.5 °C and 99.5% RH (Figure 3.10).

Similar measurements on Compound-**3** showed that it has a high resistance which couldn't be reliably measured at 22.5 °C and 99.5% RH (Figure 3.6c). The significant difference between conductivity values may be related to the framework charge. However, given the significant differences in other structural features, multiple factors could contribute to the different values among these In-MOFs.
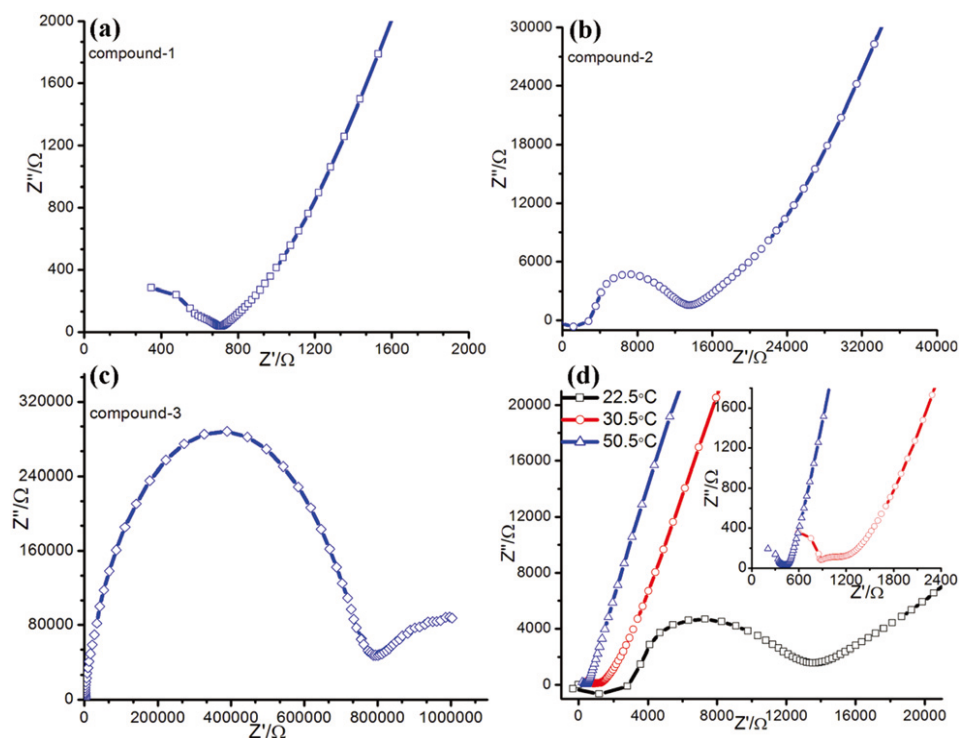
Figure 3.6 Nyquist plots of (a) the pellet sample Compound-**1** at 22.5 °C and 99.5% RH, $S = 1.327$ cm^2, $L = 0.097$ cm; (b) the pellet sample Compound-**2** at 22.5 °C and 99.5% RH, $S = 1.327$ cm^2, $L = 0.120$ cm; (c) the pellet sample Compound-**3** at 22.5 °C and 99.5% RH, $S = 1.327$ cm^2, $L = 0.051$ cm; (d) the pellet sample Compound-**2** at various temperatures and 99.5% RH (inset, enlarged for 50.5 °C and 30.5 °C).
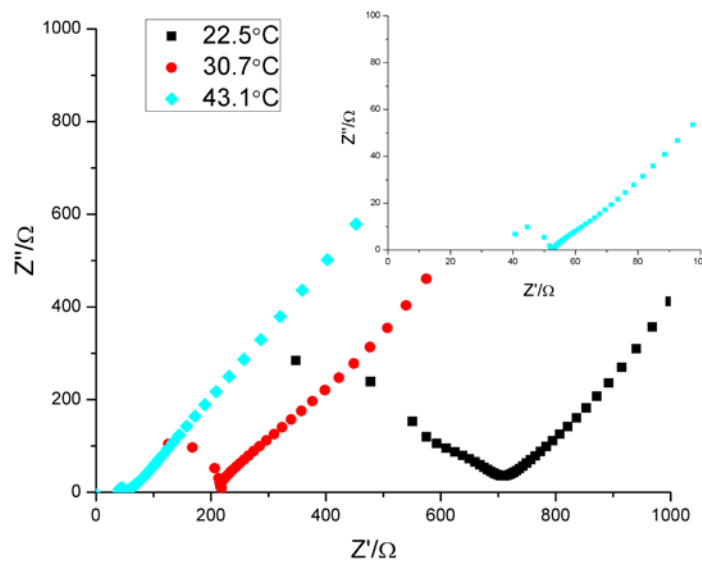
Figure 3.7 Nyquist plots of the pellet sample Compound-**1** at various temperatures and 99.5% RH condition, $S = 1.327$ cm^2, $L = 0.097$ cm. The inset shows Nyquist plot of the pellet sample Compound-**1** at 43.1 °C and 99.5% RH condition.

70
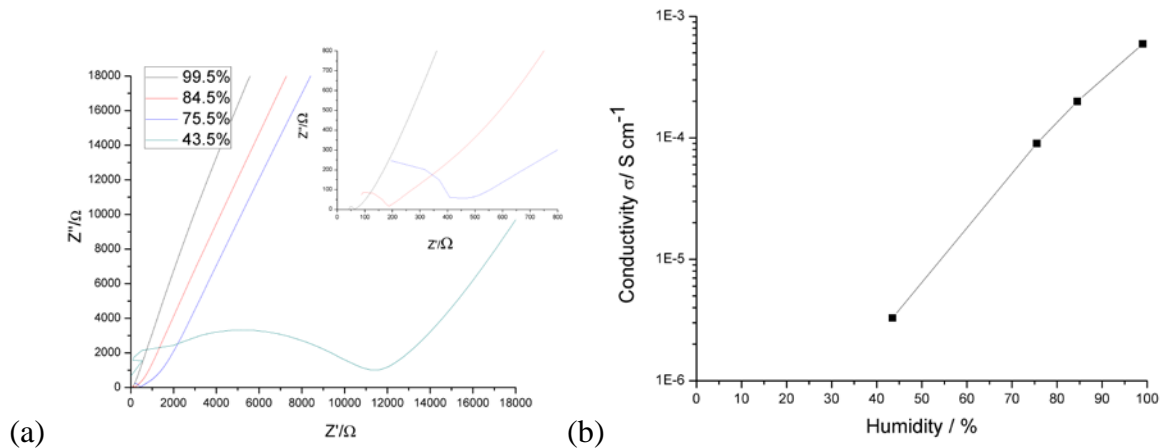
Figure 3.8 (a) Nyquist plots of the pellet sample Compound-**1** at 22.5 °C and various RH conditions, $S = 1.327$ cm^2, $L = 0.050$ cm. The inset shows Nyquist plots of Compound-**1** at 22.5 °C and 43.5% RH, 75.5% RH and 84.5% RH; (b) Humidity dependence of conductivity at 25 °C for the pellet sample Compound-**1**.
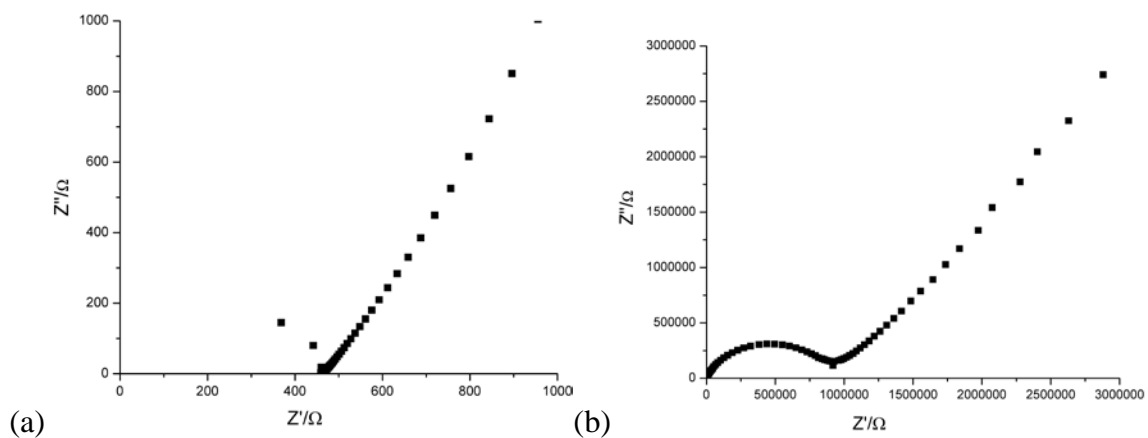
Figure 3.9 Nyquist plots of the pellet sample Compound-**2** at 22.5 °C and 99.5% RH (a) and 84.5% RH (b), $S = 1.327$ cm^2, $L = 0.114$ cm.

(a)

(b)

(c)
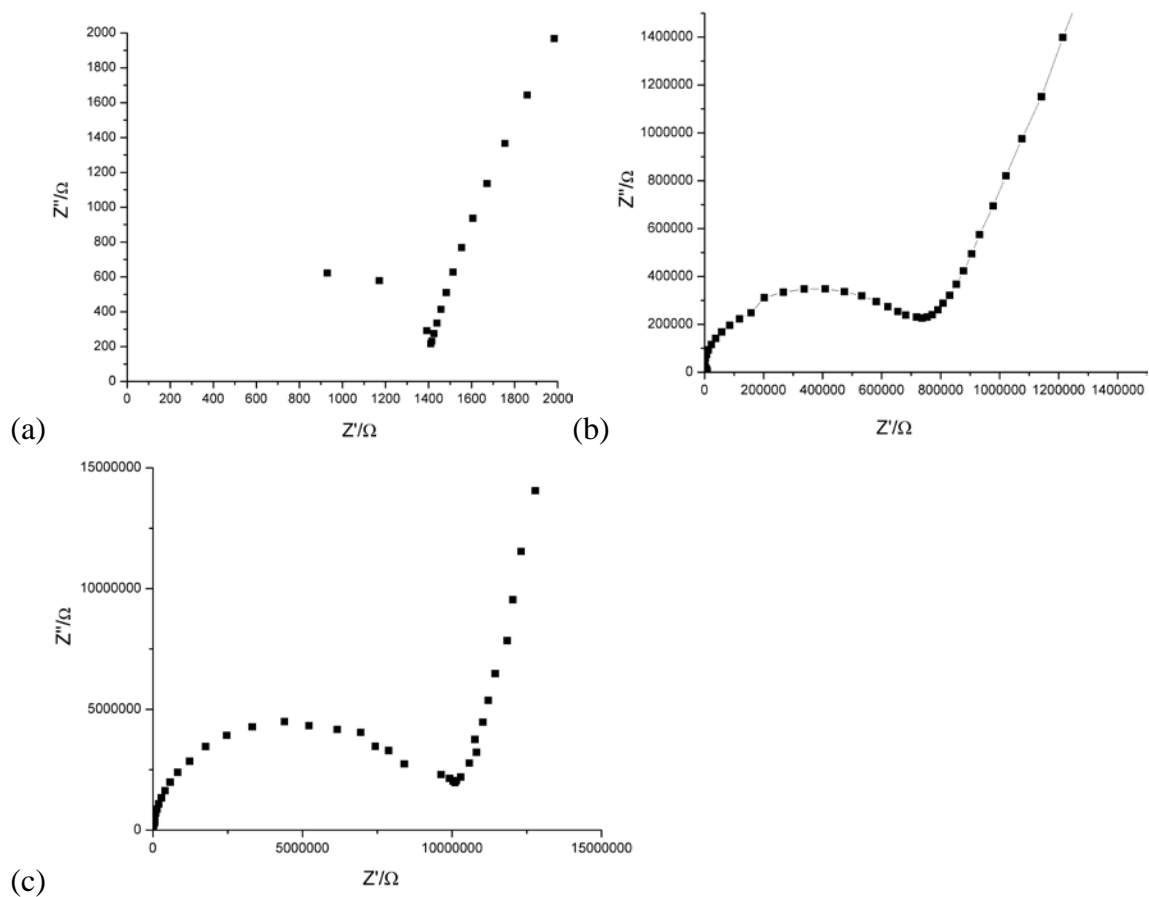
Figure 3.10 Nyquist plots of the single crystal sample Compound-**2** at 22.5 °C and 99.5% RH (a), 84.5% RH (b) and 75.5% RH (c), $S = 4.57 \times 10^{-5}$ cm^2, $L = 0.0099$ cm.

The phase purity of the samples was supported by comparing powder X-ray diffraction (PXRD) patterns of as-synthesized samples to simulated PXRD patterns (Figure 3.11a).

Thermogravimetric analysis showed that all these three frameworks can be stable until 250 °C and then the frameworks will collapse (Figure 3.11b).

The gas adsorptions of Compound-**1** and Compound-**3** were also tested. Both samples showed moderate CO_2 and C_2H_2 adsorptions at 273.15 K (Figure 3.12), but there was no adsorption for H_2 and N_2. In addition to the weaker host–guest inter actions

involving H_2 and N_2, the larger kinetic diameter of N_2 could also contribute to its lack of adsorption (N_2, 3.64-3.80 Å, CO_2, 3.3 Å, C_2H_2, 3.3 Å).[42]
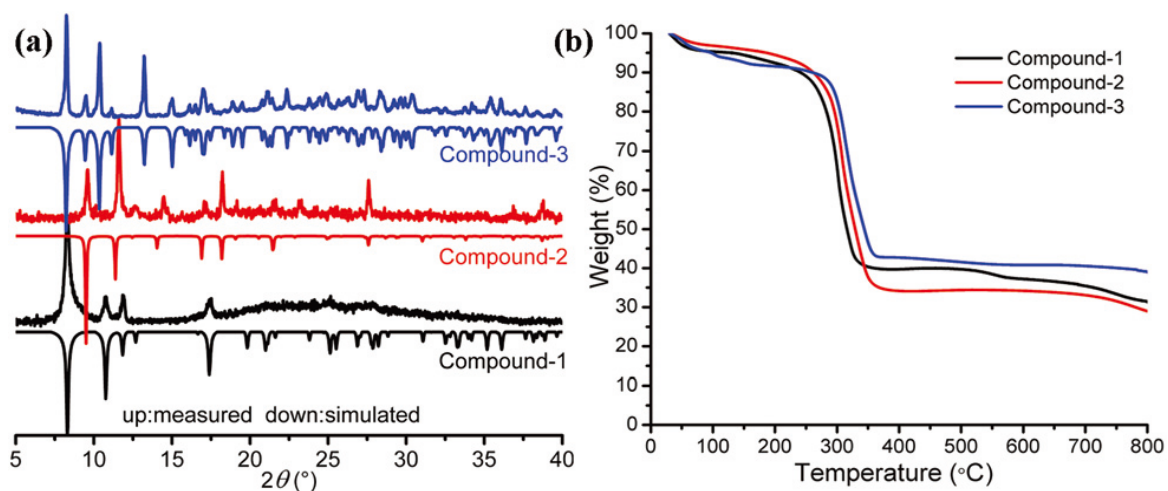
Figure 3.11 (a) Powder XRD patterns and (b) TGA curves for Compounds-**1**, -**2**, and -**3**.
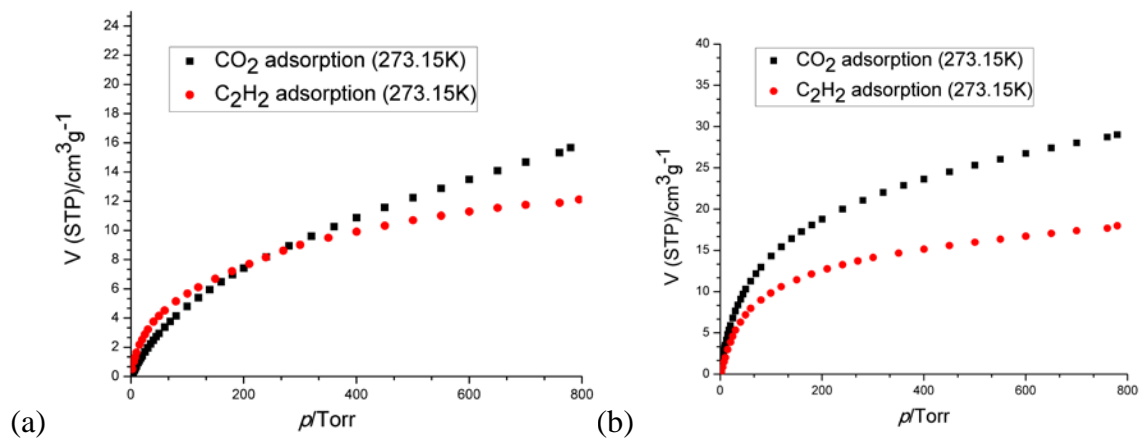
Figure 3.12 CO_2 and C_2H_2 adsorption isotherms of Compounds-**1** and -**3**.

3.4 Conclusion

This study shows that by starting from the same ditopic ligand (2,5-furandicarboxylic acid) and varying synthetic conditions, particularly the In^{3+}/FDA ratio, it is possible to access three key building blocks of indium (trimer, monomer, and chain) with variable In^{3+}/COO− ratio. Of particular interest are the different charges of these different structural building blocks which directly translate into different charges on the frameworks. While Compounds-**1** and -**2** with cationic and anionic charges show appreciable proton conductivity, Compound-3 with the neutral framework has much lower conductivity under comparable conditions.

3.5 References

(1)   M. Yoon, K. Suh, S. Natarajan and K. Kim, *Angew. Chem. Int. Ed*. **2013**, *52*, 2688813.

(2)   Rosenbaum, F. Zhao, U. Schroder and F. Scholz, *Angew. Chem. Int. Ed*. **2006**, *45*, 6658.

(3)   T. Yamada, K. Otsubo, R. Makiurac and H. Kitagawa, *Chem. Soc. Rev*. **2013**, *42*, 6655.

(4)   S. Li and Q. Xu, *Energy Environ. Sci*. **2013**, *6*, 1656.

(5)   H. Furukawa, J. Kim, N. Ockwig, M. O'Keeffe and O.M. Yaghi, *J. Am. Chem. Soc*. **2008**, *130*, 11650.

(6)   P. Li, Y. He, H. Arman, R. Krishna, H. Wang, L. Weng and B. Chen, *Chem. Commun*. **2014**, *50*, 13081.

(7)   Z. Kang, M. Xue, L. Fan, L. Huang, L. Guo, G. Wei, B. Chen and S. Qiu, *Energy Environ. Sci*. **2014**, *7*, 4053.

(8)   J. Perry IV, J. Perman and M. Zaworotko, *Chem. Soc. Rev*. **2009**, *38*, 1400.

(9)   H. Furukawa, K. Cordova, M. O'Keeffe and O. M. Yaghi, *Science*. **2013**, *341*, 974.

(10)   X. Yang, M. Xie, C. Zou, Y. He, B. Chen, M. O'Keeffe and C. Wu, *J. Am. Chem. Soc*. **2012**, *134*, 10638.

(11)   F. Bu, Q. Lin, Q. Zhai, L. Wang, T. Wu, S. Zheng, X. Bu and P. Feng, *Angew. Chem. Int. Ed*. **2012**, *51*, 8538.

(12)   X. Zhao, X. Bu, T. Wu, S. Zheng, L. Wang and P. Feng, *Nat. Commun*. **2013**, *4*, 2344.

(13)   J. Gao, J. Miao, P. Li, W. Teng, L. Yang, Y. Zhao, B. Liu and Q. Zhang, *Chem. Commun*. **2014**, *50*, 3786.

(14)   J. Gao, K. Ye, L. Yang, W. Xiong, L. Ye, Y. Wang and Q. Zhang, *Inorg. Chem*. **2014**, *53*, 691.

(15)   Y. He, R. Krishna and B. Chen, *Energy Environ. Sci*. **2012**, *5*, 9107.

(16) J. Zhao, Y. Wang, W. Dong, Y. Wu, D. Li, B. Liu and Q. Zhang, *Chem. Commun.* **2014**, *50*, 3786.

(17) M. Das, Q. Guo, Y. He, J. Kim, C. Zhao, K. Hong, S. Xiang, Z. Zhang, K. Thomas, R. Krishna and B. Chen, *J. Am. Chem. Soc.* **2012**, *134*, 8703.

(18) S. Zheng, F. Zuo,T. Wu, B. Irfanoglu, C. Chou, R. Nieto, P. Feng and X. Bu, *Angew. Chem. Int. Ed.* **2011**, *50*, 1849.

(19) S. Zheng, T. Wu, C. Chou, A. Fuhr, P. Feng and X. Bu, *J. Am. Chem. Soc.* **2012**, *134*, 4517.

(20) M. Katz, Z. Brown, Y. Colon, P. Siu, K. Scheidt, R. Snurr, J. Hupp and O. Farha, *Chem. Commun.* **2013**, *49*, 9449.

(21) H. Furukawa, F. Gandara, Y. Zhang, J. Jiang, W. Queen, M. Hudson and O. Yaghi, *J. Am. Chem. Soc.* **2014**, *136*, 4369.

(22) J. Jiang, F. Gandara, Y. Zhang, K. Na, O. Yaghi and W. Klemperer, *J. Am. Chem. Soc.* **2014**, *136*, 13844.

(23) J. Park, D. Feng and H. Zhou, *J. Am. Chem. Soc.* **2015**, *137*, 1663.

(24) D. Feng, Z. Gu, Y. Chen, J. Park, Z. Wei,Y. Sun, M. Bosch, S. Yuan and H. Zhou, *J. Am. Chem. Soc.* **2014**, *136*, 17714.

(25) D. Feng, K. Wang, J. Su, T. Liu, J. Park,Z. Wei, M. Bosch, A. Yakovenko, X. Zou and H. Zhou, *Angew. Chem. Int. Ed.* **2006**, *54*, 149.

(26) X. Zhao, T. Wu, S. T. Zheng, L. Wang, X. Bu and P. Feng, *Chem. Commun.* **2011**, *47*, 5536.

(27) S. Nagarkar, S. Unni, A. Sharma, S. Kurungot and S. Ghosh, *Angew. Chem. Int. Ed.* **2014**, *53*, 2638.

(28) W. Phang, W. Lee, K. Yoo, D. Ryu, B. Kim, C. Hong and O. M. Yaghi, *Angew. Chem. Int. Ed.* **2014**, *53*, 8383.

(29) G. Xu, K. Otsubo, T. Yamada, S. Sakaida and H. Kitagawa, *J. Am. Chem. Soc.* **2013**, *135*, 7438.

(30) P. Ramaswamy, R. Matsuda, K. Kosaga, G, Akiyama, H. Jeon, S. Kitagawa, *Chem. Commun.* **2014**, *50*, 1144.

(31)   S. Kim, K. Dawson, B. Gelfand, J. Taylor and G. Shimizu, *J. Am. Chem. Soc*. **2013**, *135*, 963.

(32)   J. Taylor, K. Dawson and G. Shimizu, *J. Am. Chem. Soc*. **2013**, *135*,1193.

(33)   T. Panda, T. Kundu and R. Banerjee, *Chem. Commun*. **2012**, *48*, 5464.

(34)   S. Sen, N. Nair, T. Yamada, H. Kitagawa and P. Bharadwaj, *J. Am. Chem. Soc*. **2012**, *134*, 19432.

(35)   T. Yamada, M. Sadakiyo and H. Kitagawa, *J. Am. Chem. Soc*. **2009**, *131*, 3144.

(36)   T. Panda, T. Kundu and R. Banerjee, *Chem. Commun*. **2013**, *49*, 6197.

(37)   Y. Liu, J. Eubank, A. Cairns, J. Eckert, V. Kravtsov, R. Luebke and M. Eddaoudi, *Angew. Chem. Int. Ed*. **2007**, *46*, 3278.

(38)   Q. Zhai, C. Mao, X. Zhao, Q. Lin, F. Bu, X. Chen, X. Bu and P. Feng, *Angew. Chem. Int. Ed*. **2015**, *54*, 7886.

(39)   S. Zheng, J. T. Bu, Y. Li, T. Wu, F. Zuo, P. Feng and X. Bu, *J. Am. Chem. Soc*. **2010**, *132*, 17062.

(40)   S. Chen, J. Zhang, T. Wu, P. Feng and X. Bu, *J. Am. Chem. Soc*. **2009**, 131, 16027.

(41)   J. Zhang, J. Bu, S. Chen, T. Wu, S. Zheng, Y. Chen, R. Nieto, P. Feng and X. Bu, *Angew. Chem. Int. Ed*. **2010**, *49*, 8876.

(42)   J. R. Li, R. J. Kuppler and H.C. Zhou, *Chem. Soc. Rev*. **2009**, *38*, 147.

Chapter 4

Development of New Zirconium Organic Frameworks and Their Properties as Precursors for Oxygen Reduction Reaction

4.1 Introduction

Zirconium Organic Frameworks have been intensively investigated since Zr-based metal organic framework (MOF) Uio-66 was reported.[1] This kind of MOFs is attractive because of their outstanding thermal and chemical stabilities. Uio-66 was synthesized by the reaction of Zr ions and 1,4-benzene-dicarboxylates (BDC). As it is shown in Figure 4.1, this MOF has only one secondary building unit (SBU), $[Zr_6(\mu_3\text{-}O)_4(\mu_3\text{-}OH)_4(O_2C)_{12}]$. In this building unit, six Zr cations are bonded by μ_3-O and μ_3-OH groups to form a core. And every two Zr cations are bridged by one carboxylate from BDC. Therefore, each SBU is 12 connected and contribute to the formation of 3D framework. Thermogravimetric analysis showed the weakest point of the structure is the bond between benzene ring and the carboxylate, not the bond between Zr ion and carboxylate group.[1] The excellent stability of Uio-66 motivates people to use different ligands, especially ligands with carboxylates, to develop new Zr-MOFs.[2-11]

Metalloporphyrins are widely used as light harvesters, oxygen carriers, and biocatalysts. Recently, they are also used in the synthesis of MOFs for the applications in gas adsorption, heterogeneous catalysis, light harvest and selective sorption in liquid or gas.[12-19] So far, some MOFs which have exceptional stability, high surface area, excellent

catalytic properties have been developed by using metalloporphyrins and different metals. Among them, zirconium-(metallo)porphyrin frameworks (ZPFs) are of great interest because these materials are expected to have good stability and excellent catalytic properties.[20-22]

MOFs with good stability are believed to be excellent precursors for the development of catalysts for oxygen reduction reaction (ORR), because they are expected to retain their porous structures after being carbonized. Pt is frequently used as electrochemical catalyst for ORR. But scientists are always trying to develop and find noble-metal free catalysts.[23-27] It has been found that noble-metal free catalysts that are prepared from zeolitic imidazolate frameworks (ZIFs) possess good catalytic properties.[28-33] For example, by using cobalt-containing benzimidazolate MOF (termed as Co-ZIF-9) as co-catalyst, Xinchen Wang et al promoted the reduction of CO_2 to CO with light (Figure 4.2).[34] Compared to ZIFs, ZPFs have two advantages of being used as precursors of catalysts for ORR: 1. the ultra-stability of ZPFs makes the carbonized products be more like to retain the high surface area of the precursors; 2. while ZIFs are only made of limited metals, such as Zn and Co, ZPFs can contain many different metals with different oxidation states, thus making them contain different active sites.[35-39]

In this work, we report a series of ZPFs that are denoted as CPM-99X (CPM = crystalline porous material, X = H_2, Zn, Co, Fe). The carbonized product of Fe-containing ZPF (denoted CPM-99Fe/C) showed an excellent ORR activity comparable to the commercial catalyst 20% Pt/C in both alkaline and acidic media.
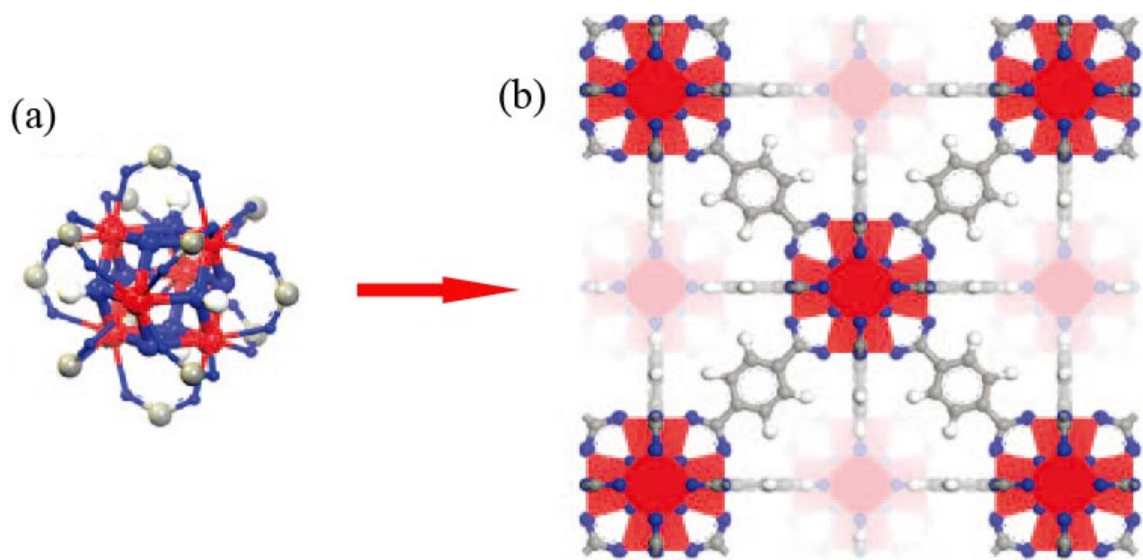
Figure 4.1 (a) SBU of Uio-66, $[Zr_6(\mu_3\text{-}O)_4(\mu_3\text{-}OH)_4(O_2C)_{12}]$; (b) Framework of Uio-66, constrcuted by Zr cations and BDC. Zr red, O blue, C grey, H, white.[1]
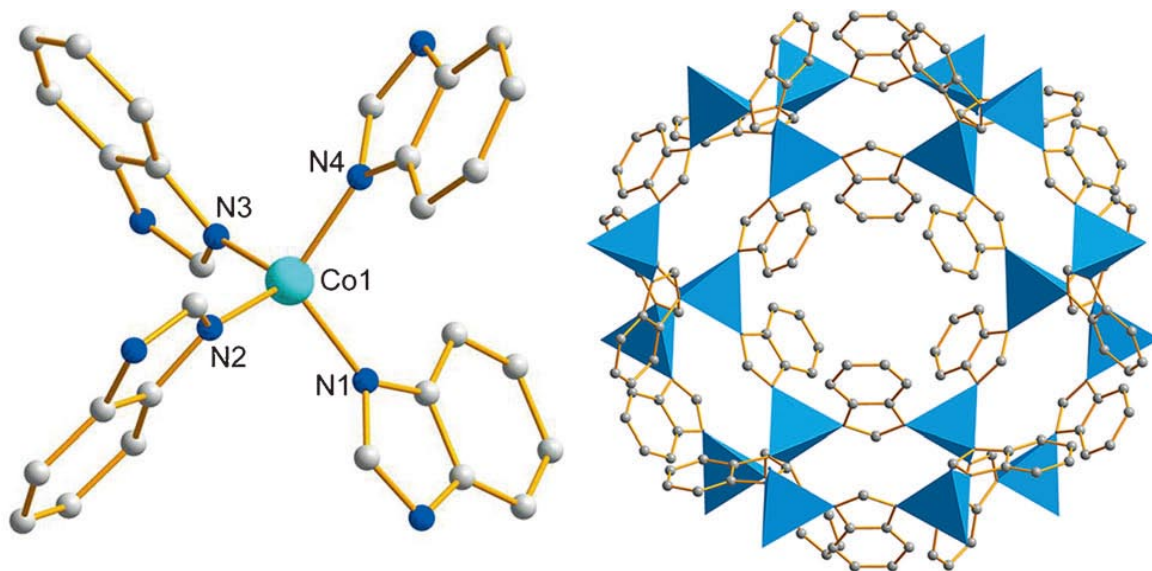
Figure 4.2 (a) Coordination environment around Co in Co-containing ZIF-9; (b) 3D framework of ZIF-9. Co light green, N blue, C grey.[34]

4.2 Experimental Section

4.2.1 Synthesis of the Ligands

All reactants and solvents were commercially available. They were all used without further purification.

4-Formylphenylboronic acid (98%, $C_7H_7BO_3$, 149.94, Oakwood), ethyl 4-iodobenzoate (98%, $C_9H_9IO_2$, 276.08, Oakwood), tetrakis(triphenylphosphine)palladium(0) (= $Pd(PPh_3)_4$, 99%, 1155.56, Sigma-Aldrich), K_2CO_3 (99%, 138.21, Alfa Aesar), pyrrole (98%, C_4H_5N, 67.09, Sigma-Aldrich), propionic acid (= PrOH, 99.5%, CH_3CH_2COOH, 74.08, Sigma-Aldrich), $Zn(OAc)_2 \cdot 2H_2O$ (219.50, Acros Organics), $Co(OAc)_2 \cdot 4H_2O$ (98%, 249.08, Sigma-Aldrich), $FeCl_2 \cdot 4H_2O$ (99%, 198.81, Sigma-Aldrich),$LiOH \cdot H_2O$ (98%, 41.96, Sigma-Aldrich), zirconium (IV) chloride (= $ZrCl_4$, 98%, 233.03, Alfa Aesar), zirconylchloride octahydrate (= $ZrOCl_2 \cdot xH_2O$, 98%, 322.25, Sigma-Aldrich), benzoic acid (= PhCOOH, 98+%, $C_7H_6O_2$, 122.12, TCI), *N,N*-diethylformamide (= DEF, 99%, $C_5H_{11}NO$, 101.15, TCI).

Synthesis of the Ligands : Tetracarboxybiphenylporphyrin (TCBPP-X, X = H_2, Zn, Co, Fe) ligands were all synthesized based on method in reference.[40-41] Typically, these ligands were synthesized by four steps. As illustrated in Scheme 4.1.
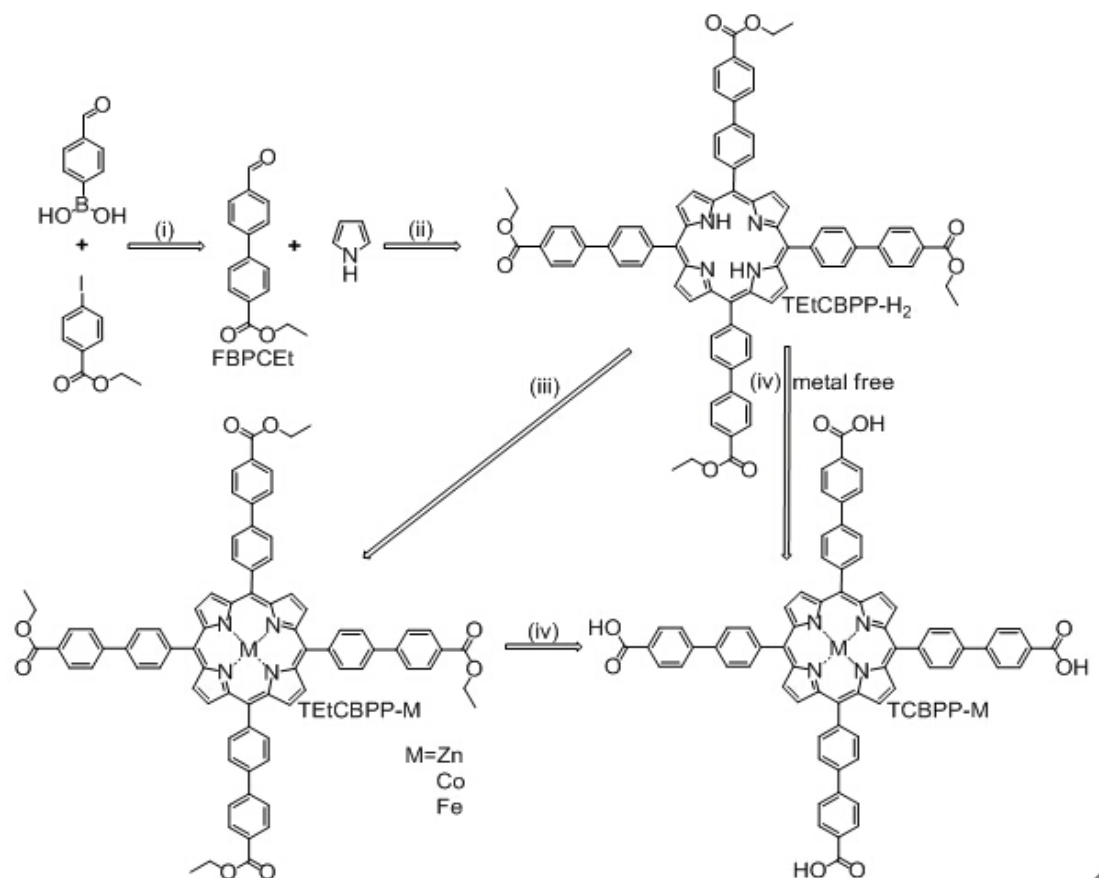
Scheme 4.1 Synthetic route for TCBPP-X (X = H$_2$, Zn, Co, Fe). Reagents and conditions: (i) Pd(PPh$_3$)$_4$, K$_2$CO$_3$, toluene/ethanol/H$_2$O, 90°C, 36 hrs; (ii) propionic acid, reflux, 3 hrs; (iii) Zn(OAc)$_2$·2H$_2$O or Co(OAc)$_2$·4H$_2$O or FeCl$_2$·4H$_2$O, DMF/MeOH/CHCl$_3$, reflux, 12 hrs; (iv) LiOH, dioxane/MeOH/CHCl$_3$, reflux, 12 hrs.

(1) 4'-Formyl-biphenyl-4-carboxylic acid ethyl ester (FBPCEt):

4-formylbenzeneboronic acid (7.5 g, 50 mmol), K$_2$CO$_3$ (13.8 g, 100 mmol), and

Pd(PPh$_3$)$_4$ (1.2 g, 1 mmol), were added degassed toluene (50 ml) and ethyl

4-iodobenzoate (14 g, 50 mmol) under Ar. The mixture was stirred at 90 °C for 36 h, and

cooled to room temperature. Then the solvent was removed under reduced pressure. H$_2$O

(100 ml) was added and extracted with dichloromethane (= CH$_2$Cl$_2$, 200 mL×2). The

collected organic layer was dried over MgSO$_4$ and the solvent was removed under reduced pressure. The crude product was chromatographed on silica (CH$_2$Cl$_2$: hexane) to yield 11.9 g (94%) of title compound. ^{1}H NMR (CDCl$_3$) δ 10.066 (s, 1H), 8.148-8.128 (d, J = 7.8 Hz, 2H), 7.783-7.763 (d, J = 7.8 Hz, 2H), 7.783-7.763 (d, J = 7.8 Hz, 2H), 7.699-7.678 (d, J = 8.0 Hz, 2H), 4.413-4.395 (q, J = 7.1 Hz, 2H), 1.412 (t, J = 7.1 Hz, 3H). MS (EI+) calcd for C$_{16}$H$_{14}$O$_3$ [M]$^+$ 254.0943. found 254.0944.

(2) 5, 10, 15, 20-Tetrakis(4-ethylcarboxybiphenyl)porphyrin (TEtCBPP-H$_2$): 4'-Formyl-biphenyl-4-carboxylic acid ethyl ester (= FBPCEt, 10.2 g, 40 mmol) was stirred in propionic acid (300 mL) and heated to reflux. Pyrrole (2.77 mL, 40 mmol) was added to refluxed FBPCEt-propionic acid solution. Then the solution was refluxed for 3 hrs in darkness. After cooled to room temperature, raw purple crystals were collected by suction-filtration. The crude product was chromatographed on silica (CHCl$_3$/hexane = 5/1) to yield 3.6 g (30%). ^{1}H NMR (CDCl$_3$) δ 8.93 (s, 8H), 8.28 (t, J = 8.7 Hz, 16H), 7.97 (d, J = 7.8 Hz, 16H), 4.49 (q, J = 7.1 Hz, 8H), 1.51 (t, J = 7.1 Hz, 12H), -2.66 (s, 2H). MS (FAB) calcd for C$_{80}$H$_{63}$N$_4$O$_8$ [M+H]$^+$ 1207.46. found 1207. FTIR: v = 3680 (m), 2990 (s), 1700 (m), 1390 (m), 1260 (s), 1070 (s), 798 (m), 746 (m) cm^{-1}. EA data: C, 78.23; H, 5.15; N, 4.55. Calculated: C, 79.58; H, 5.18; N, 4.64.

(3) 5, 10, 15, 20-Tetrakis(4-ethylcarboxybiphenyl)porphyrin-X (TEtCBPP-X): 5, 10, 15, 20-Tetrakis(4-ethylcarboxybiphenyl)porphyrin-Zn(II) (TEtCBPP-Zn). 100 mL of DMF (mixed by 30 mL of CHCl$_3$) was added to TEtCBPP-H$_2$ (1.2 g, 1.0 mmol) and Zn(OAc)·2H$_2$O (2.19 g, 10 mmol), and the mixture was heated at 120 °C for 12 hrs. After cooled down to room temperature, the chloroform was removed under reduced pressure.

Then 150 mL of H_2O was added. The obtained solid was washed three times with water and dried to give quantitative dark red crystals.

5, 10, 15, 20-Tetrakis(4-ethylcarboxybiphenyl)porphyrin-Co(II) (TEtCBPP-Co). 100 mL of DMF (mixed by 30 mL of $CHCl_3$) was added to TEtCBPP-H_2 (1.2 g, 1.0 mmol) and Co(OAc)·4H_2O (2.49 g, 10 mmol), and the mixture was heated at 120 °C for 12 hrs. After cooled down to room temperature, the chloroform was removed under reduced pressure. Then 150 mL of H_2O was introduced. The obtained solid was washed three times with water and dried to give quantitative dark red crystals.

5, 10, 15, 20-Tetrakis(4-ethylcarboxybiphenyl)porphyrin-Fe(II) (TEtCBPP-Fe). 100 mL of DMF was added to TEtCBPP-H_2 (1.2 g, 1.0 mmol) and FeCl$_2$·4H_2O (1.60 g, 8 mmol), and the mixture was heated at 120 °C for 12 hrs. After cooled down to room temperature, the chloroform was removed under reduced pressure. Then 150 mL of H_2O was introduced. The obtained solid was washed three times with water and dried to give quantitative dark red crystals.

(4) 5, 10, 15, 20-Tetrakis(4-carboxybiphenyl)porphyrin-X (TCBPP-X): 5, 10, 15,2 0-Tetrakis(4-carboxybiphenyl)porphyrin (TCBPP-H_2). The obtained ester TEtCBPP-H_2 was stirred in mixed solvent of dioxane (150 mL) and $CHCl_3$ (50 mL), to which a solution of LiOH (2.1 g, 50 mmol) in MeOH (50 mL) was introduced. The mixture was refluxed for 12 hrs. After cooled down to room temperature, dioxane, $CHCl_3$ and MeOH were evaporated. Additional water was added to the resulting residue and the mixture was heated until the solid was fully dissolved, then the solution was acidified with 1M HCl until no further precipitate was detected (pH ≈ 2). The black solid was

collected by filtration, washed with water and dried in vacuum. FTIR: $v = 3680$ (m), 2990 (s), 1700 (m), 1390 (m), 1260 (s), 1070 (s), 798 (m), 746 (m) cm^{-1}. EA data: C, 74.32; H, 4.47; N, 4.57. Calculated: C, 78.96; H, 4.23; N, 5.12. MS (FAB) calcd for $C_{72}H_{46}N_4O_8$ [M+H]$^+$ 1094.33. found 1095.

5, 10, 15, 20-Tetrakis(4-carboxybiphenyl)porphyrin-Zn(II) (TCBPP-Zn). The obtained ester TEtCBPP-Zn was stirred in mixed solvent of dioxane (150 mL) and CHCl$_3$ (50 mL), to which a solution of LiOH (2.1 g, 50 mmol) in MeOH (50 mL) was introduced. The mixture was refluxed for 12 hrs. After cooled down to room temperature, dioxane, CHCl$_3$ and MeOH were evaporated. Additional water was added to the resulting residue and the mixture was heated until the solid was fully dissolved, then the solution was acidified with 1M HCl until no further precipitate was detected (pH ≈ 3). The black solid was collected by filtration, washed with water and dried in vacuum. FTIR: $v = 2990$ (w), 1600 (s), 1170 (m), 995 (m), 769 (s), 700 (w) cm^{-1}. EA data: C, 72.10; H, 4.67; N, 5.25. Calculated: C, 74.64; H, 3.83; N, 4.84. MS (FAB) calcd for $C_{72}H_{44}N_4O_8Zn$ [M+H]$^+$ 1157.24. found 1157.

5, 10, 15, 20-Tetrakis(4-carboxybiphenyl)porphyrin-Co(II) (TCBPP-Co). The obtained ester TEtCBPP-Co was stirred in mixed solvent of dioxane (150 mL) and CHCl$_3$ (50 mL), to which a solution of LiOH (2.1 g, 50 mmol) in MeOH (50 mL) was introduced. The mixture was refluxed for 12 hrs. After cooling down to room temperature, dioxane, CHCl$_3$ and MeOH were evaporated. Additional water was added to the resulting residue and the mixture was heated until the solid was fully dissolved, then the solution was acidified with 1M HCl until no further precipitate was detected (pH ≈ 3). The black

solid was collected by filtration, washed with water and dried in vacuum. FTIR: $v = 1600$ (s), 1230 (m), 1170 (s), 769 (s), 698 (w) cm^{-1}. EA data: C, 70.14; H, 4.19; N, 4.30. Calculated: C, 75.06; H, 3.85; N, 4.86. MS (FAB) calcd for $C_{72}H_{44}N_4O_8Co$ [M+H]$^{+}$1151.25. found 1151.

5, 10, 15, 20-Tetrakis(4-carboxybiphenyl)porphyrin-Fe(II) (TCBPP-Fe). The obtained ester TEtCBPP-Fe was stirred in mixed solvent of dioxane (150 mL) and CHCl$_3$ (50 mL), to which a solution of LiOH (2.1 g, 50 mmol) in MeOH (50 mL) was introduced. The mixture was refluxed for 12 hrs. After cooled down to room temperature, dioxane, CHCl$_3$ and MeOH were evaporated. Additional water was added to the resulting residue and the mixture was heated until the solid was fully dissolved, then the solution was acidified with 1M HCl until no further precipitate was detected (pH $\approx$ 3). The black solid was collected by filtration, washed with water and dried in vacuum. FTIR: $v = 2100$ (w), 1850 (w), 1600 (s), 1230 (w), 1170 (m), 1000 (m), 769 (w) cm^{-1}. EA data: C, 69.57; H, 4.13; N, 4.53. Calculated: C, 75.26; H, 3.86; N, 4.86. MS (FAB) calcd for $C_{72}H_{44}N_4O_8Fe$ [M+H]$^{+}$ 1148.25. found 1148.

4.2.2 Characterization of the ligands

(1) 1H NMR spectrum

Solution 1H NMR spectroscopic data were recorded for samples in 5 mm tubes (outer diameter) with a Varain Inova 300 NMR spectrometer.
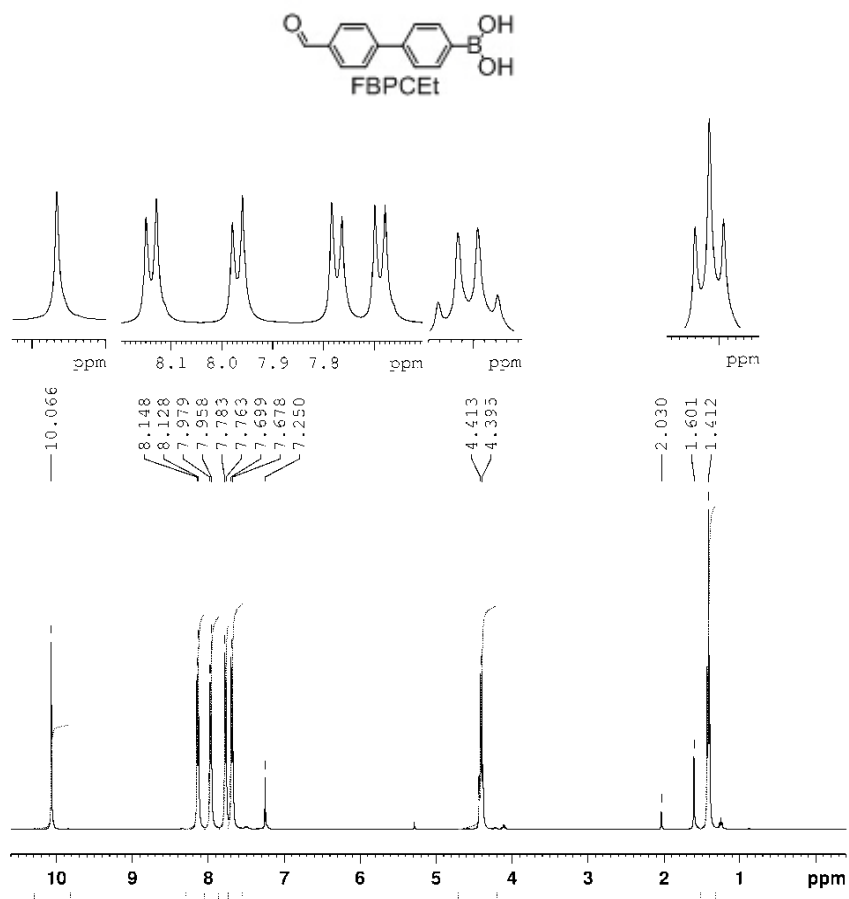
Figure 4.3 ^{1}H NMR spectrum of 4'-formyl-biphenyl-4-carboxylic acid ethyl ester (FBPCEt) in CDCl$_3$ solution.
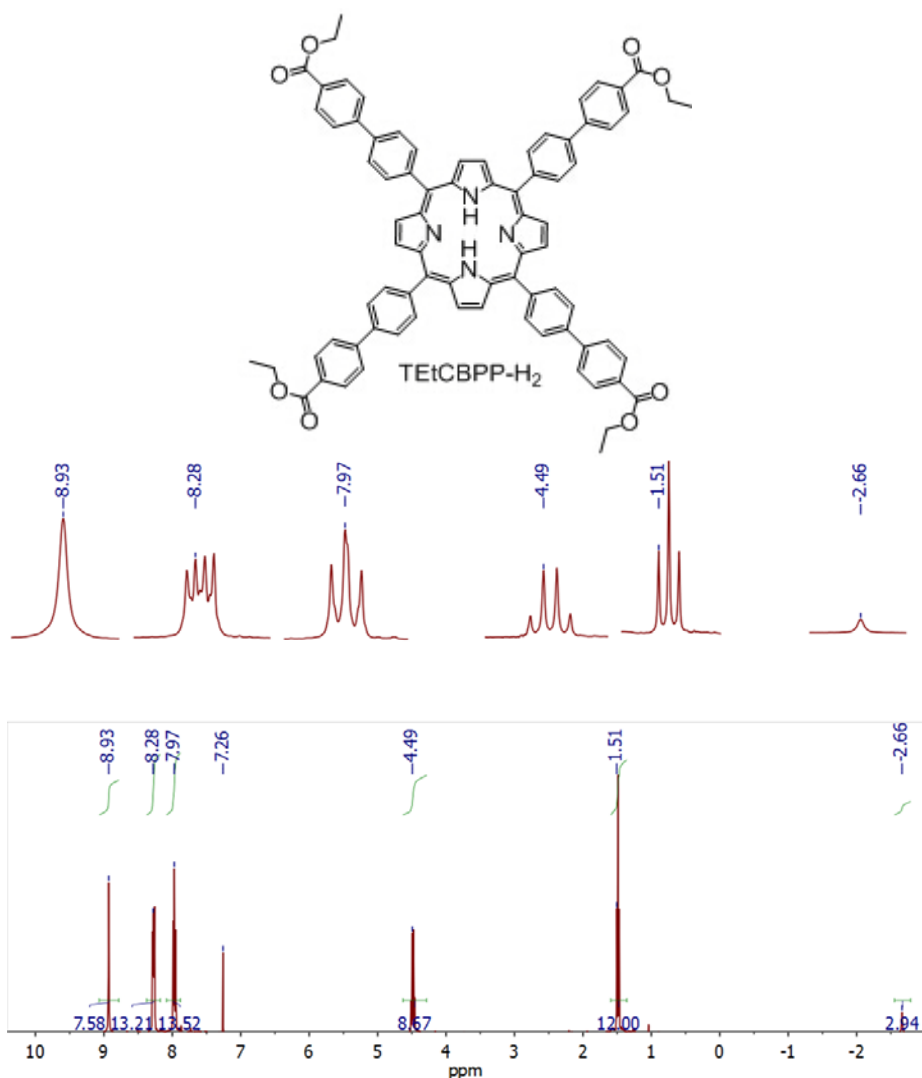
Figure 4.4 ^{1}H NMR spectrum of 5, 10, 15, 20-tetrakis(4-ethylcarboxybiphenyl)porphyrin (TEtCBPP-H$_2$) in CDCl$_3$ solution.

(2) Fourier transformed-infrared (FT-IR) spectroscopy

Fourier transformed-Infrared spectroscopy (FT-IR) was performed on a Thermo Nicolet Avatar 6700 FT-IR with cesium iodide optics allowing the instrument to observe from 525-4000 cm^{-1}.
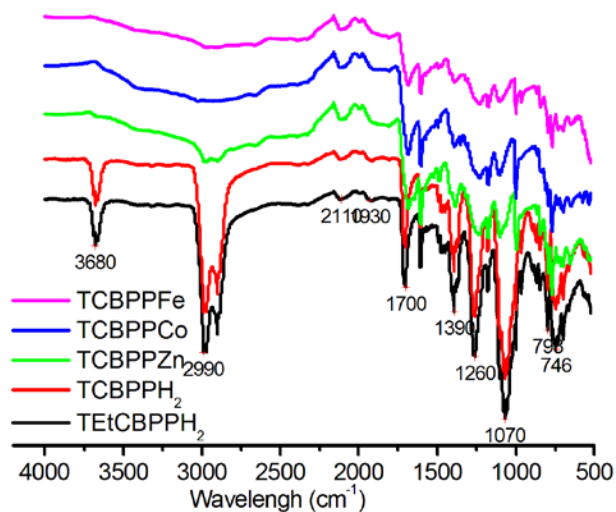
Figure 4.5 FTIR spectra of metal-free and metalizated tetracarboxybiphenylporphyrin ligands.

(3) UV-vis spectroscopy

UV-Vis (liquid absorption and solid-state diffuse reflectance) spectra were recorded on a Shimadzu UV-3101PC spectrophotometer.
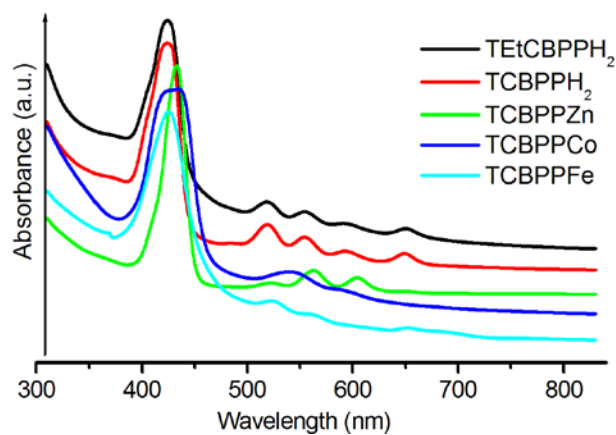
Figure 4.6 UV-vis absorbance of metal-free and metalizatedtetracarboxybiphenylporphyrin ligands in DMSO solution.

4.2.3 Synthesis of CPM-99

(1) **CPM-99(H$_2$)**: ZrOCl$_2$·xH$_2$O (0.15 g, [or 0.10 g ZrCl$_4$]), TCBPP-H$_2$ (0.15 g) and benzoic acid (7.5 g) in 75 mL of DEF were ultrasonically dissolved in a beaker, then divided into 15 glass vials of 20 mL capacity. The mixture was heated in 120 °C oven for 5 days. After cooled down to room temperature, dark cube-shaped crystals were harvested by filtration (47% yield based on TCBPP-H$_2$). FTIR: v = 2930 (w), 1600 (s), 1400 (s), 1000 (w), 717 (s) cm^{-1}. EA data: C, 55.20; H, 5.05; N, 6.25. Calculated: C, 65.43; H, 3.61; N, 4.24.

(2) **CPM-99(Zn)**: ZrOCl$_2$·xH$_2$O (0.15 g), TCBPP-Zn (0.15 g) and benzoic acid (7.5 g) in 75 mL of DEF were ultrasonically dissolved in a beaker, then divided into 15 glass vials of 20 mL capacity. The mixture was heated in 120 °C oven for 5 days. After cooled down to room temperature, dark cube-shaped crystals were harvested by filtration (48% yield based on TCBPP-Zn). FTIR: v = 1600 (s), 1400 (s), 1000 (s), 777 (w) cm^{-1}. EA data: C, 49.83; H, 3.48; N, 3.98. Calculated: C, 61.02; H, 3.22; N, 3.95.

(3) **CPM-99(Co)**: ZrOCl$_2$·xH$_2$O (0.15 g), TCBPP-Co (0.15 g) and benzoic acid (7.5 g) in 75 mL of DEF were ultrasonically dissolved in a beaker, then divided into 15 glass vials of 20 mL capacity. The mixture was heated in 120 °C oven for 5 days. After cooled down to room temperature, dark cube-shaped crystals were harvested by filtration (43% yield based on TCBPP-Co). FTIR: v = 1600 (s), 1380 (s), 1000 (w), 777 (m) cm^{-1}. EA data: C, 59.46; H, 1.67; N, 4.49. Calculated: C, 61.31; H, 3.24; N, 3.97.

(4) **CPM-99(Fe)**: ZrOCl$_2$·xH$_2$O (0.15 g), TCBPP-Fe (0.15 g) and benzoic acid (7.5 g) in 75 mL of DEF were ultrasonically dissolved in a beaker, then divided into 15

glass vials of 20 mL capacity. The mixture was heated in 120 °C oven for 5 days. After

cooled down to room temperature, dark cube-shaped crystals were harvested by filtration

(53% yield based on TCBPP-Fe). FTIR: v = 1590 (m), 1400 (s), 997 (s), 775 (m) cm^{-1}.

EA data: C, 46.15; H, 3.01; N, 4.74. Calculated: C, 60.69; H, 3.07; N, 3.93.

4.2.4 Characterization of CPM-99X

    (1) Single crystal X-ray diffraction

    Single Crystals of CPM-99X were collected on a Bruker APEX II diffractometer

equipped with a fine focus, 2.0 kW sealed tube X-ray source (MoK radiation, λ =

0.71073 Å) operating at 50 kV and 30 mA. The empirical absorption correction was

based on equivalent reflections. Structure was solved by direct methods followed by

successive difference Fourier methods. Computations were performed using SHELXTL

and final full-matrix refinements were against F^2.

    Crystal data and Structure Refinements for these compounds can be found in table

4.1. All these data is contained in CCDC 1044848-1044851, which can be obtained free

of charge from The Cambridge Crystallographic Data Centre via

www.ccdc.cam.ac.uk/data_request/cif.

Table 4.1 Crystal data and structure refinements for CPM-99 in this study.

Compound ref.	CPM-99(H_2)	CPM-99(Zn)	CPM-99(Co)	CPM-99(Fe)
Chemical formula	$C_{216}H_{142}N_{12}O_{32}Zr_6$	$C_{216}H_{136}N_{12}O_{38}Zn_3Zr_6$	$C_{216}H_{136}N_{12}O_{38}Co_3Zr_6$	$C_{216}H_{130}N_{12}O_{35}Fe_3Cl_3Zr_6$
Formula mass	3964.91	4251.03	4231.66	4274.71
Crystal system	Cubic	Cubic	Cubic	Cubic
a/Å	25.4023(4)	25.4084(8)	25.3669(10)	25.4287(2)
b/Å	25.4023(4)	25.4084(8)	25.3669(10)	25.4287(2)
c/Å	25.4023(4)	25.4084(8)	25.3669(10)	25.4287(2)
α/°	90.00	90.00	90.00	90.00
β/°	90.00	90.00	90.00	90.00
γ/°	90.00	90.00	90.00	90.00
Unit cell volume/Å^3	16391(5)	16403.3(9)	16323.1(11)	16442.7(2)
Temperature/K	296(2)	296(2)	296(2)	296(2)
No. of formula units per unit cell, Z	1	1	1	1
No. of reflections measured	38433	40406	41606	51623
No. of independent reflections	2223	2139	2130	2145
R_{int}	0.0941	0.0870	0.0976	0.1162
Final R_1 values ($I> 2\sigma(I)$)	0.0817	0.1012	0.0768	0.0870
Final $wR(F^2)$ values ($I> 2\sigma(I)$)	0.2083	0.2521	0.2205	0.2466
Final R_1 values (all data)	0.1385	0.1451	0.1160	0.1024
Final $wR(F^2)$ values (all data)	0.2503	0.2980	0.2581	0.2713
Goodness of fit on F^2	1.042	1.086	1.019	1.061

$R_1 = \sum||F_o| - |F_c||/\sum|F_o|$, $wR = \{\sum w[(F_o)^2 - (F_c)^2]^2/\sum w[(F_o)^2]^2\}^{1/2}$.

(2) Powder X-ray diffraction

Powder X-ray diffraction (PXRD) patterns of as-synthesized samples were compared to simulated PXRD patterns to support the phase purity of CPM-99X (Figure 4.7).

The experiments were performed on a Bruker D8 Advance X-ray powder diffractometer operating at 40 kV and 40 mA (CuKα radiation, λ =1.5418 Å). All the

tests were performed with a step size of 0.02° and counting time of 2s per step. The

simulated powder XRD patterns were obtained based on the single-crystal data.
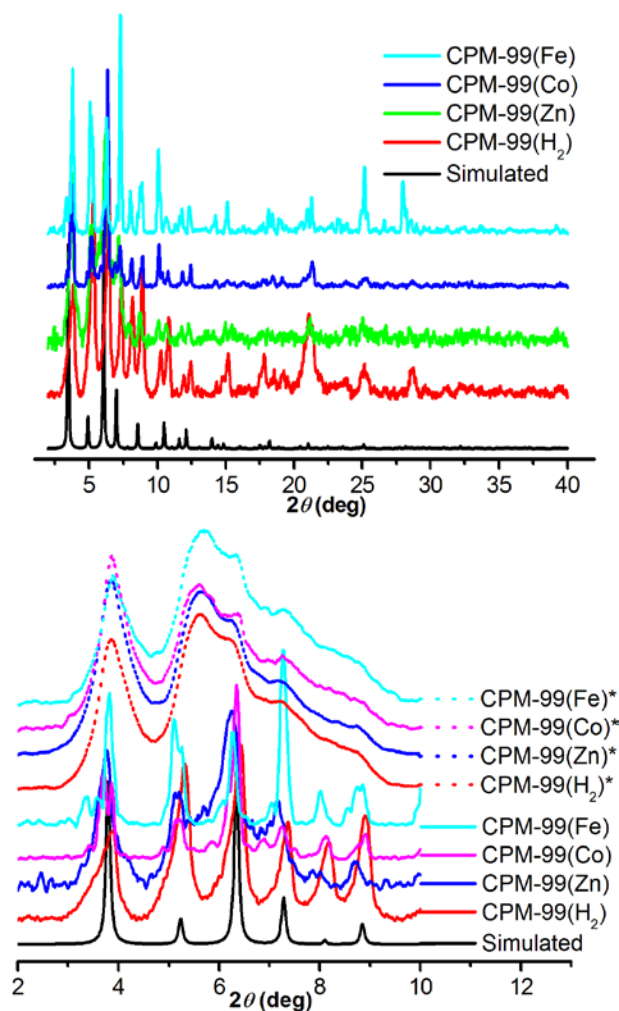
Figure 4.7 PXRD patterns of the CPM-99(X) (*denotes 200°C thermo -vacuum treatment).

(3) Microscopic imaging

Microscopic imaging was carried out at the UCR Microscopy Core at the Institute

for Integrative Genome Biology (IIGB).

(4) UV-vis spectroscopy
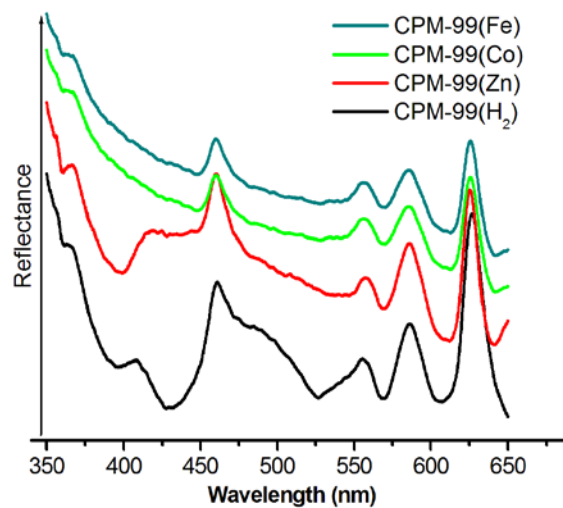
Figure 4.8 Normalized solid-state diffuse reflectance spectra of the CPM-99.

(5) Thermal analysis

The thermogravimetric analysis (TGA) was performed on a TA Instruments TGA Q500 apparatus. All the experiments were performed in the temperature range of 30 $^{\circ}$C to 800 °C under N_2 flow at a heating rate of 5 $^{\circ}$C/min.
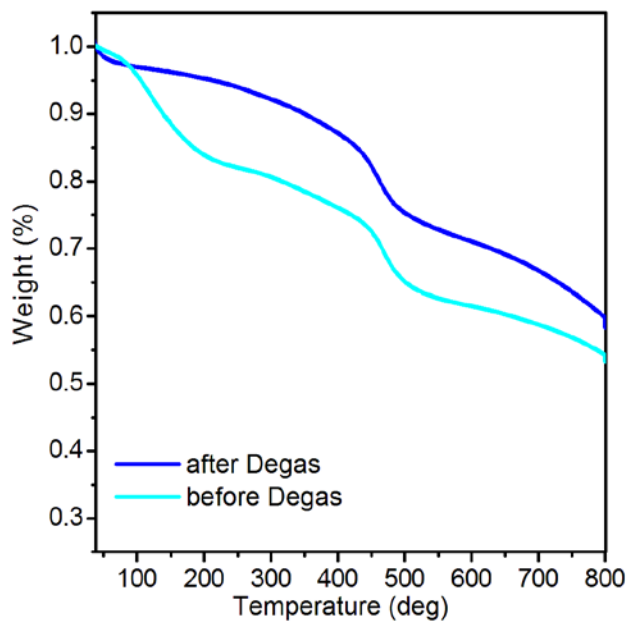
Figure 4.9 TGA of the CPM-99(Fe) (before and after degas on ASAP2020 for 12 hours at 100 °C).

(6) Gas adsorptions

Gas adsorption measurements were carried out on a Micromeritics ASAP 2020 (or 2010) Physisorption Analyzer. Prior to the measurement, the as-synthesized crystal sample was soaked in methanol for 1 day during which period the methanol bath was refreshed twice. After being filtered and dried in the vacuum oven overnight, the crystalline sample was further dried by using the "degas" function of the surface area analyzer for 12 hrs at 200 °C.
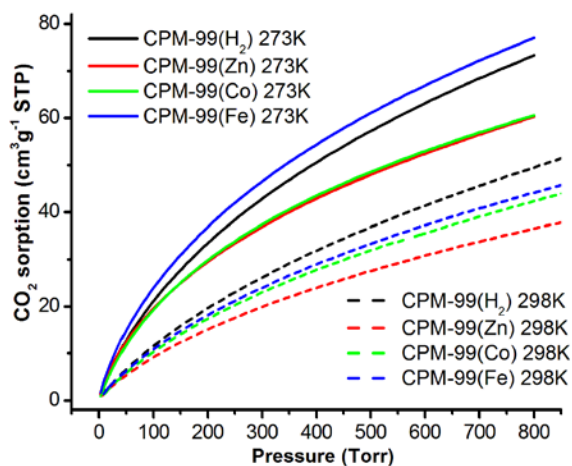
Figure 4.10 CO_2 adsorption of CPM-99.

4.2.5 Pyrolysis of CPM-99

The pyrolysis reactions of CPM-99s were carried out in quartz tubes (with two open ends) that were put in tube furnace under an argon atmosphere. As exemplified by CPM-99(Fe), the sample was heated from the room temperature to 600°C, or 700°C, or 800°C or 900 °C with a heating rate of 3 °C/min. Then the sample was pyrolyzed at set temperature for 4 hours in Ar gas. The CPM-99(Fe) samples that were pyrolyzed at 600°C, 700°C, 800°C and 900 °C were denoted to CPM-99(Fe)/C-600, -700, -800 and -900. All the experimental procedures are similar to those for the preparation of

CPM-99(H$_2$)/C-700, CPM-99(Zn)/C-700, and CPM-99(Co)/C-700, the suffixal 700 refers

to heating temperature in the pyrolysis stage. CPM-99(X)/C-700 is also labeled as

CPM-99(X)/C (X = H$_2$, Zn, Co, Fe; C denotes carbonization to carbon).

4.2.6 Characterization of CPM-99/C

(1) Powder X-ray diffraction (PXRD)
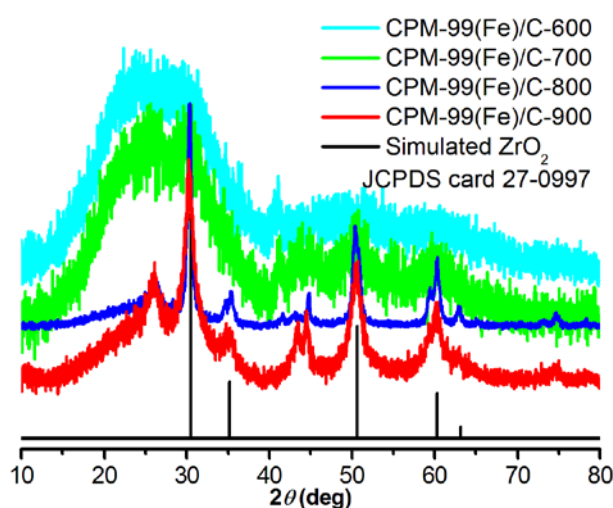
Figure 4.11 PXRD patterns of the CPM-99(Fe)/C carbonized at different temperatures.

(2) UV-vis spectroscopy
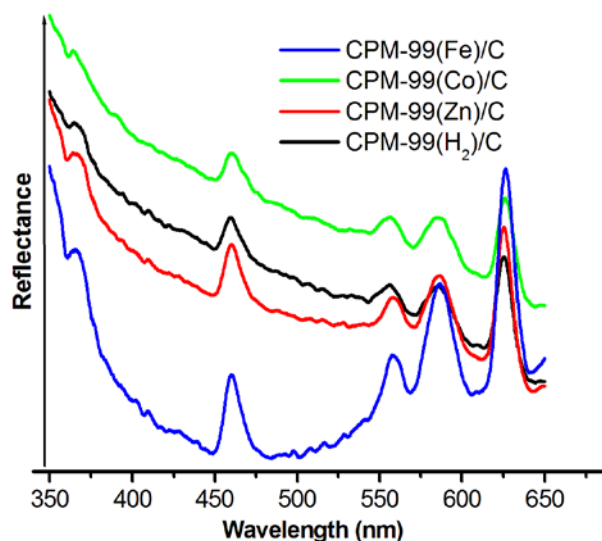
Figure 4.12 Normalized solid-state diffuse reflectance spectra of the CPM-99/C.

(3) X-ray photoelectron spectroscopy (XPS)

X-ray photoelectron spectrum (XPS) measurements were made on a Kratos analytical AXIS Ultra Delay-Line Detector (DLD) Imaging XPS equipped with a vacuum ultraviolet light source, using C 1s (284.8 eV) as a reference to correct the binding energy (Francisco Zaera Surface Group, UCR).
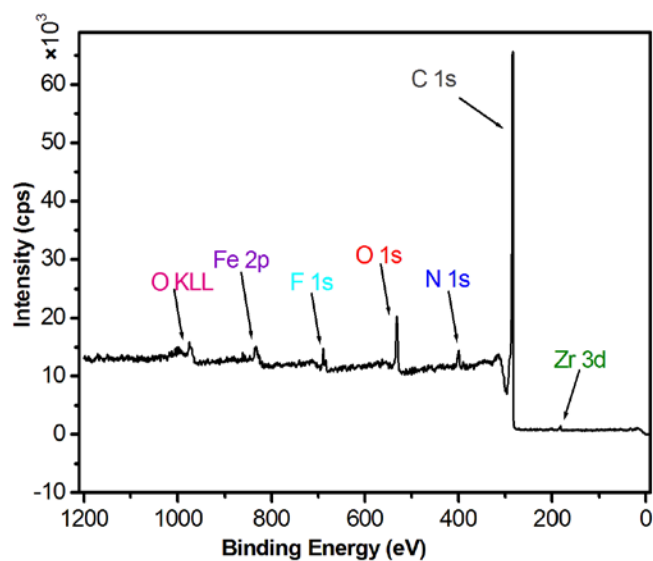
Figure 4.13 XPS survey spectrum of the CPM-99(Fe)/C.
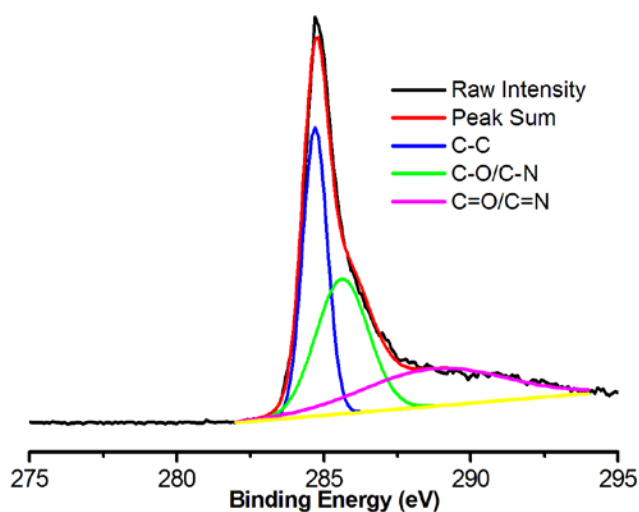
Figure 4.14 XPS C1s spectrum of the CPM-99(Fe)/C.

(4) Gas sorption
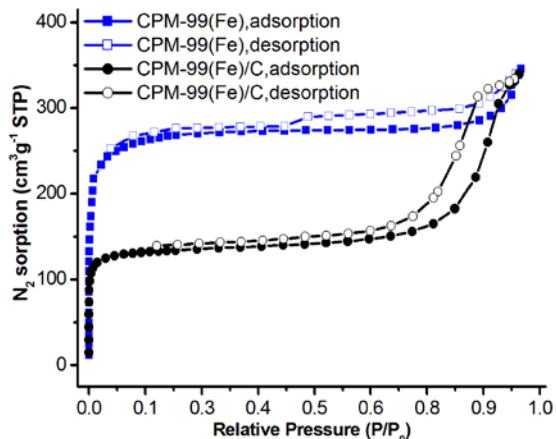
Figure 4.15 N_2 sorption of CPM-99(Fe)/C-700 and its non-pyrolytic CPM-99(Fe) at 77 K.

(5) Electrocatalytic activities for ORR

Cyclic voltammetry (CV) and rotating disk electrode (RDE) techniques on a CHI-650 electrochemical analyzer were used to test the electrocatalytic activities of as-prepared samples. A three-electrode cell was used with a glass carbon RDE (5 mm in diameter, Pine) as working electrode, an Ag/AgCl, KCl (3 M) electrode as the reference electrode, and a Pt wire electrode as the counter electrode. The ORR experiments were performed in 0.1 M KOH or 0.1 M $HClO_4$ solution. The potential was $-1\leftrightarrow+0.2$ (base) or $-0.2\leftrightarrow+1$ (acid) V (vs Ag/AgCl) at a scan rate of 10 mV s^{-1} at the ambient temperature after purging O_2 or Ar gas for 20 min.

All the working electrodes were prepared as following: 5 mg of catalysts and 40 μL of Nafion solution (5 wt%) were dispersed in 600 μL of ethanol. Then the solution was sonicated for 30 min to form a homogeneous ink. Then, 5 (base) or 15 (acid) μL of ink was loaded onto polished glassy carbon rotating disk electrode, and the electrode was

dried at room temperature. Electrolyte was saturated with oxygen by bubbling O_2 prior to the measurements. A flow of O_2 was maintained over the electrolyte during the measurements.

Commercial 20 wt% Pt/C catalysts obtained from Alfa Aesar were used for comparison. The catalyst loading of active Pt-free catalysts on the working electrode is 0.2 (base) or 0.6 (acid) mg cm^{-2} in 0.1 M KOH or $HClO_4$ solution. For Pt/C, the loading of active material is 10 μg Pt cm^{-2} (0.1 mg Pt/C cm^{-2}). All the potentials were calibrated to the potentials vs RHE (Potentials vs RHE = potential vs Ag/AgCl+0.949 (base), +0.268 (acid) V).

4.3 Results and Discussion

4.3.1 Structure Description

CPM-99 series were synthesized by solvothermal reactions of TCBPP-X (X = H_2, Zn, Co, Fe), $ZrOCl_2 \cdot 8H_2O$ and benzoic acid in DEF for 5 days at 120 °C.[42] The high quality of cube-shape single crystals makes structures of CPM-99X be easily determined by single-crystal X-ray diffraction (Figure 4.16e).

The 3D framework is constructed by $[Zr_6(\mu_3\text{-O})_4(\mu_3\text{-OH})_4(O_2C)_{12}]$ clusters. Each cluster is 12 connected as the 12 carboxylates are from 12 TCBPP-X. The clusters serve as vertexes in a cubic cage while the faces of cube are capped by TCBPP-X. The packing of cubes forms a ftw framework. It was found that pore size expansion for cubic structures through longer bridging units leads to lower framework stability and less desired interpenetration.[43,45] In this work, interpenetration is avoided and high stability is retained.
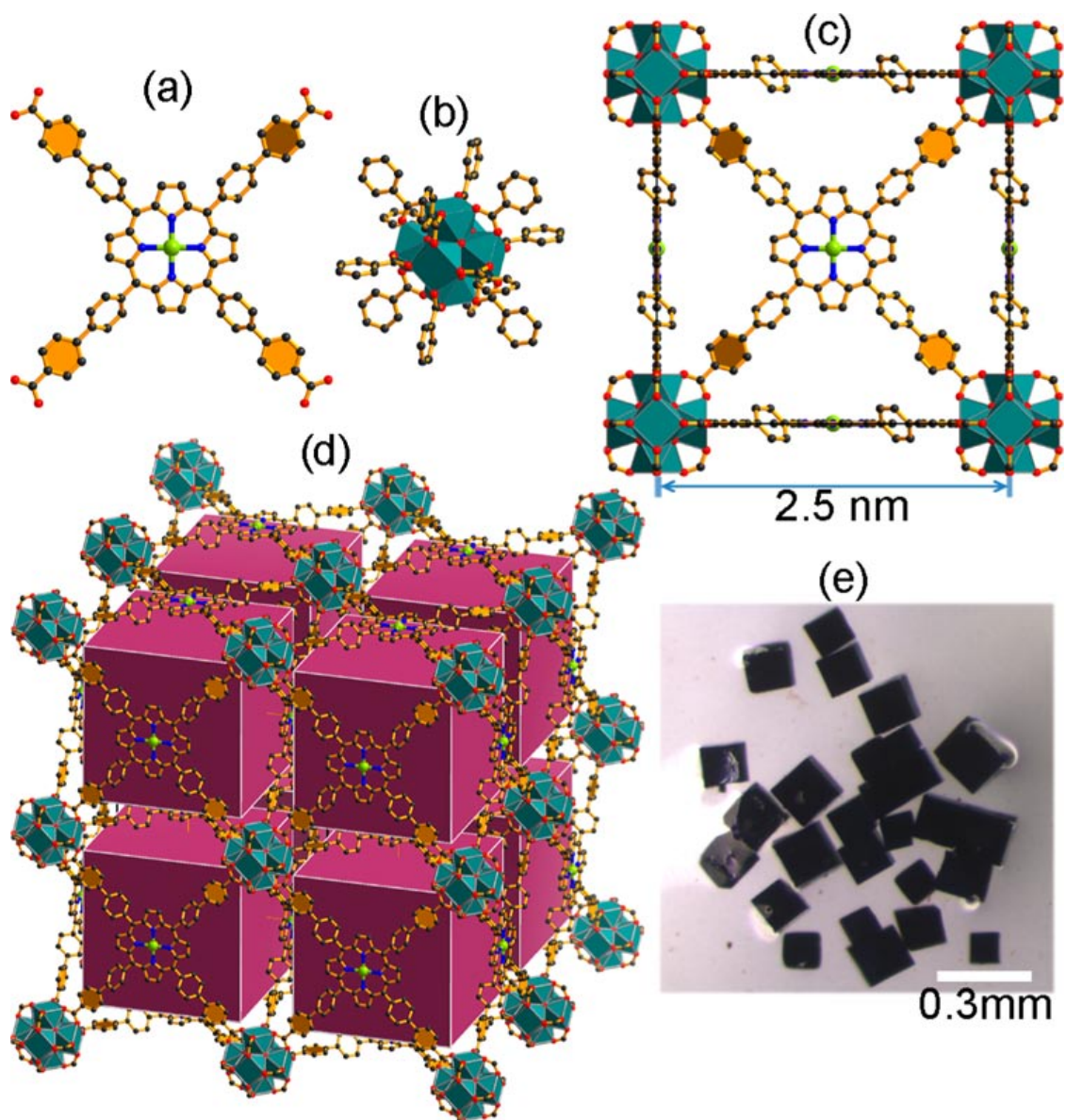
Figure 4.16 (a) TCBPP-X (X = H$_2$, Zn, Co, Fe) ligand; (b) [Zr$_6$(μ_3-O)$_4$(μ_3-OH)$_4$(O$_2$C)$_{12}$] clusters; (c) Cubic cage is constructed by Zr$_6$ clusters and TCBPP-X, the length of edge is 2.5 nm; (d) The packing of cubic cages forms a ftw framework, Zr teal, X lime, O red, N blue, C gray; (f) Photograph of single crystals.

4.3.2 Analysis of Properties

The PLATON-calculated data shows that CPM-99Fe is highly porous and its solvent accessible volume is 82%, indicating its highly porous nature. Despite such large pores, its thermal stability is quite excellent. Powder X-ray diffraction (PXRD) patterns remained nearly unchanged after the sample was degassed at 200 °C (Figure 4.7). Thermogravimetric analysis showed that CPM-99Fe retained its crystallinity up to approximately 450 °C (Figure 4.9).

The gas adsoprion properties of CPM-99X were analyzed. The CO_2 uptake of CPM-99 (H_2, Zn, Co and Fe) reached 73, 60, 61, 76 $cm^3 g^{-1}$ at 760 Torr and 273 K, respectively (Figure 4.10). These are quite high among Zirconium and/or porphyrin-based MOFs.[46-48] The porosity of CPM-99X was analyzed based on the nitrogen adsorption at 77 K. Take CPM-99Fe as representative example, the N_2 uptake of CPM-99 Fe is 450 $cm^3 g^{-1}$ (STP), and Brunauer-Emmett-Teller (BET) surface area of CPM-99 Fe is 1030 $m^2 g^{-1}$. The second increase at $P/P_0 = 0.02$ in the isotherm of CPM-99Fe indicates the presence of mesopores (Figure 4.15).

In the N_2 adsorption-desorption isotherms (77 K) of CPM-99Fe/C, there is a steep increase at low relative pressures, which demonstrates microporous characteristics. The slight hysteresis of the desorption isotherm at high relative pressure demonstrates the presence of mesopores (Figure 4.15).

The crystals of CPM-99X were carbonized to produce (metallo)porphyrinic carbons that would be used as catalysts for ORR. They were denoted as CPM-99X/C (X = H_2, Zn, Co, Fe). Based on our experiments, 700 °C is the optimum annealing

temperature. The peaks of PXRD at □ 25 and 44° correspond to the diffractions from the (002) and (100) planes of graphitic carbon, respectively. This shows the presence of long-range ordering in the carbon matrix. There are also some sharp peaks that match ZrO_2 (Figure 4.11). After being treated with HF (5 wt% in water), no diffraction peaks of ZrO_2 were observed.

UV-Vis (solid-state diffuse reflectance) spectra of CPM-99Fe and CPM-99Fe/C showed that the carbonized products somewhat retained the porphyrinic characteristic (Figures 4.8, Figure 4.12, and Figure 4.17c).

These studies may help us conclude that CPM-99X/C somewhat retain the high porosity and other properties of CMP-99X, which make them serve as good templates to encapsulate the resulting electrocatalytic nano-fragments.

The electronic states of Fe, N, and C in CPM-99X/C were analyzed by XPS measurements. As it is illustrated in Figure 4.17a (Fe 2p XPS spectrum), there are 2p3/2 and 2p1/2 peaks in 710.8 and 722.9 eV, respectively, which match well with those for Fe(II).[39] The raw N 1s spectrum is constituted by three peaks which are at 398.5, 399.6, and 400.9eV. They correspond to nitrogen species in pyridinic, metal-coordinated, and graphitic, respectively (Figure 4.17b).[38, 49]Based on these results, we conclude that the Fe ions are associated with N atoms to form catalytically active sites.[50, 51]In the C 1s spectrum, peaks that correspond to the porous carbon are centered at ~285 eV and are slightly asymmetric (Figure 4.14). These are common for nitrogen-doped graphitic carbon.[37]

ORR activities of CPM-99X/C-derived electrodes were tested and compared to benchmark carbon supported Pt (viz. 20% Pt/C). Among the four samples, CPM-99Fe/C showed the highest ORR activity.

The tests were firstly performed in 0.1M KOH solution, as it is shown Figure 4.18a, the ORR peak of CPM-99Fe/C is at the most positive potential of 0.836 V. The ORR activities of these four samples are in the order: Fe > Co >Zn$\approx$H$_2$. This is supported by the linear sweep voltammetry measurements on a RDE. As it is shown in Figure 4.18b, the onset and half-wave potentials of CPM-99Fe/C (0.950 and 0.802 V, determined at the polarization curves at 1600 rpm) are close to those (0.978 and 0.818 V) of the 20 wt % Pt/C. Moreover, compared to Pt/C, the CPM-99Fe/C catalyst showed better long-term durability (Figure 4.19). Through continuous potential cycling, a slight peak current decrease was observed for CPM-99Fe/C after 10000 cycles, while the deterioration of 20 wt % Pt/C catalyst resulted in larger decrease.

The ORR activity of the CPM-99X/C-derived electrodes in O$_2$-saturatedacidic medium (0.1 M HClO4 electrolyte) was also studied. Among four CPM-99X/C electrodes, the CPM-99Fe/C-electrode showed the best electrocatalytic activity. The onset potential of CPM-99Fe/C-electrode was 0.875 V, which was comparable to the Pt/C (0.880 V). The onset potential and current density of the CPM-99Co/C, CPM-99Zn/C and CPM-99H$_2$/C electrodes were much lower (Figure 4.18c). The ORR activities of these four samples in the acid solution showed the same order: Fe > Co > Zn $\approx$ H$_2$. It is believed that the unique structural and compositional features of CPM-99Fe,

such as high porosity, excellent stability, uniform distribution of FeN_4 active sites,

contribute to the high electrocatalytic activities of CPM-99Fe/C-derived electrode.
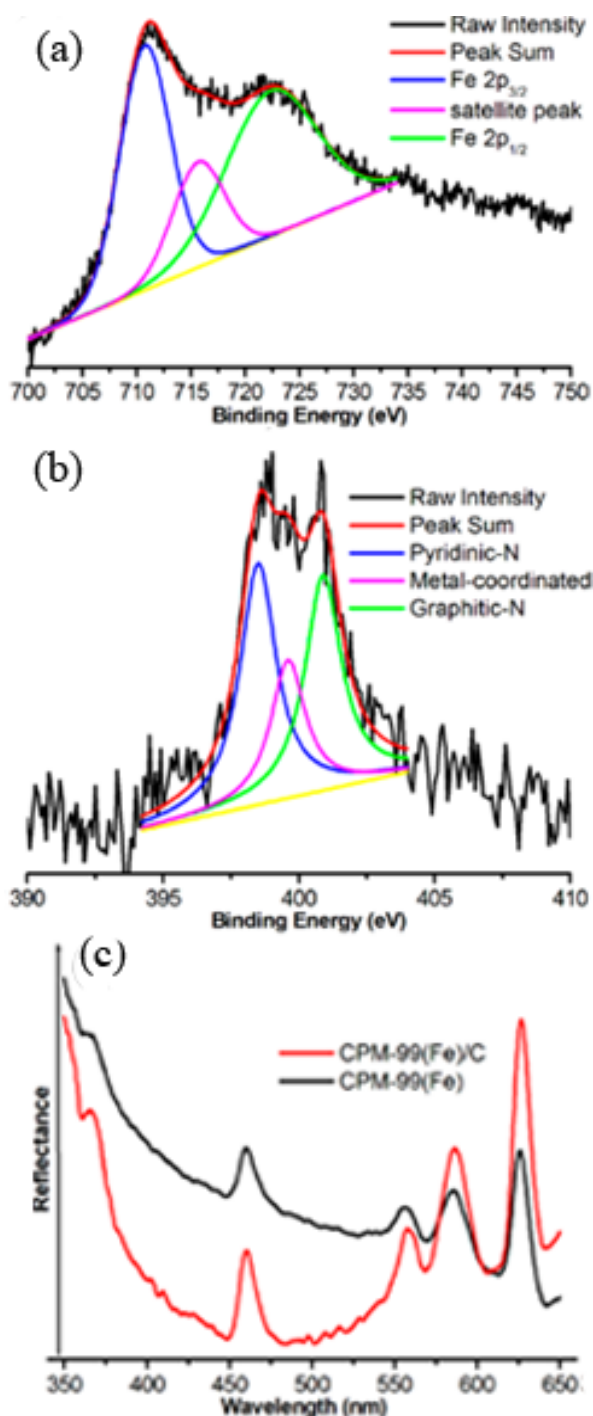
Figure 4.17 (a) Fe 2p XPS spectrum of CPM-99Fe/C; (b) N 1s spectra of the CPM-99Fe/C; (c) UV-vis diffuse reflectance spectra of CPM-99Fe and CPM-99Fe/C.
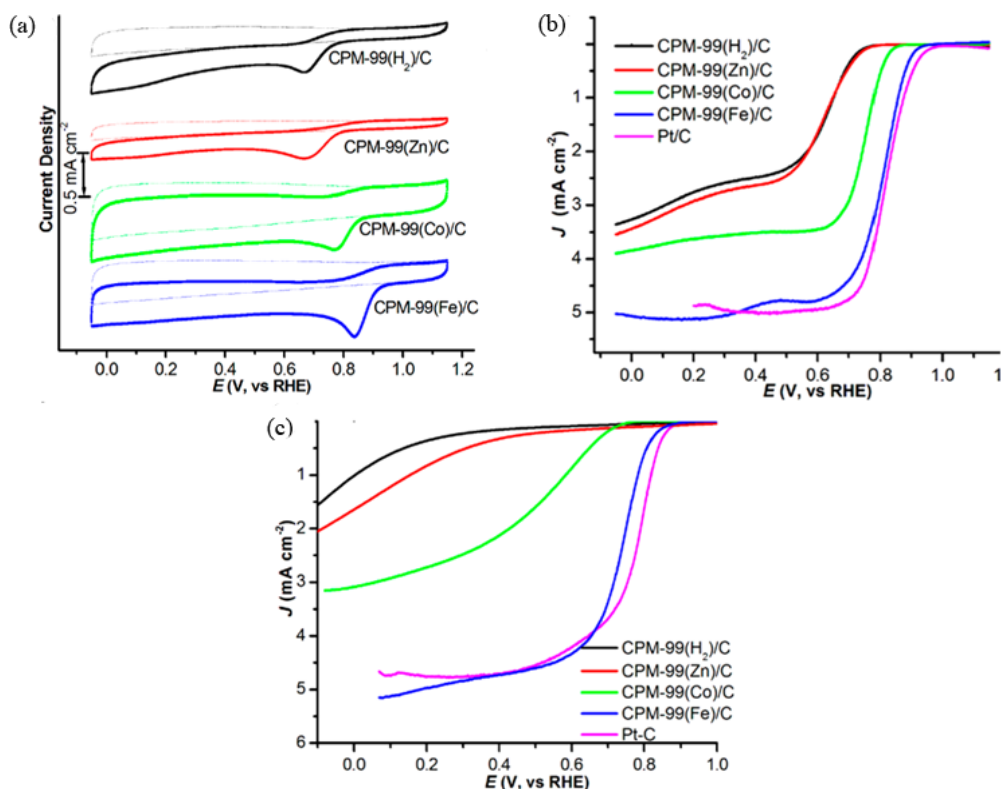
Figure 4.18 (a) CV curves of CPM-99X/C in 0.1 M KOH solution; (b) RDE polarization curves of CPM-99X/C and 20% Pt/C in 0.1 M KOH solution; (c) RDE polarization curves of CPM-99X/C and 20% Pt/C in 0.1 M HClO$_4$ solution. The catalyst loadings on the electrodes were 0.2 (in KOH) or 0.6 (in HClO$_4$) mg·cm^{-2} for the CPM- 99X/C and 0.1 mg·cm^{-2} for Pt/C. The scan rate is 10 mV·s^{-1}.
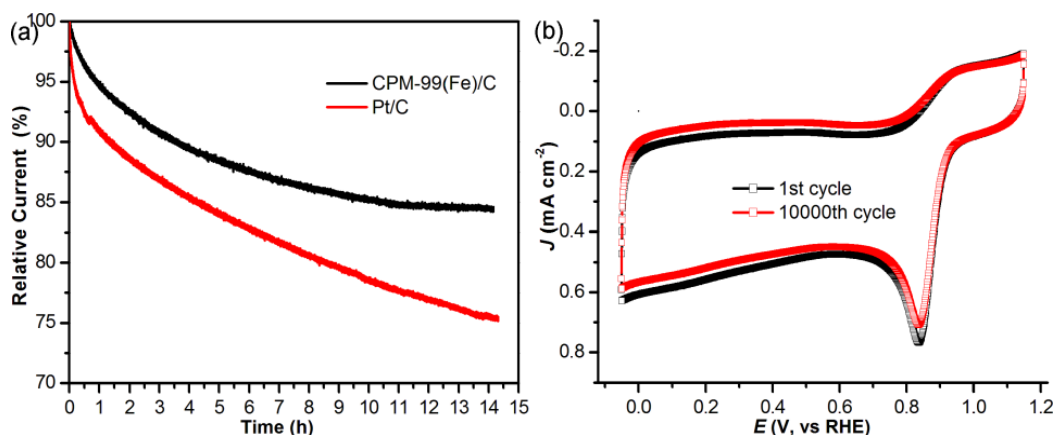
Figure 4.19 (a) Current-time (*i-t*) chronoamperometric response; (b) Cycling CVs over CPM-99(Fe)/C in O$_2$-saturated 0.1 M KOH solution.

4.4 Conclusion

By reasonable design, we developed a series of zirconium-(metallo)porphyrin frameworks (ZPFs). These materials have high porosity, excellent stability and uniformly distributed active metal sites. These make them be ideal precursors for synthesizing highly active noble-metal- free catalysts for the ORR. The carbonized catalysts of CPM-99Fe exhibited high ORR activity which was comparable to 20% Pt/C catalyst. The high electrocatalytic activity of CPM-99Fe/C can be attributed to its unique precursor, which has large cavity, high proportion of active center and hard template. This work demonstrates a successful design and synthesis of porphyrin-functionalized zirconium frameworks with desired properties for developing highly active non-precious metal electrocatalysts.

4.5 References

(1)   J. Cavka, S. Jakobsen, U. Olsbye, N. Guillou, C. Lamberti, S. Bordiga, K. Lillerud, *J. Am. Chem. Soc*. **2008**, *130*, 13850.

(2)   M. Kandiah, M. Nilsen, S. Usseglio, S. Jakobsen, U. Olsbye, M. Tilset, C. Larabi, E. Quadrelli, F. Bonino, K. Lillerud, *Chem. Mater*. **2010**, *22*, 6632.

(3)   A. Schaate, P. Roy, A. Godt, J. Lippke, F. Waltz, M. Wiebcke, P. Behrens, *Chem. Eur. J*. **2011**, *17*, 6643.

(4)   M. Katz, Z. Brown, Y. Colon, P. Siu, K. Scheidt, R. Snurr, J. Hupp, *Chem. Commun*. **2013**, *49*, 9449.

(5)   L. Shen, S. Liang, W. Wu, R. Liang, L. Wu, *J. Mater. Chem. A*. **2013**, *1*, 11473.

(6)   L. Shen, W. Wu, R. Liang, R. Lin, L. Wu, *Nanoscale*. **2013**, *5*, 9374.

(7)   G. Shearer, S. Chavan, J. Ethiraj, J. Vitillo, S. Svelle, U. Olsbye, C. Lamberti, S. Bordiga, K. Lillerud, *Chem. Mater*. **2014**, *26*, 4068.

(8)   M. Cliffe, W. Wan, X. Zou, P. Chater, A. Kleppe, M. Tucker, H. Wilhelm, N. Funnell, F. Coudert, A. Goodwin, *Nat. Commun*. **2014**, *5*, 4176.

(9)   M. Zhang, Y. Chen, M. Bosch, T. Gentle, K. Wang, D. Feng, Z. Wang, H. C. Zhou, *Angew. Chem. Int. Ed*. **2014**, *53*, 815.

(10)   H. Furukawa, F. Gandara, Y. Zhang, J. Jiang, W. Queen, M. Hudson, O. M. Yaghi, *J. Am. Chem. Soc*. **2014**, *136*, 4369.

(11)   Z. Wei, Z. Gu, R. Arvapally, Y. Chen, R. McDougald, J. Ivy, A. Yakovenko, D. Feng, M. Omary, H. C. Zhou, *J. Am. Chem. Soc*. **2014**, *136*, 8269.

(12)   H. Wu, T. Yildirim, W. Zhou, W. *J. Phys. Chem. Lett*. **2013**, *4*, 925.

(13)   L. Pan, S. Kelly, X. Huang, J. Li, *Chem. Commun*. **2002**, 2334.

(14)   C. Zou, Z. Zhang, X. Xu, Q. Gong, J. Li, C. Wu, *J. Am. Chem. Soc*. **2012**, *134*, 87.

(15)   A. Fateeva, P. Chater, C. Ireland, A. Tahir, Y. Khimyak, P. Wiper, J. Darwent, M. Rosseinsky, *Angew. Chem. Int. Ed*. **2012**, *51*, 7440.

(16) H. Son, S. Jin, S. Patwardhan, S. Wezenberg, N. Jeong, M. So, C. Wilmer, A. Sarjeant, G. Schatz, R. Snurr, O. Farha, G. Wiederrecht, J. Hupp, *J. Am. Chem. Soc*. **2013**, *135*, 862.

(17) J. Park, D. Feng, S. Yuan, H. C. Zhou, *Angew. Chem. Int. Ed*. **2015**, *54*, 430.

(18) D. Feng, Z. Gu, J. R. Li, H. Jiang, Z. Wei, H. C. Zhou, *Angew. Chem. Int. Ed*. **2012**, *51*, 10307.

(19) H. Jiang, D. Feng, K. Wang, Z. Gu, Z. Wei, Y. Chen, H. C. Zhou, *J. Am. Chem. Soc*. **2013**, *135*, 13934.

(20) D. Feng, W. Chung, Z. Wei, Z. Gu, H. Jiang, Y. Chen, D. Darensbourg, H. C. Zhou, *J. Am. Chem. Soc*. **2013**, *135*, 17105.

(21) W. Morris, B. Volosskiy, S. Demir, F. Gandara, P. McGrier, H. Furukawa, Cascio, J. Stoddart,O. M. Yaghi, *Inorg. Chem*. **2012**, *51*, 6443.

(22) D. Yuan, D. Zhao, D. Timmons, H. C. Zhou, *Chem. Sci*. **2011**, *2*, 103.

(23) Y. Zhou, Y. Chen, Y. Hu, G. Huang, S. Yu, H. Jiang, *Chem. Eur. J*. **2014**, *20*, 14976.

(24) F. Jaouen, E. Proietti, M. Lefèvre, R. Chenitz, J. Dodelet, G. Wu, H. Chung, C. Johnston, P. Zelenay, *Energy Environ. Sci*. **2011**, *4*, 114.

(25) L. Dai, *Acc. Chem. Res*. **2013**, *46*, 31.

(26) G. Wu, P. Zelenay, *Acc. Chem. Res*. **2013**, *46*, 1878.

(27) H. Wang, H. Dai, *Chem. Soc. Rev*. **2013**, *42*, 3088.

(28) I. Katsounaros, S. Cherevko, A. Zeradjanin, K. Mayrhofer, *Angew. Chem. Int. Ed*. **2014**, *53*, 102.

(29) S. Ma, G. Goenaga, A. Call, D. Liu, *Chem. Eur. J*. **2011**, *17*, 2063.

(30) A. Aijaz, N. Fujiwara, Q. Xu, *J. Am. Chem. Soc*. **2014**, *136*, 6790.

(31) D. Zhao, J. Shui, L. Grabstanowicz, C. Chen, S. Commet, T. Xu, J. Lu, D. Liu, *Adv. Mater*. **2014**, *26*, 1093.

(32) S. Wang, Y. Hou, S. Lin, X. Wang, *Nanoscale*. **2014**, *6*, 9930.

(33)　S. Wang, J. Lin, X. Wang, *Phys. Chem. Chem. Phys*. **2014**, *16*, 14656.

(34)　S. Wang, W. Yao, J. Lin, Z. Ding, X. Wang, *Angew. Chem. Int. Ed*. **2014**, *53*, 1034.

(35)　K. Park, Z. Ni, A. Cote, J. Choi, R. Huang, F. Uribe-Romo, H. Chae, M. O'Keeffe, O. M. Yaghi, *Proc. Natl. Acad. Sci. U. S. A*. **2006**, *103*, 10186.

(36)　O. Karagiaridi, W. Bury, A. Sarjeant, C. Stern, O. Farha, J. Hupp, J. T. *Chem. Sci*. **2012**, *3*, 3256.

(37)　S. Yuan, J. Shui, L. Grabstanowicz, C. Chen, S. Commet, B. Reprogle, T. Xu, L. Yu, D. Liu, *Angew. Chem. Int. Ed*. **2013**, *52*, 8349.

(38)　Z. Wu, L. Chen, J. Liu, K. Parvez, H. Liang, J. Shu, H. Sachdev, R. Graf, X. Feng, K. Mullen, *Adv. Mater*. **2014**, *26*, 1450.

(39)　Z. Xiang, Y. Xue, D. Cao, L. Huang, J. Chen, L. Dai, *Angew.Chem. Int. Ed*. **2014**, *53*, 2433.

(40)　A. D. Adler, F. R. Longo, J. D. Finarelli, J. Goldmacher, J. Assour, L. J. Korsakoff, *J. Org. Chem*. **1967**, *32*, 476.

(41)　T. Aya and A. D. Hamilton, *Bioorg. Med. Chem. Lett*. **2003**, *13*, 2651.

(42)　T. Liu, D. Feng, Y. Chen, L. Zou, M. Bosch, S. Yuan, Z. Wei, S. Fordham, K. Wang, H. C. Zhou, H. C. *J. Am. Chem. Soc*. **2015**, *137*, 413.

(43)　M. Eddaoudi, J. Kim, N. Rosi, D. Vodak, J. Wachter, M. O'Keeffe, O. M. Yaghi, *Science*. **2002**, *295*, 469.

(44)　B. Chen, N. Ockwig, A. Millward, D. Contreras, O. M. Yaghi, *Angew. Chem*. **2005**, *117*, 4823.

(45)　A. Coskun, M. Hmadeh, G. Barin, F. Gandara, Q. Li, E. Choi, N. Strutt, D. Cordes, A. Slawin, J. Stoddart, J. Sauvage, O. M. Yaghi, *Angew. Chem. Int. Ed*. **2012**, *51*, 2160.

(46)　W. Gao, L. Wojtas, S. Ma, *Chem. Commun*. **2014**, *50*, 5316.

(47)　X. Wang, L. Meng, Q. Cheng, C. Kim, L. Wojtas, M. Chrzanowski, Y. Chen, X. Zhang, S. Ma, *J. Am. Chem. Soc*. **2011**, *133*, 16322.

(48)　W. Gao, M. Chrzanowski, S. Ma, *Chem. Soc. Rev*. **2014**, *43*, 5841.

(49) H. Liang, W. Wei, Z. Wu, X. Feng, K. Mullen, *J. Am. Chem. Soc*. **2013**, *135*, 16002.

(50) J. Wu, W. Li, D. Higgins, Z. Chen, *J. Phys. Chem. C*. **2011**,*115*, 18856.

(51) Y. Zhao, K. Watanabe, K. Hashimoto, *J. Am. Chem. Soc*. **2012**, *134*, 19528.

Chapter 5

Concluding Remarks and Future Prospects

In this dissertation, we have demonstrated the synthesis of complicate MOF architecture, zeolite framework within zeolite framework. We also showed how to tune the charge of frameworks that are built from same metal and same ligand. Finally, we provide a new method to develop noble metal free electrochemical catalyst based on MOFs.

MOFs have been investigated for 30 years and lots of frameworks including zeolitic frameworks have been developed. But framework@framework architecture is quite rare and meaningful, because this unique structure can make different environments exist independently in one system. The different pore sizes of outer and inner frameworks can selectively absorb different molecules. If different functional groups can be grafted onto the surface of frameworks, respectively, the resulting material will has multi-functions. The construction of reported materials provides people with valuable guide for future work. Before our work, all cage@cage, cage@framwork, framework@framework structures are realized based on muti-functional ligands. Our work shows that inorganic building unit can also serve as a bridge between inner and outer cages. More complicate and fantastic architectures will be developed as people start to use various inorganic building units as bridges.

The charge of MOFs has a great effect on the properties of gas adsorption, proton conductivity and ion exchange. In trimer and In monomer are two of the most common

SBUs in In-MOFs, and they can exist in the same structure. By carefully tuning the reaction factors, such as ratio of In^{3+}/carboxylate ligands, not only complicate frameworks, such as cage-within-cage, can be formed, but also desired framework charge can be obtained. Similar method should be used to develop other SBUs with same metals but different charges.

In the past 5 years, Zr-MOFs that are synthesized by using carboxylate ligands gain lots of interest because of their excellent stability. However, all reported Zr-MOFs are based on 12-connected, 8-connected and 6-connected Zr$_6$ cluster ([Zr$_6$(μ_3-O)$_4$(μ_3-OH)$_4$(O$_2$C)$_{12}$], [Zr$_6$(μ_3-O)$_4$(μ_3-OH)$_4$(O$_2$C)$_8$], [Zr$_6$(μ_3-O)$_4$(μ_3-OH)$_4$(O$_2$C)$_8$]). This limits the diversity of Zr-MOFs. More efforts need be put to investigate the assembly mechanism of Zr-MOFs. Meanwhile, the potential applications of reported Zr-MOFs should be continuously explored, as the stability of these MOFs allows them to be post-functionalized in various harsh conditions.